

SUSTAINABLE FABRICATION OF NITROGEN-DOPED
CARBON QUANTUM DOTS FROM *ELAEIS*
GUINEENSIS EMPTY FRUIT BUNCHES FOR SOLAR
PHOTOCATALYSIS TOWARDS ORGANIC DYES

UMAIRAH BINTI ABD RANI

DOCTOR OF PHILOSOPHY OF CHEMICAL
ENGINEERING

LEE KONG CHIAN FACULTY OF
ENGINEERING AND SCIENCE
UNIVERSITI TUNKU ABDUL RAHMAN

FEBRUARY 2023

**SUSTAINABLE FABRICATION OF NITROGEN-DOPED CARBON
QUANTUM DOTS FROM *ELAEIS GUINEENSIS* EMPTY FRUIT
BUNCHES FOR SOLAR PHOTOCATALYSIS TOWARDS ORGANIC
DYES**

By

UMAIRAH BINTI ABD RANI

A thesis submitted to the Department of Chemical Engineering
Lee Kong Chian Faculty of Engineering and Science
Universiti Tunku Abdul Rahman
in part fulfillment of the requirements of the degree of
Doctor of Philosophy of Chemical Engineering

February 2023

ABSTRACT

SUSTAINABLE FABRICATION OF NITROGEN-DOPED CARBON QUANTUM DOTS FROM *ELAEIS GUINEENSIS* EMPTY FRUIT BUNCHES FOR SOLAR PHOTOCATALYSIS TOWARDS ORGANIC DYES

Umairah Binti Abd Rani

Empty fruit bunches (EFB) are one of the palm oil mill's most abundant sources of agricultural waste. Even though EFB has a high carbon, oxygen and hydrogen content, they are not well-explored for fabricating carbon-based nanoparticles. This study introduces a sustainable approach to fabricate nitrogen-doped carbon quantum dots (NCQDs) through hydrothermal treatment using lignin extracted from EFB as a raw material. The performance and stability of the fabricated NCQDs from EFB were evaluated through photocatalysis. This study discusses the photocatalytic degradation of methyl green dye using NCQDs through the Taguchi approach. At room temperature and methyl green dye solution of pH 7, functionalized NCQDs performed as effective photocatalysts in degrading 99% of methyl green dye under UV-light irradiation (302 nm) within 20 min. The average particle size of NCQDs was found to be 3.4 nm. The NCQDs showed greenish-blue fluorescence under a UV lamp owing to their excellent optical properties and the optical properties of NCQDs remained unchanged after several hours of UV-light exposure.

NCQDs fabricated from EFB showed outstanding stability and reactivity in which they could retain their photocatalytic capability by storing at 5 °C for twelve months. Around 99% of methyl green dye could be degraded in the first cycle and the NCQDs could be reused in photocatalysis for at least five repeated cycles while maintaining their photo-degradability of methyl green at above 70%. The NCQDs produced from EFB successfully degraded 98% of malachite green, 97% of methylene blue and 50% of methyl orange within 120, 180, and 300 min of sunlight irradiation, respectively. The photocatalytic degradation rate of methylene blue and malachite green dyes followed first-order kinetics based on the Langmuir-Hinshelwood model. Meanwhile, the kinetic rate of degradation for methyl green dye followed the pseudo-second-order model. NCQDs fabricated from EFB biomass show great potential and stability in treating wastewater contaminated with organic dyes.

ACKNOWLEDGEMENT

Firstly, I'm so thankful and praise Allah the Almighty for His generosity of blessings. I would like to express my highest appreciation to my supervisor, Dr. Ng Law Yong for his continuous guidance, supervision, advice and attention throughout the period of my candidature.

I would like to extend my deepest gratitude to my co-supervisor, Dr. Ng Yee Sern for his continuous encouragement, advice, and providing me with the sincere guidance throughout the research project, and Dr. Ong Ying Hui for her guidance in research field and sharing of knowledge and encouragement in journal publications and conferences.

Also, I would like to express my appreciation to Dr. Ebrahim Mahmoudi from Faculty of Engineering and Built Environment, Universiti Kebangsaan Malaysia for providing me with the research facilities and services as well as his guidance me in understanding the research project in quantum dots.

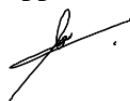
This work was mainly supported by Universiti Tunku Abdul Rahman through UTAR Research Fund (UTARRF). I would also like to acknowledge UTAR Research Scholarship Scheme (RSS) under vote number 6540/U01 for the monthly stipend for the duration of 36 months of my study.

Special thanks to all UTAR laboratory staff, for their assistance in the research facilities and analyses. To my family and all my friends, I wish to express my best regards and gratitude for assisting and providing me with moral support in many aspects, their prayers and support throughout the period of my study.

APPROVAL SHEET

This thesis entitled "**SUSTAINABLE FABRICATION OF NITROGEN-DOPED CARBON QUANTUM DOTS FROM *ELAEIS GUINEENSIS* EMPTY FRUIT BUNCHES FOR SOLAR PHOTOCATALYSIS TOWARDS ORGANIC DYES**" was prepared by UMAIRAH BINTI ABD RANI and submitted as partial fulfillment of the requirements for the degree of Doctor of Philosophy in Chemical Engineering at Universiti Tunku Abdul Rahman.

Approved by:



(Dr. Ng Law Yong)
Assistant Professor/Supervisor
Department of Chemical Engineering
Lee Kong Chian Faculty of Engineering Science
Universiti Tunku Abdul Rahman

Date: 13 February 2023

Ng Yee Sern

(Dr. Ng Yee Sern)
Assistant Professor/Co-supervisor
Department of Chemical Engineering
Lee Kong Chian Faculty of Engineering Science
Universiti Tunku Abdul Rahman

Date: 13 February 2023



(Dr. Ong Ying Hui)
Assistant Professor/Co-supervisor
Department of Chemical Engineering
Lee Kong Chian Faculty of Engineering Science
Universiti Tunku Abdul Rahman

Date: 13 February 2023

SUBMISSION SHEET

**LEE KONG CHIAN FACULTY OF ENGINEERING AND SCIENCE
UNIVERSITI TUNKU ABDUL RAHMAN**

Date: 13 February 2023

SUBMISSION OF THESIS

It is hereby certified that **Umairah Binti Abd Rani** (ID No: 1805889) has completed this thesis entitled “SUSTAINABLE FABRICATION OF NITROGEN-DOPED CARBON QUANTUM DOTS FROM *ELAEIS GUINEENSIS* EMPTY FRUIT BUNCHES FOR SOLAR PHOTOCATALYSIS TOWARDS ORGANIC DYES” under the supervision of Dr. Ng Law Yong (Supervisors), Dr. Ng Yee Sern (Co-Supervisor) and Dr. Ong Ying Hui (Co-Supervisor) from the Department of Chemical Engineering, Lee Kong Chian, Faculty of Engineering and Science, Universiti Tunku Abdul Rahman. I understand that the University will upload softcopy of my thesis in pdf format into UTAR Institutional Repository, which may be made accessible to UTAR community and public.

Yours truly,



(Umairah Binti Abd Rani)

DECLARATION

I UMAIRAH BINTI ABD RANI hereby declare that the thesis is based on my original work except for quotations and citations which have been duly acknowledged. I also declare that it has not been previously or concurrently submitted for any other degree at UTAR or other institutions.



(UMAIRAH BINTI ABD RANI)

Date: 13 February 2023

TABLE OF CONTENTS

	Page
ABSTRACT	i
ACKNOWLEDGEMENT	iii
APPROVAL SHEET	iv
SUBMISSION SHEET	v
DECLARATION	vi
LIST OF TABLES	xi
LIST OF FIGURES	xii
LIST OF ABBREVIATIONS	xiv
CHAPTER	
1.0 INTRODUCTION	1
1.1 Background of study	1
1.2 Problem statements	3
1.3 Research objectives	4
1.4 Thesis outlines	5
2.0 LITERATURE REVIEW	6
2.1 Introduction	6
2.2 Empty fruit bunches (EFB)	7
2.2.1 Definition of EFB	7
2.2.2 Production of EFB in Malaysia	7
2.2.3 Properties of EFB	8
2.2.4 Application of EFB	8

2.2.5	Lignin extracted from EFB	10
2.3	Photocatalysis	11
2.3.1	Introduction to photocatalysis	11
2.3.2	Fabrication of photocatalysts	11
2.3.3	Functionality of photocatalysts	13
2.3.4	Improvement of photocatalysis	14
2.4	Carbon quantum dots (CQDs)	15
2.4.1	Introduction to carbon quantum dots	15
2.4.2	Properties of CQDs	16
2.4.3	Raw material used in the fabrication of CQDs	18
2.4.4	CQDs-based biomass precursors	20
2.4.5	Method used to fabricate CQDs	21
2.5	Dopant elements used in the fabrication of CQDs	31
2.6	Application of NCQDs as photocatalyst	34
2.7	Stability of CQDs	37
3.0	RESEARCH METHODOLOGY	42
3.1	Introduction	42
3.2	Fabrication of carbon quantum dots	43
3.2.1	Lignin extraction method	43
3.2.2	Production of NCQDs and CQDs	44
3.3	Characterisation study of CQDs and NCQDs	45
3.4	Photocatalytic degradation of organic dyes	47
3.5	Optimisation study by Taguchi approach	48
3.6	Photocatalytic kinetic study	51

3.7	Stability and reactivity study	52
3.8	Evaluation of the degraded dyes	52
3.9	Determination of active species	53
4.0	RESULT AND DISCUSSION	54
4.1	Introduction	54
4.2	Fabrication mechanism of NCQDs from EFB	55
4.3	Characterisation study on CQDs and NCQDs	61
4.3.1	Functional group determination	61
4.3.2	Elemental analysis	63
4.3.3	Observation on the surface carbon phases	64
4.3.4	Photoluminescence (PL) properties	66
4.3.5	Light absorption and optical properties	69
4.3.6	Surface charges evaluation	71
4.3.7	Particle sizes distribution	72
4.3.8	Surface morphological studies	75
4.4	Photocatalytic degradation of organic dyes by NCQDs	76
4.4.1	Malachite green	76
4.4.2	Methylene blue	78
4.4.3	Methyl orange	80
4.4.4	Methyl green	81
4.4.5	Mechanism of photocatalytic degradation by NCQDs	82
4.4.6	Determination of active species	89
4.5	Optimisation by Taguchi approach	90
4.6	Photocatalytic kinetic study	94

4.6.1	First-order kinetics model	94
4.6.2	Pseudo-second-order kinetics model	96
4.7	Stability and reactivity study	97
4.8	Evaluation on the degraded dyes	100
4.9	Comparisons of CQDs and NCQDs performance	101
5.0	CONCLUSIONS AND RECOMMENDATION	106
5.1	Summary of study	106
5.2	Recommendations of future works	108
	REFERENCES	110
	PUBLICATIONS	157

LISTS OF TABLES

Table		Page
2.1	Application of EFB in wastewater treatment.	9
2.2	Fabrication and applications of photocatalysts.	12
2.3	Summarize of the CQDs fabrication methods.	22
2.4	Fabrication of CQDs through hydrothermal treatment.	30
2.5	Application of NCQDs as photocatalyst.	35
3.1	Experimental design for four factors and three levels.	49
3.2	Taguchi L ⁹ (3 ⁴) orthogonal array and results of dye degradation in percentage.	50
4.1	Elements present in the CQDs and NCQDs with their respective atomic percentages.	64
4.2	The degradation process of organic dye solutions using the NCQDs as photocatalyst in the presence and absence of the scavenger agents.	89
4.3	SN ratios for each factor corresponding to its level.	91
4.4	TOC values before and after the photocatalytic degradation by NCQDs.	100
4.5	Photocatalytic degradation of dye using CQDs, NCQDs and without catalyst.	103
4.6	Photocatalytic degradation performance towards organic dyes reported from other studies.	105

LISTS OF FIGURES

Figure		Page
2.1	Role of photocatalyst in degrading organic pollutants.	13
2.2	The appearance of the CQDs solution under UV-light irradiation and daylight.	17
3.1	Flowchart of research methodology.	43
3.2	The illustration scheme of the photocatalysis by the fabricated NCQDs form EFB.	47
4.1	FTIR spectrum of lignin extracted from EFB.	56
4.2	Fabrication process of NCQDs through a hydrothermal treatment.	57
4.3	A postulated mechanism of NCQDs fabrication.	59
4.4	An illustration of the self-assembly process in the formation of NCQDs.	61
4.5	FTIR spectra of CQDs and NCQDs produced from EFB.	62
4.6	Elemental mapping for CQDs and NCQDs.	63
4.7	XRD pattern for CQDs and NCQDs produced from EFB.	65
4.8	XRD pattern for NCQDs from EFB.	66
4.9	PL spectra for (a) CQDs excitation, (b) NCQDs excitation, (c) CQDs emission and (d) NCQDs emission.	67
4.10	The fluorescence lifetime of the fabricated NCQDs from EFB.	69
4.11	UV-Vis spectra for (a) CQDs and (b) NCQDs produced from EFB	70
4.12	Zeta potential analysis of (a) CQDs and (b) NCQDs	72
4.13	TEM images for CQDs surfaces in (a) 50 nm scale, (b) 100 nm scale, (c) a histogram of the particle size distribution of CQDs and (d) SAED pattern of CQDs.	74
4.14	HR-TEM images for NCQDs surfaces in (a) 20 nm scale, (b) 100 nm scale, (c) a histogram of the particle size distribution of NCQDs and (d) SAED pattern of NCQDs.	74

4.15	(a) SEM image at a magnification of 50.00 kx for CQDs and (b) FE-SEM image of NCQDs produced from empty fruit bunches.	75
4.16	The proposed mechanism of MAG degradation without CQDs/NCQDs once exposed to sunlight	76
4.17	The proposed mechanism of MB degradation without CQDs/NCQDs once exposed to sunlight.	79
4.18	The degradation rates of MO dye solution at pH 7 (a) without CQDs/NCQDs and (b) with NCQDs under sunlight irradiation before and after 300 min of sunlight irradiation exposure.	80
4.19	Plot of UV-light absorption spectra for the degradation of MEG dye within 30 min and (b) photocatalytic degradation efficiency of MEG dye by NCQDs under UV-light irradiation within 30 min.	81
4.20	The adsorption-desorption equilibrium of different dyes over the NCQDs within 60 min in dark.	82
4.21	Photocatalytic degradation efficiency of MAG, MB and MO dyes by NCQDs under sunlight irradiation within 180 min.	83
4.22	The proposed photocatalytic degradation mechanism of malachite green.	85
4.23	The proposed photocatalytic degradation mechanism of methylene blue	86
4.24	The proposed photocatalytic degradation mechanism of methyl green.	88
4.25	Mean of signal-to-noise ratios for four parameters in the photocatalytic degradation of MEG dye.	92
4.26	Graphs of $\ln (A_0/A_t)$ versus sunlight irradiation time for photocatalytic degradation of organic dyes: (a) MB dye in the presence of NCQDs; (b) MB dye in the absence of NCQDs; (c) MAG dye in the presence of NCQDs and (d) MAG dye in the absence of NCQDs.	95
4.27	A plot of t/C_t versus UV-light irradiation time for photocatalytic degradation of MEG dye.	96
4.28	The reusability of NCQDs for at least five consecutive cycles.	97
4.29	(a) The degradation rate of MEG dye using NCQDs before storage for twelve months and (b) the degradation rate of MEG dye using NCQDs that have been stored for twelve months.	99

4.30	Comparison of the degradation rate of dyes in the presence and in the absence of NCQDs, versus UV-light irradiation exposure time: (a) MB dye and (b) MAG dye.	102
------	--	-----

LISTS OF ABBREVIATIONS

EFB	Empty fruit bunch
CQDs	Carbon quantum dots
NCQDs	Nitrogen-doped carbon quantum dots
MB	Methylene blue
MAG	Malachite green
MEG	Methyl green
MO	Methyl orange
OA	Orthogonal array
SN	Signal to noise
UV	Ultra-violet
TOC	Total organic carbon
BQ	Benzoquinone
IPA	Isopropyl alcohol
PL	Photoluminescence
FTIR	Fourier transform infrared spectroscopy
EDX	Energy-dispersive X-ray
XRD	X-ray diffraction
TEM	Transmission electron microscopy

CHAPTER 1

INTRODUCTION

1.1 Background of study

Water pollution remains one of the main challenges to be overcome in most countries in meeting the high water consumption. Organic compounds, such as dyes, appear to be one of the primary pollutants in contaminating the water streams, generated by textile, paint, tannery, and leather industries (Cui et al., 2022). The dye effluents are hazardous to the aquatic organism, blocking sunlight penetration and reducing photosynthesis activity (Tammina et al., 2018). Excessive exposure to organic dye is harmful to humans as it may cause nervous system disorders, cardiovascular damages, carcinogenesis and respiratory toxicity.

Photocatalysts can be the ideal candidates in degrading the organic dye pollutants due to their low initiation energy requirement, high effectiveness, ease of scaling up, and low maintenance cost (Fauzi et al., 2022). However, existing photocatalysts may source from inorganic materials, expensive raw materials or other materials with limited access. Researchers have taken efforts in replacing the conventional photocatalysts with more sustainable raw materials with wide availability. Biomass from the palm oil industry in Malaysia appears to be a good candidate in supplying the raw materials in the fabrication of photocatalysts, as a mass of 95,000,000 tonnes of empty fruit bunches production in a year has been reported (Ahmad Farid et al., 2020).

However, it is worth noting that the application of EFB is still quite limited and it is continually explored to maximize its application at current stage. Biomass can be used as raw materials in producing an effective photocatalyst such as carbon quantum dots (CQDs). CQDs are nano-sized semiconductors with photoluminescence properties, which can emit a fluorescent light when irradiated by the UV light irradiation (Munishwar et al., 2018). Besides, the structure of CQDs can be easily modified while complying quantum characteristics (Bai et al., 2018). CQDs can be doped with various elements in producing CQDs with different properties (Makkar and Viswanatha, 2018).

One of the potential elements for doping onto the CQDs is nitrogen (Cui and Xue, 2022) to produce nitrogen-doped carbon quantum dots (NCQDs). NCQDs are a class of carbon-based nanoparticles which are comprised of quasi-spherical nanoparticles with particle sizes of 1-10 nm. NCQDs not only have a strong quantum confinement effect but also has excitation wavelength-dependent emission and tuneable photoluminescence (Kondee et al., 2022).

In this study, lignin from empty fruit bunches has been selected as a primary carbon precursor in the production of NCQDs. In addition to its wide availability, lignin has good biocompatibility with an abundance of aromatic macromolecules. It contains several carbon and oxygen-based functional groups (C-H, C=C, and C-O) and hydroxyl groups (Joseph et al., 2017).

The performance of NCQDs produced from the lignin, which can be extracted from the EFB, will be explored as a feasible way of producing photocatalysts for organic dye degradation.

1.2 Problem statements

Malaysia produces many empty fruit bunches (EFB) annually from the palm oil mill industries, which have quite limited applications and underutilization. Sustainable biomass appears to be an ideal source for the fabrication of NCQDs at minimum cost while reducing the impacts on the environment.

However, none of the existing works has reported the fabrication of NCQDs from EFB without any oxidizing agents. The fabrication of NCQDs without oxidizing agents such as hydrogen peroxide, nitric acid and sulfuric acid appears to be a more environmentally friendly approach for sustainable development.

Besides, NCQDs sourced from the EFB in the absence of other semiconductors have not been evaluated for their photocatalytic behaviours towards the organic dyes. However, the photocatalytic performance of NCQDs produced from EFB is required to understand their stability and effectiveness towards the photodegradation of organic dyes using light sources. The photocatalytic degradation of organic dyes using NCQDs may have some complications due to multiple variables such as amount of NCQDs, initial dye concentration, pH of dye solution and reaction time during the photocatalysis. Thus, contribution factors by each variable need to be scientifically identified and evaluated.

1.3 Research objectives

The objectives in this study are:

1. To fabricate nitrogen-doped carbon quantum dots using hydrothermal treatment method in the absence of oxidizing agent.
2. To investigate the chemical and physical properties of nitrogen-doped carbon quantum dots fabricated from empty fruit bunches using Fourier Transform Infrared spectroscopy, Energy-dispersive X-ray analysis, X-ray diffraction analysis, photoluminescence spectroscopy, UV-Vis spectrophotometer, Zeta potential analysis, scanning electron microscopy and transmission electron microscopy.
3. To evaluate the performance of nitrogen-doped carbon quantum dots in the photocatalytic degradation of organic dyes such methylene blue, malachite green, methyl green, and methyl orange under UV-light and solar irradiation.
4. To investigate the stability and reactivity of the fabricated nitrogen-doped carbon quantum dots in terms of storage duration and the potential reusability in the photocatalytic degradation activity.

1.4 Thesis outlines

Chapter 1 introduces the research background, including the current progress in the development of NCQDs. Besides, the problem statements and hypotheses are included in this chapter. The research objectives are highlighted in this chapter. Chapter 2 presents a literature review, which focuses on the previous studies related to the raw materials, the dopant elements and the methods applied in producing CQDs. This section will highlight the application of NCQDs in degrading organic dyes and the stability of NCQDs.

Chapter 3 reports the research methodology in the fabrication of CQDs and NCQDs, methods for characterization, photocatalytic degradation of organic dyes by NCQDs, stability and reactivity study on the fabricated NCQDs and the Taguchi approach. This study used the total organic carbon analysis to evaluate the degraded dyes.

Chapter 4 is the result and discussion section. This chapter will highlight the performance of the fabricated NCQDs as photocatalysts in degrading organic dyes with their physical and optical characterization. The evaluation of the degraded dyes and the stability of the fabricated NCQDs have been discussed in this chapter. The Taguchi approach and the photocatalytic kinetic study are also discussed in this section. In addition, investigation on the active species during photocatalysis and the comparative performance of CQDs and NCQDs will be included. Chapter 5 is the summary of the study, which specifies the attainment of the research objectives and the recommendation of future works.

CHAPTER 2

LITERATURE REVIEW

2.1 Introduction

This chapter elaborates specific reviews on the previous works that are related to the background information of empty fruit bunches including the production of empty fruit bunches in Malaysia, their properties and applications. Information about lignin that are extracted from EFB are also discussed in this chapter. Besides, an overview on the photocatalysis including the fabrication of photocatalyst composites, the functionality of photocatalyst in degrading organic pollutants, the application of photocatalysts in degrading organic pollutants as well as the improvement of photocatalysts in wastewater treatment is also included in this chapter.

This chapter also reviews the carbon quantum dots (CQDs), the raw precursors and the methods applied in the fabrication of CQDs. The dopant elements used in the fabrication of CQDs will also be reviewed. In this study, the nitrogen, which is the main element for nitrogen-doped carbon quantum dots (NCQDs) is also reviewed from the view of the potential application of NCQDs as photocatalysts in the photocatalytic degradation of organic pollutants. Lastly, the optical and fluorescent properties of NCQDs are also reviewed in this section in order to determine their stability, reactivity, and the reusability as photocatalyst.

2.2 Empty fruit bunches (EFB)

2.2.1 Definition of EFB

Empty fruit bunches (EFB) are classified as biomass wastes which are produced from the oil extraction mills process. The EFB for *Elaeis guineensis* is a bulky brown bunch, which is a side product of the extraction of fruits and oils through a rotary thresher drum technology (Chang, 2014).

The average yield of EFB fibers is approximately 400 g per bunch (Ramlee et al., 2021). EFB, contains 73% fibres, 30% cellulose, 20% hemicellulose, and 35% lignin (Derman et al., 2018; Or et al., 2017). Due to their high lignin and cellulose structure, an approximately abundance of hydrocarbons and esters at 15.85% and 44.37%, respectively, can be produced via EFB pyrolysis.

2.2.2 Production of EFB in Malaysia

The palm oil industries in Malaysia are developing rapidly in order to fulfil the local and global markets demand. To date, Malaysia is contributing 28% of global palm oil production and 33% of global exportation (Chan et al., 2021). The high palm oil production activities produce approximately 95 million tonnes of empty fruit bunches annually (Ahmad Farid et al., 2020; Aizat et al., 2021), and the uncontrolled handling of these EFB wastes would pose a severe environmental pollution. Therefore, the investigation on the utilisation of EFB fibers as renewable carbon sources to produce a variety of value-added products is highly emphasized.

2.2.3 Properties of EFB

EFB is a biodegradable and non-toxic materials, which has high lignocellulosic content and fiber yield. The main elemental composition of EFB are carbon, oxygen, hydrogen, nitrogen and sulphur (Amal et al., 2008). The carbon contents, which are the major components in the EFB structure, could be used as a promising natural carbon feedstock for valuable agricultural end-products (Karunakaran et al., 2019).

2.2.4 Application of EFB

EFB can be developed in the production of carbon-based nanoparticles, and their applications are continually explored. To date, the production of carbon-based nanoparticles from EFB materials has received significant interest due to they are rich in hydrocarbons and oxygenated-functional groups (Yaqoob et al., 2021). These outstanding properties of EFB were introduced into various applications, including nanocomposite materials, membrane technologies, and carbon-based nanoparticles.

Furthermore, EFB can be used as an alternative ingredient in the fabrication of multiple functional nanocomposites, which are to be used for wastewater treatment. A summary on the application of EFB as different component structures in wastewater treatment is as tabulated in Table 2.1. Nevertheless, the wide utilisation of EFB materials is still limited due to their high moisture, low calorific value and low energy density.

Table 2.1: Application of EFB in wastewater treatment

EFB components	Applications	References
Cellulose	Production of EFB-based nanocellulose as super-adsorbent for water remediation	(Septevani et al., 2020)
	Preparation nanocrystalline cellulose for enhancing the stability of antioxidant potential	(Foo et al., 2022)
	Synthesis of EFB-derived cellulose membrane for treating dye wastewater	(Haan et al., 2020)
Milled EFB biochar	Production of carbon quantum dots to be used as fluorescence sensor for copper ions detection	(Kamarol Zaman et al., 2021)
Activated biochar	Production of adsorbent for the removal of cibacron blue 3G-A dye from aqueous solution	(Jabar and Odusote, 2020)
Activated charcoal	Formation film composite for adsorptive removal of cadmium from water streams	(Rahmi et al., 2021)
Activated carbon	Production of composite photocatalyst for photocatalytic degradation of malachite green	(Loo et al., 2021)
EFB fibers	Fabrication of biosorbent for toxic hexavalent chromium removal	(Rambabu et al., 2020)
Carboxymethylcellulose	Production of nitrogen-doped carbon quantum dots	(Issa et al., 2020)
Lignin	Lignin was used as precursor for carbon fiber production	(Karunakaran et al., 2020)
	Fabrication of carbon quantum dots as photocatalysts for dye degradation	This study

2.2.5 Lignin extracted from EFB

Lignin-based carbon fibers consist of aromatic macromolecules, which are renewable resources that can be obtained from agricultural industries such as empty fruit bunches (EFB) via chemical or thermal pretreatments. Lignin is an aromaticity structure with an abundant biopolymer and high amorphous macromolecules (Hidayati et al., 2020a). It is an amorphous phenyl propylene polymer that is primarily composed of carbon, hydrogen and oxygen atoms, and it is chemically linked to hemicellulose and cellulose in EFB fibers (Goudarzi et al., 2014).

The lignin that is extracted from EFB fibers contains several carbon and oxygen-based functional groups such as C-H, C=O, C=C, and C-OH, as well as aromatic and hydroxyl groups (Joseph et al., 2017). The chemical structure of lignin also contains of phenylpropane, syringyl propanol, and guaiacyl-propane with *p*-hydroxy-propane, which are linked through various chemical bonds (Hidayati et al., 2020b).

Due to lignin's complex chemical structure, it can be used as raw materials in carbon fiber production (Karunakaran et al., 2019), polyvinyl chloride photo-stabiliser (Fadhil et al., 2022), activated carbon production (Brazil et al., 2022), and lignin-based absorbent (Y. Tan et al., 2021). Taking into account the high degree of crystallinity, high content of carbon and oxygenated-functional groups, lignin can also be considered as a potential carbon precursor in the fabrication of CQDs.

2.3 Photocatalysis

2.3.1 Introduction to photocatalysis

Photocatalysis is a promising photochemical process by converting low-density light energy into high-density chemical energy with the assistance of semiconductor photocatalytic materials. The conversion process can be stimulated by the absorption of light sources irradiation (Wu et al., 2022) and generates reactive free radicals by advanced oxidation processes in the presence of photocatalysts and light sources, which further results in photochemical changes for redox reaction. Photocatalysis involves the generation of electron-hole pairs due to the excitation of an electrons from the valence band to the conduction band initiated by light source energy. It can efficiently mineralize a significant number of pollutants to comparatively non-toxic final products such as water, carbon dioxide, and non-toxic inorganic salts in the presence of reactive oxygen species and electron-hole pairs (Pirsaheb et al., 2018). Therefore, photocatalysis can be considered as economically viable technologies for organic pollutants degradation in wastewater treatment.

2.3.2 Fabrication of photocatalyst

Photocatalysts can be produced using several carbon-based raw materials. Photocatalysts are made from carbon-based nanoparticles such as the fluorescent quantum dots materials due to their high quantum efficiency, good light absorption that enhancing the utilisation efficiency of solar energy, and the quantum surface states will increase the active reaction sites (Balakumar et al., 2021; G. Wang et al., 2021).

Table 2.2 shows several types of semiconductor composites of photocatalysts with their raw materials used and the degradation efficiency. The recent studies show that synthetic materials were normally used in the fabrication of photocatalysts instead of natural carbon source. This leads to a research gap that the sustainable manufacturing approach of photocatalysts using natural carbon sources without addition of toxic solution could be investigated.

Table 2.2: Fabrication and applications of photocatalysts

Raw materials	Photocatalyst composites	Degradation efficiency	References
Cellulose nanofiber hydrogel and titanium dioxide	Carbon quantum dots/titanium dioxide	Up to 92% of methylene blue could be degraded.	(Gong et al., 2022)
Citric acid, polyvinylpyrrolidone, zinc nitrate and sodium hydroxide	Graphene quantum dots/zinc oxide	Up to 99% of metronidazole could be degraded	(Hsieh et al., 2022)
Thiourea, sulfuric acid, carbide nanosheets,	Nitrogen carbide quantum dots doped carbide nanosheets	Up to 99.1% of organic pollutants could be degraded	(Duan et al., 2022a)
Carbon nitride nanosheets, bismuth tungstate, methyl alcohol, ethanol, citric acid.	Carbon quantum dots-carbon nitride nanosheets/bismuth tungstate	Up to 90% of norfloxacin could be degraded	(Liu et al., 2022)
Citric acid, bismuth nitrate, nitric acid, sodium tungstate dehydrate, ethanol	Graphene quantum dots/bismuth tungstate	Up to 88% of nitric oxide could be degraded	(Cui et al., 2021)
Graphitic carbon nitride, urea, ethanol, tungsten oxides	Tungstate oxide quantum dots-carbon nitride	Up to 89% of antibiotics could be degraded	(Huang et al., 2021)

2.3.3. Functionality of photocatalysts

Semiconductor photocatalysts are photocatalytic materials that possess light-harvesting behaviour. A potential photocatalyst must be a good light absorber to provide efficient photo-generated electron-hole pairs separation. The exposure of photocatalysts to light sources leads to the generation of mobile electrons and hole pairs. The resultant electron-hole pairs will promote electrons transition from the valence bands to the conduction bands (Chengyun Zhou et al., 2020). The photo-induced electrons at conduction band show a strong reducibility and the photo-generated holes at valence band possesses great oxidation.

The photo-generated electron-hole pairs will migrate to the surface of photocatalyst, and oxygen molecules will be reduced to free radicals such as hydroxyl and superoxide radicals. These free radicals are powerful non-specific oxidants which will attack the organic pollutants and accelerate the photocatalytic degradation activity (Mukthar Ali et al., 2019). Figure 2.1 illustrates the function of photocatalysts in degrading organic pollutants to produce carbon dioxide and water.

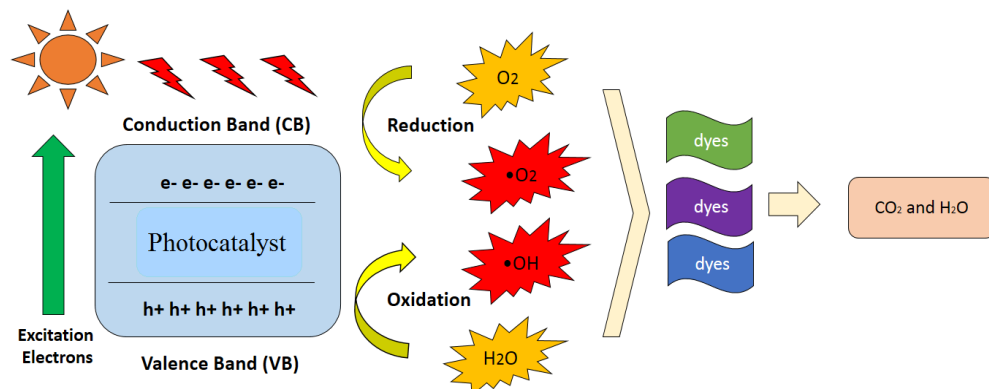


Figure 2.1: Role of photocatalyst in degrading organic pollutants.

2.3.4 Improvement of photocatalysis

Several studies have used hydrogen peroxide (H_2O_2) to improve photocatalytic degradation of organic pollutants (Cahino et al., 2019; Y. Cheng et al., 2019; Iqbal et al., 2021a). The addition of H_2O_2 could enhance the generation of active radicals during photocatalysis. However, this approach is not recommended because the high contribution of degradation performance was probably due to the presence of H_2O_2 instead of the fabricated photocatalysts.

From the view of photocatalysts improvement, study has been conducted to produce nanocomposite photocatalyst, which consists of nanocrystals that can contribute to the generation of large number of positive holes and negative electrons (Flihh and Ammar, 2021). Liu et al. (2021) has reported that the fabrication of nanocellulose-based photocatalyst enhanced the photocatalytic degradation of methyl orange (Liu et al., 2021). The degradation efficiency could be achieved up to 99.72% within 120 min of degradation due to the high specific area and low recombination rate of the fabricated photocatalyst.

Other than the large surface area, photoluminescence properties of semiconductor photocatalysts are also significant feature in the construction of an effective photocatalyst. In this case, carbon-based quantum dots can be considered as an effective component in the production of photocatalysts (Ming et al., 2021a; You et al., 2022). They not have high active surface area, but also fascinating luminescence properties and outstanding electron transport performance.

Recent study has proven that the presence of quantum dots materials in the fabricated photocatalysts enhance the light harvesting ability, promoted photo-generated charges separation, and generate abundant of active sites (Ming et al., 2021b). Hence, luminescence quantum dots materials can be a good photocatalyst as a significant candidate in degrading organic pollutants.

2.4 Carbon quantum dots (CQDs)

2.4.1 Introduction to CQDs

CQDs are a new product of fluorescence carbon nanoparticles that consist of carbonaceous materials with particle sizes around ten nm (Xue et al., 2019). The structure of CQDs is a single-atom-thick material which comprises of a honeycomb lattice with atoms arranged in sp^2 hybridization. The arrangement of atoms similar to the bulk material, but with more surface atoms on their structure (Reshma and Mohanan, 2019). They contain high number of well-defined electrons, discrete quantum states and possesses electronic properties intermediate between bulk and discrete elementary particles (Reshma and Mohanan, 2019).

CQDs have confine energy band gaps and delocalized charge carriers, which resulting in additional properties of high specific area and excellent transporting ability. Thus, CQDs with lateral particle sizes have been considered to better electron transporters and acceptors that make them the optimal candidates for photocatalytic materials. Besides, they also can be well-dispersed in various organic solvents to carry out chemical reactions and achieve high electron mobility in solution processes.

2.4.2 Properties of CQDs

CQDs are fluorescent nanosized-materials with unique photoluminescent and outstanding optical electronic properties (Joshi et al., 2018). The variety functional groups on the CQDs surfaces have modified their surfaces and particle sizes to realize their quantum fluorescent effects. Besides, the optical electronic properties of CQDs can cause the separation of photo-generated electrons (Liang et al., 2018). These unique properties make CQDs suitable to be used as photocatalytic materials.

CQDs can display highly photoluminescent signal, high fluorescent activity, chemical inertness and robustness due to their quantum confinement effect and optical stability properties (Saud et al., 2015; Shi et al., 2019a). They are potentially in treating the wastewater due to good luminescent component, high photo-stability, good biocompatibility, low cost of fabrication and less toxicity (Das et al., 2018).

Figure 2.2 shows the fluorescence of CQDs in which the appearance of CQDs solution would change to light blue fluorescent when the surfaces of CQDs absorb UV-light irradiation, resulting in excitation electrons to higher energy levels. A photon will be emitted as a glowing blue color when the electrons fall back to a lower energy state (Bajorowicz et al., 2018; Rajabi et al., 2013). This fluorescence phenomenon occurs because CQDs consist of nanoscale quantum dot particles, which proving their luminescence properties (Li et al., 2010).

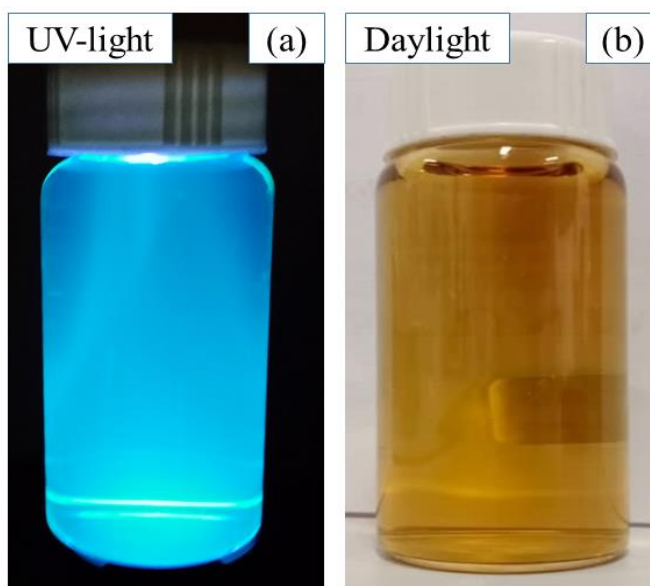


Figure 2.2: The appearance of the CQDs solution under (a) UV-light irradiation and (b) daylight.

CQDs possess effective ability in trapping and transferring electrons (charge transport), as well as inhibiting recombination of photo-generated charges (Aghamali et al., 2018). The charge transport is depends on the particle size and optical properties in which the space between charge carriers are slightly less than the carrier diffusion distance (Hemmateenejad et al., 2015).

The edge-abundant properties of CQDs are also highly beneficial for photocatalysis as this reaction generally occurs at the edges area. CQDs are very sensitive towards UV-light irradiation, which can convert the sunlight spectrum to the desired wavelength, resulting in highly performance of photocatalysis (Wang et al., 2018; Yadegari et al., 2019). The nanoscale features of CQDs can encourage the redox reaction during photocatalysis (Qiankun et al., 2019).

2.4.3 Raw materials used in the fabrication of CQDs

Different types of carbon precursors can be used to produce CQDs, owing to their complex organic structures (Dong et al., 2012; Papaioannou et al., 2018). Among the notable are citric acid (Ahlawat et al., 2021; Cui et al., 2019; Sistani and Shekarchizadeh, 2021a; Q. Wang et al., 2019; Z. Wang et al., 2021a; L. Zhou et al., 2019), graphitic micro-particles (Arvind et al., 2019), chitosan and acetic acid (Bai et al., 2022), zein biopolymer (Azizi et al., 2019), sodium hydroxide and acetone (Gao et al., 2021), ethylene glycol (Hagiwara et al., 2021a), bacteria (Wu et al., 2021), commercial carbon black (Youh et al., 2021), *m*-phenylenediamine (Yang et al., 2022), ammonium citrate (L. Fang and Zheng, 2021), sweet potatoes (Saboorizadeh et al., 2021a), gelatin (Latief et al., 2021), 2,4,6-trihydroxybenzoic acid (Latief et al., 2021), humic acid (J. Cheng et al., 2019), ascorbic acid (Q. Wang et al., 2019), shrimp shell (Elango et al., 2022), glucose (Javed et al., 2019; Xie et al., 2018), cholesterol (Kalaiyarasan and Joseph, 2019) and synthetic lignin (Myint et al., 2018; Shi et al., 2019b; Zhu et al., 2021).

Different chemical structures of precursors will result in different optical properties of CQDs (Shen et al., 2018). CQDs produced from glucose showed better crystalline structure, more efficient in charge carriers separation and higher electronic transfer ability compared to those produced using citric acid as the precursor. This could be explained by the intermolecular dehydration of glucose during the hydrothermal carbonization, which is a more complete reaction compared to when using citric acid.

Variety aromatic hydrocarbon can be used as raw carbon materials, which significantly produced fluorescent CQDs due to their abundance in oxygen-containing functional groups (Xue et al., 2019). The formation of oxygen-containing functional groups in the CQD structures can contribute to an outstanding excitation-dependent fluorescent emission, resulting in excellent optoelectronic properties. In addition, the rich of hydrophilic functional groups in the raw materials also contribute to the hydrophilicity of CQDs and the hydrodynamic surface charges of CQDs (Dhandapani et al., 2020).

From the view of quantum size, the types of raw materials used in the CQDs fabrication will result in different CQDs particle sizes. A comparative study has been reported where the particle sizes of CQDs produced from citric acid and glucose were different (SA et al., 2017). The particle sizes of CQDs produced from citric acid and glucose were 13 nm and 11 nm, respectively, probably due to the different concentration of free carbon atoms in the carbon precursors. In addition, different structure of carbon precursors will also result in different fluorescence of CQDs. Recent study has designed fluorescent CQDs from the greengage juice through a hydrothermal treatment (Alvandi et al., 2021). The designed CQDs could be appeared in multicolor fluorescent when exposed to UV-light irradiation. Another study has produced a highly green fluorescent CQDs from fish scale (Dhandapani et al., 2020). To produce a yellow luminescent purified CQDs solution, researchers have used ethylene glycol and 9,10-dinitroanthracene as raw materials in which the obtained CQDs were dispersed in ethanol (Hagiwara et al., 2021b).

2.4.4 CQDs-based biomass precursor.

To date, the use of waste biomass has not been widespread in fabricating CQDs. To be in line with the direction on the realisation of near zero-discharge of wastes, discoveries in fabricating waste material based CQDs are indispensable, which this approach can be one of the initiatives in minimizing waste materials, especially from palm oil mill industries, food industries and other agricultural industries. Sustainable raw materials that contain high carbon precursors such as plant-based waste fibers, by-product of food and beverage powders and palm oil industry waste materials are good biocompatibility, which can be used to replace the common raw materials such as citric acid in the fabrication (Piri et al., 2019).

The benefits of using green carbon sources to fabricate CQDs are cost-effectiveness, eco-friendliness and wide availability in nature. In addition, the production of high fluorescent CQDs using renewable carbon sources without chemical exposure is also highly recommended in order to achieve sustainable development.

Due to the rapid development of the palm oil sector which produces a large number empty fruit bunches that contain high carbon and oxygen content, and complex structure of polyphonic macromolecules that can be generated frequently (Rosli et al., 2017; Salifairus et al., 2016), they could be used as a potential carbon precursor in order to produce high-performance CQDs.

2.4.5 Methods used to fabricate CQDs

There are several primary methods in fabricating CQDs including laser ablation technique (Cui et al., 2020), microwave-assisted synthesis (W. Liu et al., 2019), electrochemical exfoliation (Sui et al., 2019), ultrasonic process (Xie et al., 2018), and hydrothermal treatment (Sabet and Mahdavi, 2019).

In general, most of the CQDs are fabricated through controllable carbonisation from significant organic molecules. Specifically, CQDs are fabricated through the physical and chemical approach by breaking the large carbon structures to the small-particle sized CQDs. A bulk carbon structure of raw materials is cutting down into smaller units of particle size with fluorescent characteristics (Chen et al., 2018). The fabrication stage undergoes carbonisation, oxidation, condensation, and polymerization processes, resulting in fluorescent CQDs. However, the CQDs preparation still suffers from certain concerns such as the use of toxic reagents, special equipment, time-consuming, strong oxidising agents, and quantum efficiency. Therefore, it is highly desired to study the significant approach for effective fabrication CQDs in a low-cost manner and low-energy consumption.

Each of the fabrication method will produce the CQDs at different physical and chemical properties in terms of surface properties, quantum yields, fluorescence properties, photoluminescence intensity, solubility and particle size distribution. However, these varieties can be optimised by some modification within the fabrication process or some post-treatments. The features of different synthetic methods for the preparation of CQDs are summarized in Table 2.3.

Table 2.3: Summarize of the CQDs fabrication methods

Method used	Raw materials	Solution/chemicals	Method condition	Fabrication Duration	Yield (%)	Particle sizes (nm)	References
Laser ablation	Carbon cloth	Dimethylsulfoxide and ethyl acetate	Frequency (10 Hz), wavelength (1064 nm), pulse width (6 ns), pulse energy (20 mJ),	10 min	35.4	3.8	(Cui et al., 2020)
	Graphite target	Polyethylenimine	Frequency (10 Hz), wavelength (532 nm), pulse width (10 ns), pulse energy (35 mJ),	15 min	54.6	0.3	(Kaczmarek et al., 2021)
	Platanus biomass	Deionized water and potassium hydroxide	Frequency (10 Hz), wavelength (1064 nm), pulse width (3-6 ns), pulse energy (20 mJ),	30 min	32.4	0.23	(Ren et al., 2019)
Microwave-assisted synthesis	Citric acid and phenylenediamine	Deionized water	Heating under 700 W	7 min	39.2	5.0	(Y. Zhou et al., 2019)
	Dried black carbon	Pure water	Heating under 150 W	20 min	21.3	3.5	(Ganesan et al., 2022)
	Acidic cotton linter waste	Water	Heating under 400 W	5 min	-	10.8	(Eskalen et al., 2020)
Electrochemical exfoliation	Pre-baked carbon anode	Ammonium bicarbonate as	Voltage of 15 V	12 h	1.8	25.6	(Zhou et al., 2021)

	Graphite rods	electrolyte Sodium chloride solution as electrolyte	Voltage of 15 V	10 min	-	1.8	(Li et al., 2019)
Ultrasonic process	Either coal sample	Hydrogen peroxide	Frequency 40 kHz Output power ~700 W	6 h	10.0	6.3	(Saikia et al., 2022)
	Kiwifruit juice	Ethanol	Frequency 80 kHz Output power ~320 W	3 h	2.4	6.7	(Xu et al., 2022)
	L-glutamic acid	Water	Ultrasonic generator was kept at 50% power	4 h	13.2	3.5	(Qi et al., 2021)
Hydrothermal treatment	Gelatin	Deionised water	Heating up to 200 °C	3 h	22.7	0.5	(Latief et al., 2021)
	White flowering plant	Deionised water	Heating up to 200 °C	4 h	28.2	5.0	(Arumugham et al., 2020)
	Citric acid	Distilled water	Heating up to 200 °C	4 h	21.1	4.2	(C. Wang et al., 2019)
	Tartaric acid and L-arginine	Ethanol	Heating up to 180 °C	12 h	8.3	-	(Zhu et al., 2020)
	Fish scale	Distilled water	Heating up to 180 °C	24 h	6.0	-	(Dhandapani et al., 2020)

CQDs can be produced through the direct UV-pulsed laser ablation technique by exposing the carbon materials in aqueous medium. In this technique, high energy delivered by laser beam causes ablation (Arvind et al., 2019), in which the laser beam will interact to the carbon precursors and generate a high-pressure steam and high temperature that can directly cut the bulk carbon materials into carbon nanoparticles.

The laser beam is directed to the carbon precursors at a depth of around 5 millimeters from the aqueous surface. Heat treatment supplied during the method operation caused fragmentation of carbon precursors into nanoparticles. Besides, this approach uses pulsed laser with a second harmonic wavelength to irradiate carbon particles under constant stirring in order to avoid precipitation of the fabricated CQDs. Researchers reported that this technique was able to produce CQDs with homogeneous structure, and the corresponding quantum yield of emission was as high as 35.4% (Cui et al., 2020).

Due to its long-pulse width, bubbles are formed at the laser focus, resulting in the formation carbon nanoparticles. Bubbles with different densities can be generated when the laser pulse width is modified, leading to produce CQDs with different particle sizes (R. Wang et al., 2017). The particle sizes of CQDs could be controlled by altering the laser irradiation time and optimising other parameters such as pulse repetition rate, pulse duration, and laser wavelength (H. Li et al., 2022), which can have impacts on the nucleation of CQDs. However, this method is complicated operation, high cost, harsh condition, as well as multiple-operation steps.

Another method to fabricate CQDs is microwave-assisted synthesis by applying polymerisation and carbonisation processes (Alarfaj et al., 2018). This method consumes an electromagnetic wave energy with a large wavelength range of 1 mm to 1 m, which can provide intensive energy to break off the chemical bonds of carbon precursors (R. Wang et al., 2017). However, the heating treatment in this method consumes high efficiency energy compared with conventional heating because the energy is generated directly within the carbon precursors through the molecular interactions with the electromagnetic fields.

The electromagnetic energy absorbed by the carbon precursors could be converted into heat energy. Interaction of microwave energy with the electrical dipole moment caused the rotation of polar molecules, thus producing a thermal energy (R. K. Singh et al., 2019). This thermal energy is transmitted to the carbon surfaces by the electromagnetic radiation during the microwave heating.

This method is a rapid and low-cost technique to produce CQDs in which it can provide uniform and simultaneous heating, resulting in uniform particle size distribution of CQDs (Khan et al., 2019). This method can effectively shorten the reaction time and provide simultaneous and homogeneous heating in producing the CQDs with stable and bright photoluminescence with excellent dispersion in an aqueous solution. However, this method requires high energy consumption and poor control size (Jusuf et al., 2018). Besides, this method is quite limited as the reaction consumes high temperature in short duration.

Electrochemical exfoliation method also can be used to produce CQDs by oxidising carbon source electrode (Kumar et al., 2021; R. Wang et al., 2017). In this method, graphite rods were employed as both cathode and anode, with carbon precursors and salt solution as the electrolyte solution. Alkaline environment is necessary for the formation of CQDs through the electrochemical carbonization of raw materials. Direct current at static potentials was applied through the electrochemical circuit, resulting in chipping of the graphite rods to produce CQDs (Tian et al., 2020).

Operationally, electrodes were dipped into the electrolyte and direct current was applied to the electrodes. As the voltage is applied to the electrodes reaction between hydroxide and proton ions, the process produce bubbles on the cathode surfaces (Bakhshandeh and Shafiekhani, 2018). Graphite layers are stripped from the anode surface and migrate to the electrolyte surface. Gaseous species generated during the process helps to weaken and brakes Van der Waals bonds between the graphite plates.

This approach only involved a single treatment step with high purity, controllable particles size, and the CQDs produced were found to possess desirable fluorescence properties along with high water solubility (Shaik et al., 2021). The judicious cutting via electrochemical oxidation of a graphite honeycomb layer into ultra-small particles can lead to tiny fragments of graphite, which can produce high-quality CQDs. However, this approach is quite limited due to demanding equipment, few small molecule precursors and a bit complicated operation. Besides, this method produces less functional groups compared with other common fabrication methods.

Ultrasonic treatment is another high-energy technique for the fabrication of CQDs (Ansari et al., 2021). In this method, carbon precursors in a desired solvent is exposed to ultrasonic waves, which can form bursting of vacuum bubbles. These vacuum bubbles may cause high-velocity impinging fluid jets, depolymerization, strong hydrodynamic fluid shear force, which can control the surface morphology and can reduce the surface patterns of CQDs (Yang et al., 2016). Besides, ultrasonic energy was applied to activate the particles so that the produced chemical energy can modify the carbon bond structure into nanosized CQDs.

Besides, probe sonography is applying to produce tremendous local energy, which contributes carbonisation process in the fabrication of CQDs. Furthermore, ultrasound can generate alternating low-pressure and high-pressure waves in solution, leading to the formation of small vacuum bubbles. The energy of ultrasonic waves leads to the polymerisation and carbonisation processes in generating of CQDs. Some experimental works used concentrated sulfuric acid (Javed et al., 2019) or hydrogen peroxide (Saikia et al., 2019) to accelerate the oxidation process of carbon precursors (Kaur et al., 2018).

Ultrasonic radiation applied in this technique can control surface morphology and reduce the surface defects of CQDs. This reaction can be carried out by shortening the reaction duration, resulting in good yield CQDs. However, this method requires high energy consumption as well as high instrumental cost.

CQDs can be fabricated using hydrothermal treatment (Cui et al., 2019; G. Liu et al., 2019). This treatment involves heating of carbon materials at a high pressure and temperature to allow interactions between the water molecules and the precursors (Tian et al., 2018).

When heat energy was supplied, the pressure was increased and the particle of water was deoxidised. Production of proton and hydroxyl ions caused the repulsion forces between the carbon layers (Pan et al., 2010). The resulting high-pressure can be controlled by the Teflon lined stainless steel autoclave. Formation of CQDs can be occurred by oxidising carbon materials to form a variety of oxygen-containing functional groups (Allahbakhsh and Bahramian, 2018; Kaur et al., 2018).

This method can be considered as a better route to fabricate CQDs, which is more effective in controlling the particle size distribution (S. Zhang et al., 2018). Besides, this method has been proved in improving the carbon quantum yield by 53.19 % with high stability and lower cytotoxicity (Khan et al., 2020). CQDs can also appear as bright blue fluorescent when under UV irradiation (Das et al., 2018; Xu et al., 2013), showing that the nanoparticle sizes of CQDs have been produced. Moreover, this method does not require dialysis bags to remove excess chemicals used, no alkaline solution is needed to stabilize the pH solution, and shorter fabrication time consuming. This fabrication method can be considered as a sustainable approach if waste carbon sources are used as raw carbon materials.

Among the reported methods, hydrothermal treatment is the most recommended approach to fabricate CQDs due to their less toxicity as the reaction condition is usually deionised water. Generally, natural carbon sources are able to undergo the hydrothermal treatment as they are highly soluble in water. Therefore, this method can be an easiest route to produce highly luminescent CQDs in the absence of any chemicals. However, other methods can also be used as long as the chemical structure of raw materials contains oxygenated-functional groups.

Hydrothermal treatment is conducted using the Teflon lined stainless steel autoclave reactor because it involves crystallising reactants at high temperatures and high vapour pressures (Tian et al., 2018) during the fabrication activity. This method uses deionised water as a reaction medium without addition of any strong acid or other catalyst (Wang et al., 2016). Besides, this approach can produce a high quantum yields, which are important to enhance the photoluminescent properties with better surface passivation of CQDs (Jindal and Giripunje, 2018).

Table 2.4 summarizes the hydrothermal treatment of carbon precursors to produce CQDs. From previous studies, organic molecules are the most reliable precursors to form high-quality CQDs with good quantum yield. These carbon sources generally contain multifarious heteroatoms in which they can produce CQDs packed with various surface groups and possess unique fluorescent properties without further passivation. Therefore, these raw materials are suitable to undergo the hydrothermal treatment.

Table 2.4: Fabrication of CQDs through hydrothermal treatment.

Raw material	Solution medium	Temperature (°C)	Duration (h)	Yield (%)	Particle Size (nm)	Fluorescence	References
Citric acid and ethylenediamine	Pure water	200	6	19.3	5.3	blue	(Shi et al., 2022)
Ascorbic acid and chitosan	Distilled water and acetic acid solution	180	12	-	7.8	green	(Riahi et al., 2022)
Citric acid	Distilled water	180	20	24	4.9	blue	(Sistani and Shekarchizadeh, 2021b)
Maple leaves	Deionised water	190	8	-	3.5	blue	(Chellasamy et al., 2022)
Moringa oleifera roots, diethylenetriamine, citric acid and gallic acid	Distilled water and absolute alcohol	200	10	43.4	3.6	blue	(Z. Wang et al., 2021b)
Sweet potatoes	Double distilled water	180	8	-	2.5	green	(Saboorizadeh et al., 2021b)
Ammonium citrate	Deionized water	160	4	-	2.5	blue	(L. Y. Fang and Zheng, 2021)
Gelatin	Distilled water	200	3	17	4.2	blue	(Ahmed et al., 2021)
Soot from bike exhaust	Distilled water	160	10	-	6.0	blue	(Chaudhary et al., 2022a)

2.5 Dopants elements used in the fabrication of CQDs

Heteroatom doping is an effective approach in the modification of CQDs, which can effectively enhance the surface traps of CQDs and produce surface passivation (Ansari et al., 2021). The presence of doping elements in the CQD structures can modify the carbon framework with creating new excited energy potentials, and thus, improving the functionality of fluorescent CQDs. The involvement of the doping elements in the production of CQDs is significantly improving the internal structure of surface state CQDs, thereby adjusting their energy band gaps and electrons density.

Dopant elements can be used in the fabrication of doped-CQDs in order to enhance their fluorescence and quantum yield. The presence of dopant elements can effectively induce charge delocalization and regulate the carbon work function of CQDs, and hence the chemical activity could be improved (Wang et al., 2022a). From the view of photocatalysis, the electron-rich dopant atoms in CQD surfaces could contribute to enhance the redox reaction capability and visible light responsivity (Jamila et al., 2020), and thus, more active site and free radicals can be generated, resulting in high performance of photocatalytic degradation activity.

In addition, the significant doping on the CQDs effectively improves the electronic and optical properties of CQDs, which can change the internal surface state of CQDs and increase the electron density (A. Tan et al., 2021), that can contribute to the considerable prospects for photoluminescence applications. Besides, the presence of doping elements in the CQD structures indicates high fluorescence intensity and high quantum effect.

Dopant elements that commonly used are nitrogen, boron, chlorine, sulfur, cerium, selenium, and phosphor (Y. Liu et al., 2019; Seng et al., 2020; Wang et al., 2020; Zhang and Fan, 2021). These elements are reported to enhance the optical properties of CQDs, which accelerates the electrons transport and resulting in good photocatalytic performance.

Among the dopant elements, nitrogen atom is the most effective dopant element that can be used because it has similar size to carbon and possess greater electronegativity than carbon, make it easier to incorporate into carbon network as well as can form strong covalent bonds with carbons via substitution doping (A. Tan et al., 2021). Furthermore, nitrogen is the effective doping element to CQDs surface due to the electron-rich nitrogen atom will enhance the electron-donating ability of CQDs. The nitrogen lone pair electrons can easily bond to carbon-based materials in the carbon skeleton, resulting in outstanding fluorescence of CQDs (Shaik et al., 2021).

Different nitrogen source is also reported to be used in preparing NCQDs. Glucosamine with dipotassium hydrogen phosphate (R. Li et al., 2022), could serve as the nitrogen and carbon sources in the production of NCQDs. Besides that, other nitrogen source such as melamine has also been used as nitrogen source in the fabrication of nitrogen doped-CQDs (Naushad et al., 2021), as the structure melamine which has carbon, hydrogen, and nitrogen atoms that can contribute to the production of high photoluminescence of NCQDs through the formation of C-N and C=N. Other than urea, ethylenediamine (Zou et al., 2022), arginine (Zhu et al., 2020), diamionaphthalene (Riaz et al., 2019) have been used as dopant elements.

Considering the excellent electronic conductivity and photo-excitation properties of nitrogen atom as dopant elements in CQD structures (Jia et al., 2020), they are expected to be used as an electronic mediator in photocatalytic materials, and hence, the contribution of nitrogen element can improve the photocatalytic degradation performance. Recent study has used nitrogen-doped CQDs in the photocatalyst composites. The presence of nitrogen elements in CQD structures has improved the photocatalytic degradation of methyl orange from 47% to 86% (Jamila et al., 2020).

Different types of dopant agents will result in different efficiency of degradation. Researchers have produced doped-CQDs by using nitrogen and bismuth as two different dopant agents (Chung Hui et al., 2021). The degradation performance proven that the nitrogen doped CQDs showed a great potential in the degradation of methylene blue in which nitrogen doped CQDs gives the highest degradation efficiency of 72.1%, compared to bismuth doped CQDs, showed only of 68.1% of degradation.

The comparative performance of dopant elements in the CQDs by using nitrogen (N) and chlorine (Cl) as dopant elements in the fabrication of N-CQDs and Cl-CQDs was also investigated (Y. Cheng et al., 2019). The results showed that the photocatalytic degradation performance on the organic dyes using N-CQDs was up to 97% while the degradation of organic dyes using Cl-CQDs was around 60%. This result suggested that the fabricated N-CQDs was more efficient in degrading organic dyes due to the unpaired electrons contributed from N atom that can integrate with CQD structures, and thus, improving the electronic state and electron transition characteristics.

2.6 Application of NCQDs as photocatalyst

NCQDs are a promising photocatalyst with high efficiency for light energy conversion. NCQDs can be an efficient photocatalyst in the photocatalytic degradation of organic pollutants owing to their strong visible-light absorption, excellent light-trapping ability, can exhibit quantum confinement in which the quantum-confined electrons are able to produce high energy photons as well as high efficiency in the separation of photo-generated charge carriers (Jamila et al., 2020; J. Zhang et al., 2018).

Researchers have shown interest in exploring the potential applications of NCQDs due to their outstanding photoluminescence properties and good photochemical stability (Y. Chen et al., 2021; Liu et al., 2020; Zheng et al., 2021). The fluorescent and luminescent NCQDs could be a potential photocatalyst because their high electron transfers capability and excellent photochemistry properties, leading to reduced charge carrier recombination. Consistent with other study (Duan et al., 2022b), NCQDs was found to possess quantum phenomena that have significant benefits in optical properties, resulting in efficiency in degrading organic dyes.

Owing to the relatively strong electron affinity of nitrogen atoms in CQDs, electrons can be easily captured by molecular oxygen, resulting in the generation of free radicals and thus, leading to the efficiency of photocatalytic degradation activity (F. Wang et al., 2017a). Hence, the fabricated NCQDs may act as an electron mediator in the photocatalytic system. The summary of the application of NCQDs as photocatalyst in degrading of organic pollutants are listed in Table 2.5.

Table 2.5: Application of NCQDs as photocatalyst

Photocatalyst composites	Fabrication method	Solution medium	Organic pollutants	Degradation Efficiency (%)	References
NCQDs with rice husks	Hydrothermal	Distilled water	Methylene blue	72.1	(Chung Hui et al., 2021)
NCQDs with graphitic carbon nitride	Hydrothermal	Ethanol	Tetracycline hydrochloride	90.0	(H. Chen et al., 2021)
Core-shell modified Ag/NCQDs bismuth vanadate	Sonication	Methanol	Tetracycline hydrochloride	80.3	(J. Zhang et al., 2021)
NCQDs with sulfur doped embedded zinc oxide	Hydrothermal	Deionised water and sodium hydroxide	Antibiotics	92.9	(Qu et al., 2020a)
NCQDs modified defect-rich graphitic carbon nitride	Ultrasonic	Anhydrous ethanol	Chromium (IV)	92.6	(Liu et al., 2020)
NCQDs with bismuth sulfide	Hydrothermal	Deionised water	Methylene blue	98.0	(L. Zhang et al., 2021)
NCQDs bismuth doping composite of titanium dioxide	Hydrothermal	Deionised water	Pharmaceutical wastewater (Diclofenac)	82.5	(Chung et al., 2022)

Table 2.5 shows that, most of NCQDs photocatalyst composites contributed to high efficiency in degrading the pollutants. This is due to NCQDs can act as an electron pool which diminishes the bandgap and the electron-hole separation could be excited using lower energy (Qu et al., 2020b).

The excellent electron conductivity of NCQDs will act as electron reservoir to accelerate the separation of photo-generated charge carrier. NCQDs has higher charge transfer ability than CQDs due to the higher electronegativity of nitrogen atoms compared with carbon atoms. This has significantly improved the performance of photocatalytic degradation of pollutants, as reported by Chen et al. (2021) where the NCQDs degraded 90% of tetracycline hydrochloride (HTC) in comparison to CQDs (73%) (H. Chen et al., 2021).

The fabricated photocatalyst that consists of NCQDs component could enhance the photocatalytic degradation by improving luminescent of the fluorescent photocatalyst. This is well supported by the work of Cheng et al. (2019), which showed that in the presence of NCQDs, about 97% of rhodamine B solution has been degraded within 240 min whilst only 4% degradation rate was observed in the absence of NCQDs (Y. Cheng et al., 2019). The presence of NCQDs could provide active sites and generate hydroxyl radicals onto the catalyst surface (Liu et al., 2020). Owing to the relatively strong electron affinity of nitrogen atoms in NCQDs, electrons can be easily captured by molecular oxygen, resulting in the generation of free radicals. Thus, photocatalytic degradation activity is improved (F. Wang et al., 2017b).

This was well observed in the work of Zheng et al. (2021) where the use of photocatalyst by NCQDs composited with dibismuth tetraoxide yielded, the degradation of methyl orange at 85% after 75 min of near-infrared light irradiation (Zheng et al., 2021). In contrast, only 65% of methyl orange have been degraded without CQDs/NCQDs. This is also agreed by Chen et al. (2021) whom reported that complete Rhodamine B dye have been degraded using NCQDs/SnO₂ nanocomposites whilst only 20.1% degradation was observed when only SnO₂ was used as the photocatalyst under the same duration (Y. Chen et al., 2021).

2.7 Stability of CQDs

CQDs possesses an outstanding stability and long-term photo-stability due to its high luminescence properties that enhance stability in water dispersion. The fabricated water soluble CQDs have acceptable photoluminescence stability with high stability to ionic solution and resistant to photo-bleaching.

The hydrophilic groups in the CQDs enhance the solubility and stability in aqueous media considerably, which lead to improved electron transfer capabilities for photo-degradation activities. In addition, the use of electron-donating nitrogen-related functional groups can further increase the excited energy states stability in CQDs structure. The CQDs with excellent photo-stability is suitable to be applied as photocatalyst due to their stability for long-term UV-light irradiation. Under different pH conditions, CQDs are reported to have excellent fluorescence intensity near the neutral pH range.

This is reported by Jiang et al. (2019) that the CQDs fluorescence intensity increased when the pH was increased from 1 to 6 and then weakened as the pH values varied from 6 to 12. This may be due to functional groups on the CQDs surfaces which may form intramolecular hydrogen bonds (Jiang et al., 2019).

Similar trend was also observed by Yu et al. (2021), where the fluorescent CQDs remained steady in the broad pH range of 5 – 10, and it dropped significantly when the pH was lower than 5 or higher than 10 (Yu et al., 2021). This trend was further supported by Shi et al. (2019) that the CQDs displayed excellent stability in the wide range of pH values from 1 to 13, and the maximum fluorescent intensity was observed at pH 7 (Shi et al., 2019a).

The decrease of CQDs fluorescence intensity under strong acidic or alkali medium can be ascribed to the change of surface charge caused by protonation-deprotonation of the functional groups on the surface of CQDs, thereby suppressing the fluorescence (Zhu et al., 2020).

In contrast, the study on the effect of saline ions on the photoluminescence stability of CQDs showed that there was no significant alteration in the luminescence intensity with an increase in the sodium chloride concentration, indicating that the CQDs have high salt tolerance (Yang et al., 2018). In fact, the CQDs were reported to show good stability for at least two hours even in a high ionic strength solution (Yu et al., 2019).

This was supported by Jian et al. (2017) who claimed that the CQDs have good stability in phosphate-buffered saline for a period of 14 days at room temperature, without changes in their fluorescence properties.

This shows that the fabricated CQDs possess high stability in buffers due to their nanoparticle sizes and higher surface charges (Jian et al., 2017). Long term stability of CQDs was also evaluated from the view of fluorescence intensity. A study by Feng et al. (2019) in evaluating the stability of CQDs showed that the fluorescence intensity of CQDs was maintained at 95% of its original intensity after one-month storage at 4 °C (F. Wang et al., 2017a). This revealed that the CQDs might possess excellent stability with power storage.

Similar observation was also reported whereby the fluorescence stability of CQDs was observed to remained unchanged after 15-30 days by Arumugam and Kim (2018) and Pan et al. (2018), which further justifying the nature of CQDs to have great dispersibility and stability over a long period (Arumugam and Kim, 2018; Pan et al., 2018). The CQDs can remain stable after long term storage and UV-light irradiation. Yu et al. (2021) reported that the CQDs remained similar activity after 2.5 months of storage or exposure to 365 nm UV-light irradiation for 180 min (Yu et al., 2021), suggesting that CQDs possess a better and stable bleaching resistance.

Similar observation was also reported by Basavaiah et al. (2018), whereby the CQDs have shown high photo-stability in that neither shift in emission wavelength nor significant reduction in fluorescence intensity was observed upon continuous exposure to UV-light irradiation from 10 min to 60 min, and 1 to 3 months preservation (Basavaiah et al., 2018), indicating its long term stability.

These findings were further strengthening by Wang et al. (2021) that claimed CQDs fluorescence intensity did not change significantly after 2 hours of exposure to UV-light irradiation, suggesting a high resistance to photo-bleaching. The as-prepared CQDs exhibit great stability in high-salt conditions, excellent photo-stability after continuous illumination for about 60 min, which guarantee the potential applications of CQDs in fluorescence fields (Guo et al., 2018).

The above observations suggested that CQDs can be used for various applications in multiple reuse cycles without reducing its reactivity and effectiveness. From the view on its reusability as photocatalysts, CQDs exhibited a relatively good stability for reuse in several runs without any significant drop in catalytic activity.

Photocatalyst-based CQDs showed good reusability for the photocatalytic degradation of amoxicillin after five successive runs (Chen et al., 2019). The CQDs composites maintained the excellent reusability and stability as they could be reused for at least five consecutive recycling experiments as photocatalyst (Balakumar et al., 2021).

The degradation rate was found to be maintain even after three cycles of reusability, as reported by Seng et al. (2020) on dye removal (Seng et al., 2020). The maintained degradation rate of photocatalyst-based CQDs was also observed for pharmaceutical compounds degradation for at least five successive cycles of CQDs reuse (Kumar et al., 2022), showing that the fabricated CQDs composites possess good stability.

The characteristic inter-planar stacking structure of the conjugated aromatic systems in the CQDs structure has contributed to the stability of carbon-based materials (Faraji and Moradi Dehaghi, 2021), which the aromatic systems with π - π stacking self-assembly principle was beneficial to the formation of carbon core structure. These potential properties could be related to structural property of CQDs that consist of π - π stacking interactions between the functional groups and the surface defects of the fabricated CQDs (F. Wang et al., 2017a).

Owing to the strong π - π stacking electrostatic interactions among CQD sheets, they were stable for repetitive photocatalysis as well as for a long-period of storage duration. Therefore, the aggregation and the loss of active photocatalysts could be efficiently inhibited, which indicated that the CQDs photocatalyst had good cycling photocatalytic degradation rate.

CHAPTER 3

RESEARCH METHODOLOGY

3.1 Introduction

Carbon quantum dots (CQDs) were fabricated from the empty fruit bunches (EFB) that were collected from Seri Ulu Langat Palm Oil Mill (Dengkil, Malaysia). Urea (99%, Merck, USA) was used as a nitrogen dopant element to fabricate nitrogen-doped carbon quantum dots (NCQDs). Both CQDs and NCQDs were fabricated through hydrothermal treatment. The CQDs and NCQDs were characterised and used as photocatalysts in the photocatalytic degradation of organic dyes. The photocatalytic degradation parameters were evaluated using the Taguchi approach.

The performance of NCQDs as photocatalysts has been evaluated based on the photocatalytic kinetic study with two kinetic models. The stability and reactivity of the fabricated NCQDs were investigated by evaluating their reusability cycles in degrading dye solutions and the duration of storage.

Evaluation study on the degraded dye solution has been carried out using the total organic carbon analyser to ensure that the dye molecules have been successfully degraded, proving that the photocatalytic degradation activity succeeded by the fabricated NCQDs.

Scavenging experiments were also carried out to investigate the active species involved during the photocatalytic degradation activity. Figure 3.1 summarized the flowchart of methodology in this study.

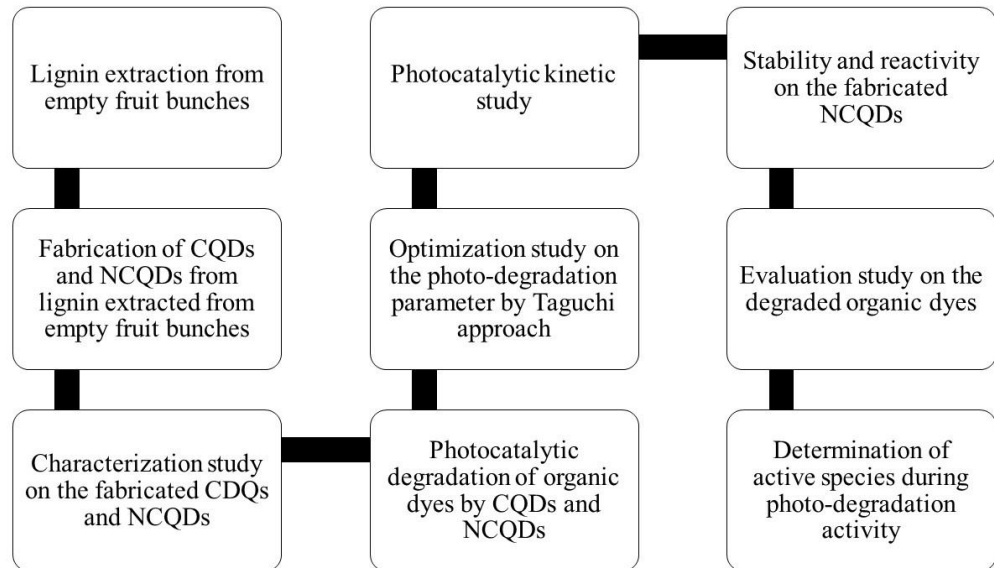


Figure 3.1: Flowchart of the research methodology

3.2 Fabrication of carbon quantum dots

3.2.1 Lignin extraction method

Lignin was extracted from EFB via the method reported by previous studies with some minor modifications (Coral Medina et al., 2015; Narapakdeesakul et al., 2013). First, the EFB fibres collected were washed for several cycles using distilled water to remove the undesired impurities.

Sodium hydroxide solution was prepared by diluting the sodium hydroxide pellets (97 %, Merck, USA) using distilled water. Afterwards, 30 g of EFB fibres were added into a 150 mL of sodium hydroxide solution (at a concentration of 0.5 M) and heated up at 120 °C for 2 h.

After that, the excess EFB residues were filtered out from the suspension. Hydrochloric acid (38 %, Merck, USA), at a concentration of 0.5 M, was added dropwise into the filtrate and stopped when the pH of the solution achieved pH 3. The mixture was left at room temperature for 24 h to allow the lignins to form precipitates.

Afterwards, the lignin was collected by vacuum filtration and washed for several cycles using distilled water to remove the remaining hydrochloric acid solution. Then, the residue containing lignins was placed into an oven at a temperature of 70 °C for drying.

3.2.2 Production of NCQDs and CQDs

NCQDs were fabricated from lignins using the hydrothermal method with some minor modifications (Liang et al., 2019). First, urea and lignin were dissolved in deionised water at a molar ratio of 1:4. After that, the mixture was transferred into a Teflon lined stainless steel autoclave reactor, the reactor was heated up at 180 °C in an oven for 8 h. Similar fabrication procedures were repeated without the addition of urea to obtain the CQDs.

After the hydrothermal process, the reactor was allowed to cool down to room temperature. Then, the solution was filtered using a filter paper having an average pore size of 20-25 µm in order to remove the unreacted raw materials. Unlike other works, this study avoided the employment of dialysis bag for purification because there were no any additional chemicals were used during the hydrothermal treatment. In the end of the process, the purity of the fabricated NCQD was confirmed through the characterization analyses with comparative studies as a benchmark.

Since without additional oxidizing agent or chemicals during the hydrothermal treatment, the obtained filtrate after the hydrothermal treatment could be directly used as photocatalysts in the photocatalytic degradation activity without affected their efficiency.

The brownish filtrate solution, which contained NCQDs or CQDs were stored at 5 °C in a refrigerator for prior to use as a photocatalyst. The concentrated brownish solution obtained after the fabrication stage consisted of the photocatalysts.

3.3 Characterisation study on CQDs and NCQDs

The fabricated solution of CQDs and NCQDs were dried using a freeze-dryer in order to obtain the CQDs and NCQDs in solid forms for analysis purposes. Functional groups on CQDs and NCQDs were analysed by Fourier Transform Infrared Spectroscopy (FTIR) (model Nicolet iS10) at a range of spectral width of 4000 to 400 cm^{-1} at a resolution of 4 cm^{-1} . The solid samples of CQDs and NCQDs were placed on the FTIR sample glasses, and the background was scanned prior to the scanning of the samples. The samples were recorded at 32 scans in order to produce a unique spectral fingerprint.

The elemental compositions of CQDs and NCQDs were determined using electron microscopy instrument with carbon fiber coating system, Energy-dispersive X-ray analysis (EDX) (model Apollo X). The solid samples of CQDs and NCQDs were coated by using chromium prior to the scanning. The EDX data consist of spectra showing the peaks corresponding to the respective elements. X-ray diffraction analysis (model Shimadzu XRD-6000) was applied in analysing the crystallinity phase of CQDs and NCQDs.

The solid sample of CQDs and NCQDs were compacted on the sample holder to make them a compact powder solid. The scanning range was between 0° to 80°. The surface morphology of CQDs and NCQDs were observed using field emission scanning electron microscopy (Hitachi S-3400N). The solid sample was placed on the sample holder. The images of FE-SEM are created by detecting the reflected electrons.

Particle sizes of CQDs and NCQDs were measured using a high resolution transmission electron microscopy (Thermo Fisher; Talos 120C). A beam of electron is transmitted through a sample to form the HR-TEM images. Meanwhile, the particle distribution of CQDs and NCQDs were calculated by measuring approximately 100 particles using the Image J Software in order to construct a particle distribution histogram.

Photoluminescent properties of the CQDs and NCQDs were evaluated using photoluminescence spectroscopy (Edinburgh Instrument FLS920) at a detection range of 200 nm to 1000 nm. Light absorption analysis on the CQDs and NCQDs solutions was observed using a double-beam UV-Vis spectrophotometer (Shimadzu UV-2600) at the absorption wavelength range of 200 nm to 800 nm. Zeta potential analysis of CQDs and NCQDs was carried out using dynamic light scattering (Malvern) to determine the hydrodynamic properties. The analysis was conducted at room temperature with distilled water at pH 7 as the aqueous medium. The solution was added into a cell that contain two gold electrodes. When voltage is applied to electrodes, particles will move towards the electrodes with opposite charges. A Doppler technique is used to measure the particle velocity.

3.4 Photocatalytic degradation of organic dyes

The potential application of the fabricated NCQDs as photocatalysts in this work was evaluated by conducting the photocatalytic degradation of methylene blue (MB), malachite green (MAG), and methyl orange (MO) solutions in the presence and absence of CQDs/NCQDs under sunlight irradiation. The photocatalytic degradation experiments were carried out between 10:00 am and 3.00 pm under sunlight irradiation with an average solar intensity of 4000–5000 Wh/m², which supported by a reported study that the monthly average of daily solar irradiation in Malaysia is recorded as 4000–5000 Wh/m² (Izadyar et al., 2016). The experimental works were conducted at the open area of Taman Bangi Avenue, Kajang, Selangor, Malaysia with a latitude and longitude of 2.9002148 and 101.7992594, respectively.

In addition, methyl green dye (MEG) was used as synthetic dye solution in the photocatalytic degradation experiments under UV-light irradiation in order to evaluate the efficiency of the fabricated NCQDs under a constant UV-light irradiation (302 nm). The illustration scheme of the photocatalysis is shown in Figure 3.2.

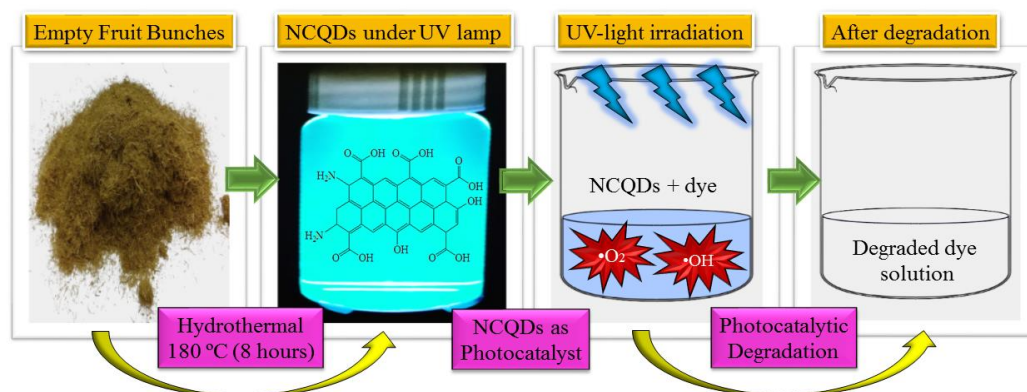


Figure 3.2: The illustration scheme of the photocatalysis by the fabricated NCQDs from EFB.

A volume of 10 mL of diluted NCQDs were added into a solution that contained 100 mL of dye solution (10 ppm). The mixture was stirred in the darkness for 60 minutes to ensure that the adsorption and desorption equilibrium were achieved between the reactants and NCQDs before sunlight irradiation. Then, the mixture was exposed to sunlight for 180 min. At the same duration, a volume of 100 mL of 10 ppm dye solution was also exposed to sunlight without the presence of NCQDs as a control run. After the experiments, the dye solutions were collected and the dye concentration was analysed using UV-Vis spectrophotometer. The absorbance values for the samples can be obtained from the UV-Vis spectrophotometer by scanning at wavelengths of 660 nm, 630 nm, and 464 nm for MB, MAG, and MO solutions, respectively. From the results, the percentage degradation of dye solutions was calculated by using Eq. (1):

$$\text{Degradation (\%)} = [(A_0 - A_t) / A_0] \times 100\% \quad (1)$$

where A_0 is the initial absorbance of dye, and A_t is the absorbance of dye at a specific time.

3.5 Optimisation study by Taguchi approach

The mixture of methyl green (MEG) dye and NCQDs solution was exposed to UV-light irradiation at a wavelength of 302 nm. The experiment was conducted at room temperature for specified duration using Nyxtechnik UV box T12621D as a UV-light irradiation source. The MEG dye concentration in the solution was analysed using a UV-Vis spectrophotometer at a wavelength of 500 – 700 nm after the photocatalytic process. The degradation efficiency for MEG dye can be calculated using Eq. (1).

The effect of operating conditions on the photocatalytic degradation of MEG dye was evaluated using the Taguchi approach, a method based on the statistical principle. In this study, the Taguchi orthogonal array (OA) of the factorial design was employed using Minitab. Four parameters were investigated, namely amount of NCQDs (A), pH of dye solution (B), duration of degradation (C), and initial dye concentration (D). There are three levels for each parameter, as shown in Table 3.1.

Table 3.1: Experimental design for four factors and three levels.

No	Code	Factors	Level 1	Level 2	Level 3
1	A	NCQDs amount (ml)	5	10	20
2	B	pH of dye solution	3	7	9
3	C	Duration (min)	10	20	30
4	D	Initial dye concentration (ppm)	10	20	30

Based on the parameters combinations, the Taguchi method has suggested that an L^9 orthogonal array design (Wong et al., 2020) is sufficient to systematically predict the significant variables and the effect of each factor on the degradation efficiency using nine sets of experiments. The arrangement of the experiments is shown in Table 3.2.

Table 3.2: Taguchi L⁹ (3⁴) orthogonal array and results of dye degradation in percentage.

Runs	Degradation factors				Dye degradation (%) (Average)
	NCQDs amount (ml)	pH of dye solution	Duration (min)	Initial dye concentration (ppm)	
1	10	9	10	20	96.7
2	10	7	30	10	74.3
3	20	7	10	30	72.9
4	20	9	20	10	99.8
5	10	3	20	30	47.7
6	20	3	30	20	10.2
7	5	7	20	20	66.3
8	5	9	30	30	99.5
9	5	3	10	10	10.7

The Taguchi method analysis was evaluated using the Signal to Noise (SN) ratio. SN ratio is a method to identify the optimum level of each factor by measuring the mean values (represents the desirable effect) and the standard deviation (represents the undesirable effect) of the data set (Sohrabi et al., 2017).

It can be classified into three categories; the larger-is-better, the nominal-is-better, and the smaller-is-better. In this study, the degradation efficiency was the desirable primary response. Therefore, the SN ratio chosen in the Taguchi method was the larger-is-better, and it can be calculated using Eq. (2).

$$SN = -10 \log_{10} \left[\frac{1}{n} \sum_{i=1}^n \frac{1}{y_i^2} \right] \quad (2)$$

where n is the number of experiments and y_i is the degradation efficiency.

3.6 Photocatalytic kinetic model

A kinetic study for the photocatalytic degradation of MEG dye was carried out using seven bottles of 100 mL MEG dye solution at a concentration of 20 ppm and pH 7. Firstly, 10 ml of 10 ppm NCQDs solution was added into each bottle. The mixtures were exposed to UV-light irradiation for the time interval of 0, 5, 10, 15, 20 and 30 min. After the irradiation, the sample bottle was taken out and analysed for MEG dye concentration in the solution using a UV-Vis spectrophotometer. The results were fitted into pseudo-second-order kinetics models, as shown in Eq. (3):

$$dC_t / dt = k(C_e - C_t)^2 \quad (3)$$

where C_e and C_t are the concentration of degraded MEG dye at the equilibrium and specific time, respectively, and k is the rate constant. The integrated equation can be expressed in Eq. (4), in which the rate constant of MEG degradation can be obtained from the intercept of the linear-line plots of t/C_t versus t .

$$t/C_t = 1 / (kC_e^2) + t / C_e \quad (4)$$

The kinetics of the photocatalytic degradation rate of MB and MAG dye solutions were fitted into first-order kinetics model, which were calculated by using (Eq. (5)):

$$\ln (A_0/A_t) = kt \quad (5)$$

where k is the reaction rate constant that can be obtained by calculating the slope of the graph, A_0 represents the initial dye absorbance, and A_t represents the dye absorbance at the time (t).

3.7 Stability and reactivity study

This study used NCQDs as the photocatalysts in liquid form as they can be well-dispersed in an aqueous medium. The used NCQDs were separated from the degraded dye solution, which were reused in the subsequent cycles after the degradation activity. Column chromatography was employed to separate and collect the NCQDs from the dye solution in which n-hexane ($\leq 100\%$, Merck USA) and silica gel (0.2-1.0 mm, Merck, USA) were used as the mobile and stationary phases, respectively. The collected NCQD solutions were further analysed using UV-Vis spectrophotometer at a 200-350 nm wavelength range.

The fabricated NCQDs' stability was evaluated by analysing their fluorescence properties after twelve months of storage in a 5 °C refrigerator by evaluating the photocatalytic degradation performance of MB, MAG and MEG dyes. The UV-light absorbance of the stored NCQDs was also observed by UV-Vis spectrophotometer at a 200-350 nm wavelength range to evaluate their stability and optical properties after being stored for up to twelve months.

3.8 Evaluation of the degraded dyes

The degree of mineralisation is important for evaluating the complete degradation of organic dyes. Therefore, total organic carbon (TOC) analysis can be used to measure the organic carbon concentration in the degraded dye solution. The TOC of the degraded organic dyes were determined using the TOC-L Analyser (Shimadzu, SSM-5000). The degraded dye solution was directly injected into a TOC-L analyser for the combustion catalytic oxidation process at the temperature of 680 °C to measure their carbon content.

The TOC removal rate can be calculated using Eq. (6):

$$\text{TOC removal (\%)} = [(C_0 - C_t) / C_0] \times 100\% \quad (6)$$

where C_0 is the initial concentration of TOC, and C_t is the concentration of TOC after the degradation activity.

3.9 Determination of active species

Trapping experiments were carried out using isopropyl alcohol and benzoquinone as the scavenging agents to confirm the roles of hydroxyl and superoxide radicals in the photocatalysis of organic dyes in this study (Huang et al., 2021). A 0.05 mol of isopropyl alcohol (IPA) and 0.05 mol of benzoquinone (BQ) were added into 20 ppm of dye solution (100 ml) in which the scavenger agents were used to trap $\cdot\text{OH}$ and $\cdot\text{O}_2$ radicals, respectively, during the photocatalytic degradation activity under a UV-light irradiation. The photocatalytic degradation was conducted based on the optimal condition as suggested by the Taguchi approach.

CHAPTER 4

RESULT AND DISCUSSION

4.1 Introduction

Nitrogen-doped carbon quantum dots (NCQDs) were fabricated from the empty fruit bunches (EFB) through a hydrothermal treatment. This section will discuss the mechanism of the hydrothermal treatment of EFB in the fabrication of NCQDs. The fabricated NCQDs were applied as photocatalyst in the photocatalytic degradation of organic dyes. In the following sections, their chemical, physical and optical properties were evaluated using the respective instruments. The performance of the fabricated NCQDs as photocatalyst was evaluated based on their ability in degrading different types of organic dyes.

In this study, Design-Expert software was employed in order to determine the factors with significant effects on the photo-degradation of organic dyes through the Taguchi approach. The experimental observations were converted into signal-to-noise (SN) ratios, which are the desirable and undesirable values for the output characteristic, respectively. In addition, an evaluation of the photocatalytic kinetic study was also presented in this chapter by discussing the first-order and pseudo-second-order kinetic models.

The stability and reactivity of the fabricated NCQDs were also evaluated in this chapter. The degraded organic dyes were analyzed using the total organic carbon analyzer in order to further indicate the degree of mineralization of the dye molecules. In addition to the evaluation on the performance of the fabricated photocatalysts, a comparative study between CQDs and NCQDs was experimentally evaluated.

4.2 Fabrication mechanism of NCQDs from EFB

Lignin from EFB fibers is one of the potential raw materials that can be used in the NCQDs fabrication due to its long hydrophobic branches with various functional groups such as hydrophilic phenolic, aromatic, carbonyl and hydroxyl side chains as proven in the FTIR spectrum as shown in Figure 4.1.

The presence of sufficient carbon, oxygen and hydrogen content in the lignin structure is also one of the reasons for using them as raw materials. Urea was used as a nitrogen dopant element in producing NCQDs because it consists of carboxyl groups that can contribute to the formation of carbon bondings among the CQD surfaces. In addition, the nitrogen atoms presented in their structure can easily construct the covalent bonds within the surfaces of CQDs to form NCQD structures.

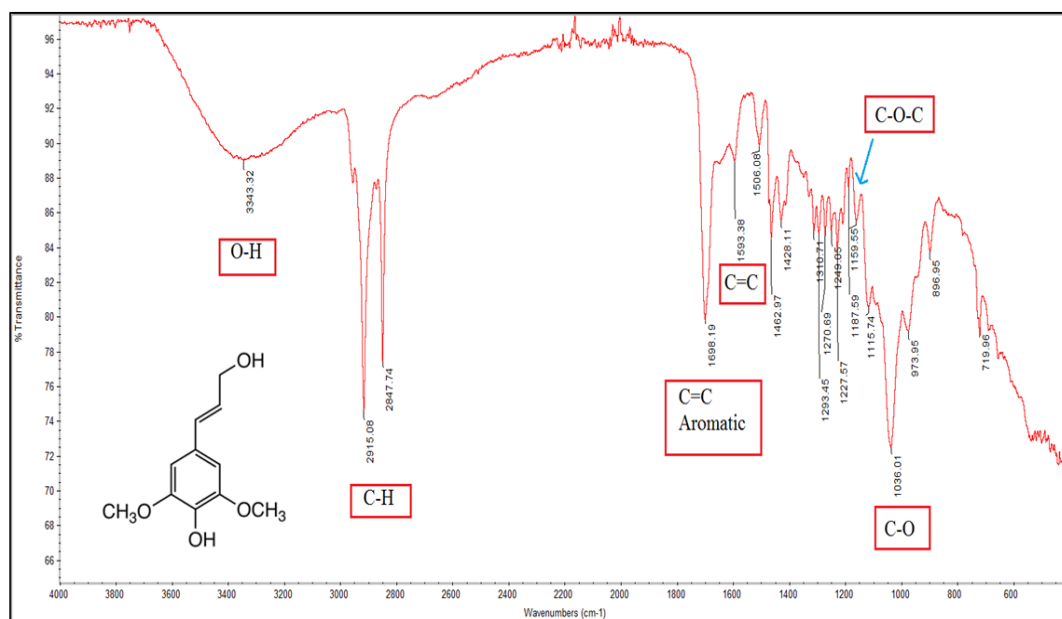


Figure 4.1: FTIR spectrum of lignin extracted from EFB

Lignin and urea consist of abundant surface hydrophilic functional groups, which have high dispersibility in aqueous medium reaction. Therefore, this study intended to apply the hydrothermal treatment in fabricating the NCQDs. The hydrothermal treatment was conducted at a heating of 180 °C for 8 h (Saboorizadeh et al., 2021b). At this condition, NCQDs could be produced in uniform particle size distribution and a high yield of quantum dots in the solution.

The reaction condition remained constant in this study to ensure a consistent photo-degradation performance as well as the quantum effect properties. During the hydrothermal treatment, water molecules were dissociated into hydrogen and hydroxide ions, leading to the formation of various functional groups on the surfaces of NCQDs. Figure 4.2 shows the overview of the fabrication of NCQDs from EFB fibers.

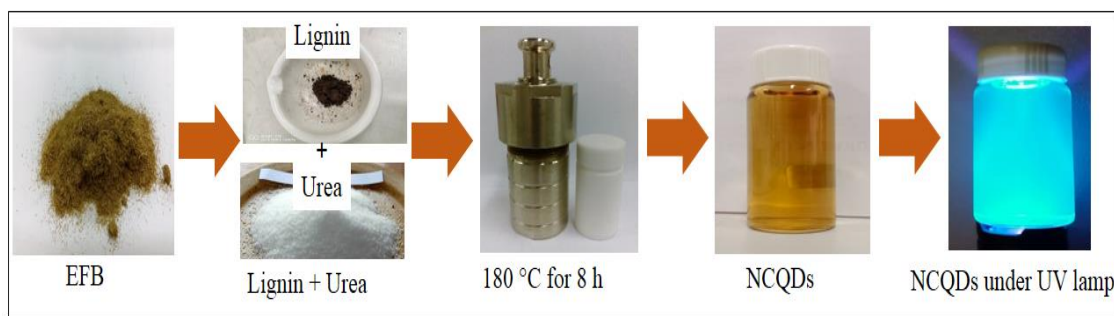


Figure 4.2: Fabrication process of NCQDs through a hydrothermal treatment.

In the hydrothermal process, deionized water was used as the reaction medium. Carbon precursors were reacted in the hydrothermal reactor at 180 °C in which the oxidation process occurred to enhance the fluorescent quantum yield. This process involved the heating of the carbon precursors at high temperature and high pressure, which allowed interactions among precursors and water molecules.

During the hydrothermal reaction, lignin and urea were oxidized and exfoliated due to the reducing strength of hydrogen bonds between the carbon sheets, and covalent bonds between the urea molecules (Li et al., 2018). In fact, urea was completely dissolved in water because it contains a carboxylic group, which has high polarity. Therefore, the formation of NH₂ groups on the surfaces of CQDs can be performed by hydrolysis of water molecules during the hydrothermal process.

The hydrothermal method is able to produce the fluorescent carbon quantum dots with good light energy conversion and high surface crystallinity. The formation of NCQDs can be achieved by oxidizing carbon sheets to produce more oxygen-containing functional groups through a self-assembly process (Allahbakhsh and Bahramian, 2018).

Various functional groups on the CQD surfaces, including surface defects contributed by the nitrogen element, would affect their optical properties and fluorescence properties, leading to the production of photocatalyst-based luminescent material. The particle sizes of reactants decreased during the reaction, producing NCQDs with strong fluorescent emission. This indicated the successful dehydration and carbonization of the lignin molecules upon pressurization. During the heating process, the colour of the solution changed from dark brown to light brown, indicating that the surface morphology of NCQDs could be gradually modified to produce nano-sized particles with high crystallinity. The crystallinity surface is necessary from the aspect of electronic transfer ability in order to enhance the photocatalytic efficiency, resulting to larger surface area and easy to react to the light irradiation.

Figure 4.3 shows a postulated mechanism of NCQDs fabrication. Based on the postulated mechanism, the reactants (lignin and urea) could be oxidized to form NH_2 , $\text{C}=\text{C}$, $\text{C}=\text{O}$ and $\text{C}-\text{C}$, which mainly composed the NCQDs. The formation of primary functional groups showed that the fabricated CQDs and NCQDs possess π system of chemical structure with electronic transition properties. Besides, the formation of the hydrophilic groups in the NCQDs structure could enhanced the solubility in aqueous solutions, which could easily interact with the dye solution. The high solubility of the fabricated NCDQs in aqueous solution could also result in high fluorescent quantum properties for the production of the photo-generated electron-hole pairs, which could facilitate a high efficiency in electron harvesting during the photo-degradation activity (Zhang et al., 2016).

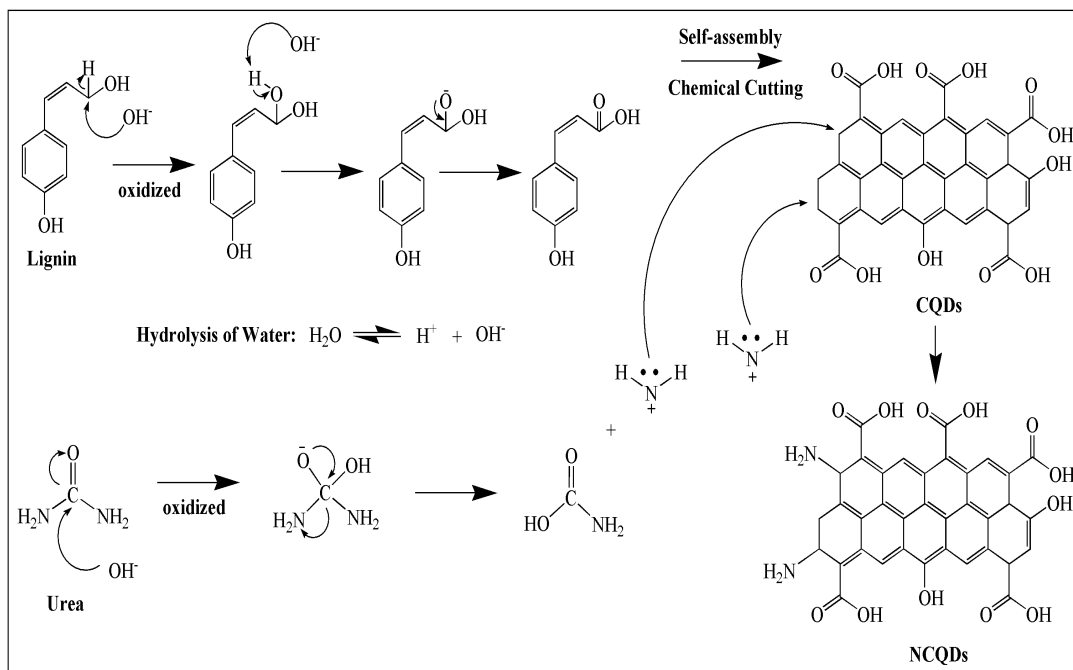


Figure 4.3: A postulated mechanism of NCQDs fabrication

The oxidative treatment using water molecules may cause the fragmentation of macroscopic carbon aggregates into nano-sized particles as well as enhances their solubility and functionality in degrading organic dye (Kumari et al., 2018). Based on the mechanisms (Figure 4.3), the hydrothermal treatment begins with the hydrolysis of water as the temperature increases, in which the water molecules dissociate into the hydrogen ions (H⁺) and hydroxide ions (OH⁻). The OH⁻ will attack the primary alcohol in the lignin structure.

The hydrogen atom on the primary alcohol in the lignin structure is removed by OH⁻ and a carbonyl group (C=O) is formed (Xu et al., 2018). In addition, water molecules will break the π - π carbon bonds in the lignin to form carboxyl and hydroxyl groups on the NCQDs surfaces (Kumari et al., 2018).

At the same time, OH^- will attack the carbonyl groups in the urea structure to form carboxylic (COOH) and amino (NH_2) groups. Afterwards, lone pairs from NH_2 will attack the aromatic rings of CQDs to form stable NH_2 groups.

During the self-assembly process of NCQDs, the hydrogen bonding interactions play an important role in the formation of the NCQD core as the covalent bonds of hydrogen (H) and oxygen (O) atoms possess great electronegativity (Wicht et al., 2019). When the concentration of the NCQDs increases, the distance between hydroxyl (OH^-) groups are significantly reduced. When an H atom is close to an O atom, the (O-H-O) bonds can be gradually formed. In fact, H atoms on the OH^- groups have only one electron for forming a covalent bond to an O atom. Therefore, electrons can be easily attracted due to the higher electronegativity of the O atom and the electron pairs are close to the O atom.

The positive and negative charges are attracted to each other to form H bonds. Thus, self-assembly of NCQDs may occur during the hydrothermal treatment in order to fabricate nano-sized NCQDs, in which, the smaller the particle size, the larger the particle surface area, the high tendency in degrading organic dyes during photocatalytic activity. In fact, the fabricated NCQD from EFB possess negatively charge functional group. More negatively charges detected, resulting in electron rich-species as well as good fluorescence properties with high crystalline surface morphology. An illustration of the self-assembly process is shown in Figure 4.4.

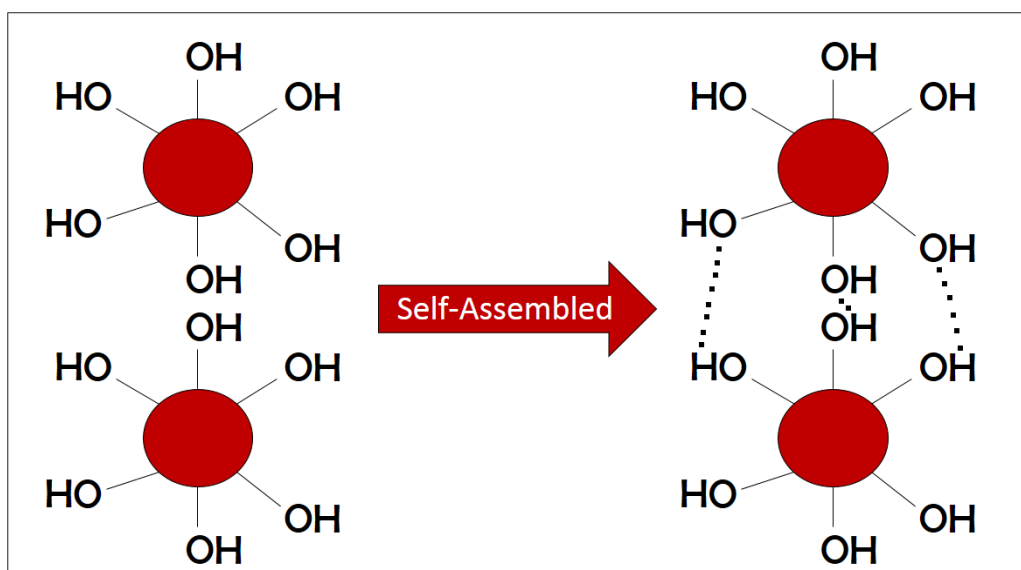


Figure 4.4: An illustration of the self-assembly process in the formation of NCQDs.

4.3 Characterisation study on CQDs and NCQDs

4.3.1 Functional group determination

Fourier transform infrared spectroscopy (FTIR) analysis was used to identify the functional groups present in CQDs and NCQDs. Figure 4.5 shows that a broad absorption band is observed around 3450.03 cm^{-1} , which can be attributed to O-H group stretching vibrations. The absorption band of the C=O groups appears at 1619.44 cm^{-1} . A peak centred at 1412.09 cm^{-1} is attributed to the stretching of C=C groups in the aromatic ring (Sabet and Mahdavi, 2019).

Another two peaks appear at 1042.02 cm^{-1} and 2924.35 , which can be attributed to the stretching of C-O and C-H bending, respectively (Khan et al., 2019; Monte et al., 2019). By further comparison between CQDs and NCQDs, vibration stretching for N-H and C-N bonds were found at wavenumbers of 3257 cm^{-1} and 1154 cm^{-1} , respectively (Huynh et al., 2001; Söderström and Ketola, 1994), proving the presence of NCQDs.

The formation of various functional groups in the CQDs and NCQDs revealed the successful oxidation reaction of raw materials used (lignin from empty fruit bunches and urea) during the hydrothermal treatment. The absence of similar peaks for CQDs FTIR spectrum verified that the nitrogen atoms were successfully bonded onto the CQDs surfaces to produce NCQDs.

Besides, some of the carbonyl groups in urea have also been changed into amide groups during the hydrothermal reaction. Different functional groups on the NCQDs surface will create different emissive traps during the excitation of electrons, resulting in high photoluminescence NCQDs.

FTIR spectra in this study have proved that the presence of several hydrophilic functional groups such as hydroxyl, carboxyl, and carbonyl groups have been bonded to the aromatic ring of the NCQDs and CQDs core structures, which made them hydrophilic materials and have high solubility in the aqueous medium (Deng et al., 2018).

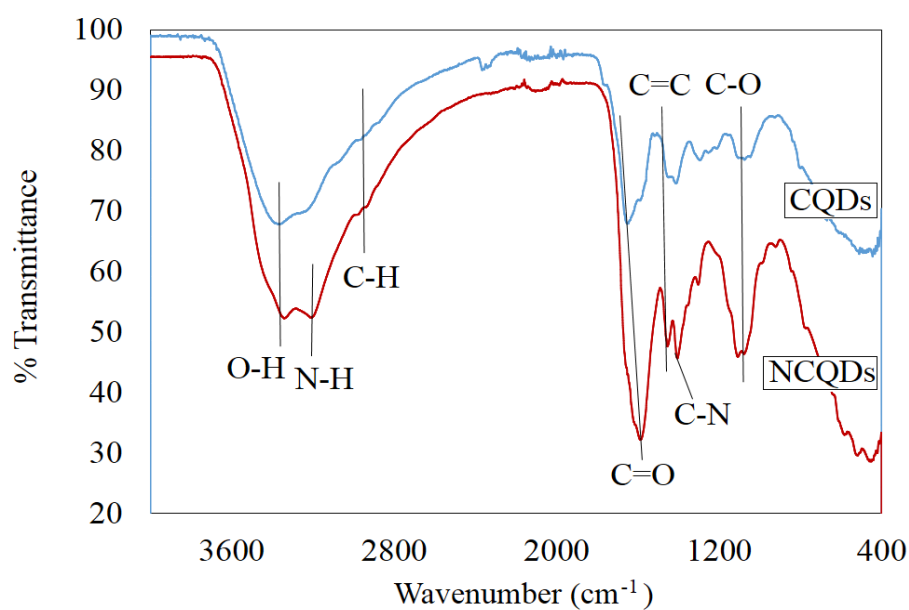


Figure 4.5: FTIR spectra of CQDs and NCQDs produced from EFB.

4.3.2 Elemental analysis

The energy-dispersive X-ray (EDX) results for CQDs and NCQDs are shown in Table 4.1 and their elemental mapping can be found in the Figure 4.6. Both CQDs and NCQDs mainly composed of carbon and oxygen atoms, which have been associated with the presence of the hydroxyl group, carbonyl group and aromatic rings.

Based on the atomic percentage from the elemental composition analysis, NCQDs have a relatively lower composition of oxygen atoms compared to CQDs because some of the oxygen atoms have been displaced by the nitrogen atoms through the formation of carbon-nitrogen single bond. The presence of nitrogen element in the NCQDs indicated the successful doping of the nitrogen onto the CQD surfaces.

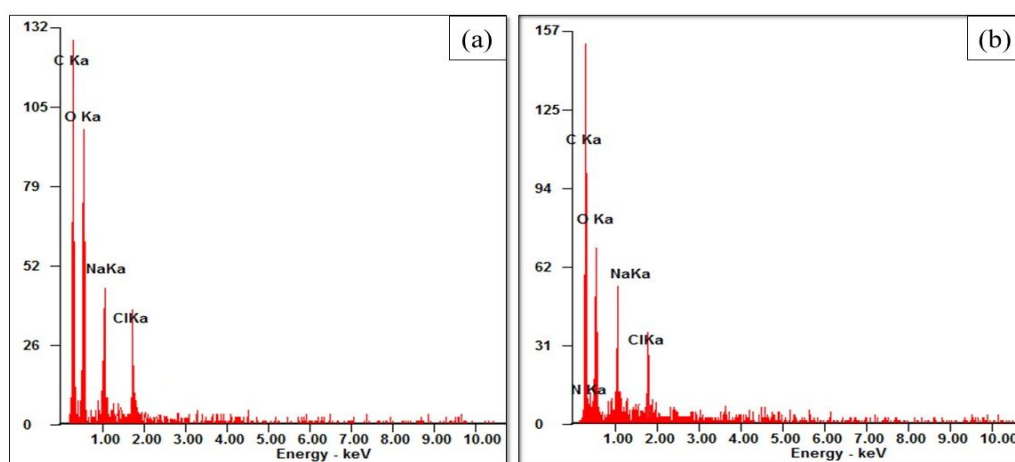


Figure 4.6: Elemental mapping for CQDs and NCQDs

Both CQDs and NCQDs showed higher content of carbon than oxygen element at a mass ratio of approximately 2:1 due to the presence of carbon-based functional groups in the quantum dot structures.

The EDX result indicated the significant elements in the CQDs and NCQDs molecular structure, which were supported by FTIR spectra. In addition, sodium and chlorine elements were also observed. These could be the elements remained after the lignin preparation stage. Nevertheless, their percentages were low and will have minimal effects on the surface characteristics of quantum dots.

Table 4.1: Elements present in the CQDs and NCQDs with their respective atomic percentages.

Elements	Atomic percentage (%)	
	CQDs	NCQDs
Carbon	61.47	60.76
Nitrogen	0.00	9.01
Oxygen	30.35	20.38
Sodium	4.65	5.93
Chlorine	3.53	3.92

4.3.3 Observation on the surface carbon phases

The X-ray diffraction (XRD) patterns of CQDs and NCQDs as shown in Figure 4.7, demonstrated a sharp and high-intensity reflection centred at 46.3° with a diffraction plane of (111) that corresponded to the existence of abundant functional groups and the graphite structure in the carbon core of CQDs and NCQDs (Zhao et al., 2019). This peak has also shown the characteristic inter-planar stacking structure of the conjugated aromatic systems, which were indexed for carbon-based materials (Faraji and Moradi Dehaghi, 2021).

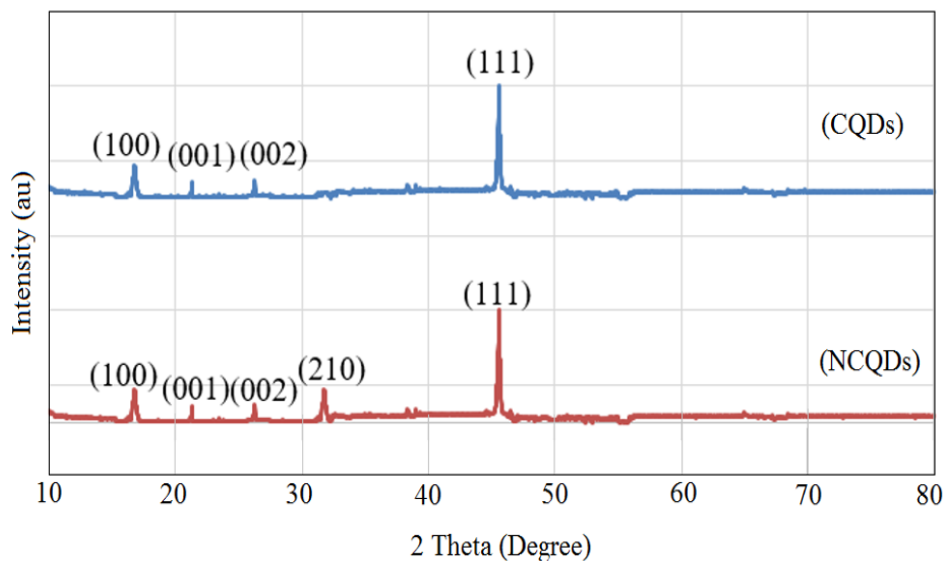


Figure 4.7: XRD pattern for CQDs and NCQDs produced from EFB.

The peaks at around 16.9° indicated the diffraction plane of (100), which certified the presence of CQDs in the compounds (Naushad et al., 2021). The diffraction pattern appeared within 10° to 50° suggested the presence of crystalline carbon phase in the fabricated CQD and NCQD surfaces. A diffraction peak appeared at around 32.7° , characteristic of (210) diffractions, indicated that some carbon atoms were doped with the dopant element, which confirmed the presence of nitrogen dopant in the fabricated CQDs (Jamila et al., 2020; Zeng et al., 2019).

The narrow diffraction peaks of XRD pattern indicated that the fabricated compound contained carbon quantum dots with high crystallinity (Yu et al., 2020). The crystallinity phases of CQDs and NCQDs that were fabricated from EFB fibres showed excellent interfacial charge transfer, improved molecular oxygen activation ability, more efficient electron pathway, and increased light-harvesting capacity, leading to enhanced photocatalytic degradation activity (Martins et al., 2016).

Based on Figure 4.8, the diffraction pattern of the NCQDs from empty fruit bunches shows peaks centred at around 20° to 30°, which were related to a highly crystalline nature and high purity of the fabricated NCQDs. A strong peak was observed at around 35°, characteristic of (010) diffractions from the graphite phase due to the agglomeration of NCQDs during the freeze-drying process.

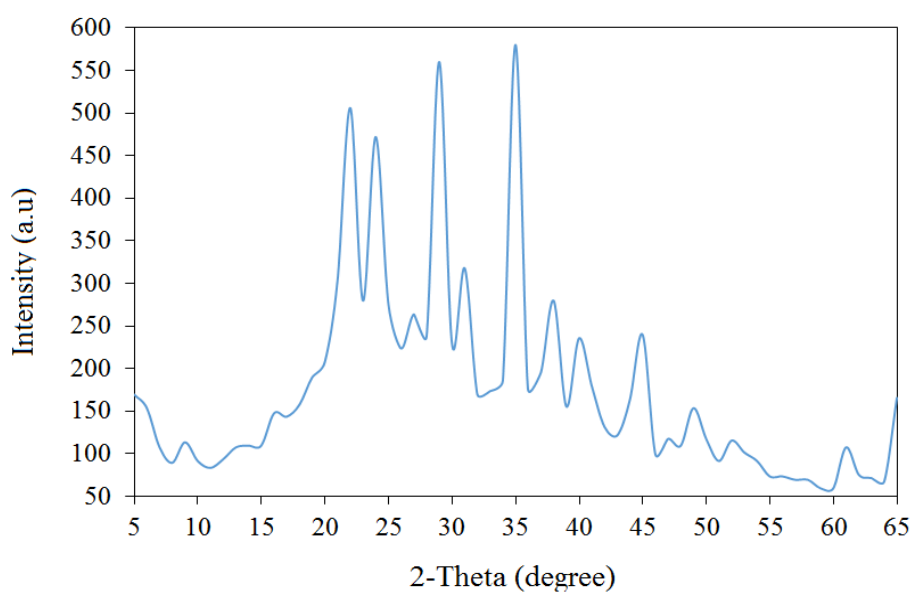


Figure 4.8: XRD pattern for NCQDs from EFB.

4.3.4 Photoluminescence (PL) properties

The photoluminescence properties of CQDs and NCQDs were evaluated by PL spectrophotometer in order to study the spontaneous emission of light under optical excitation. Figure 4.9 shows the optimal wavelength of emission and excitation in which the spectra exhibited the highest intensity, confirming that the dimension of fluorescent quantum dots ranged from 2 to 5 nm, resulting to blue fluorescence.

Based on Figure 4.9, CQDs have the optimal emission peak at 441 nm upon excitation at 361 nm. When nitrogen was added to the CQD surfaces, the emission peak shifted slightly towards the higher energetic region, 468 nm at an excitation wavelength of 386 nm. The PL result in this work is consistent with the PL results of several other studies (Chaudhary et al., 2022b; Das et al., 2022; Qi et al., 2022; Wang et al., 2022b).

The wavelength intensity for excitation and emission of NCQDs was higher than CQDs due to the nitrogen-dopant element, which enhanced the luminescent properties that could be attributed to the effect of surface passivation functionality. The lone pairs from nitrogen atoms have contributed to the creation of new electronic transition in the NCQDs, which could then increase the photoluminescent intensity (C. Zhou et al., 2019).

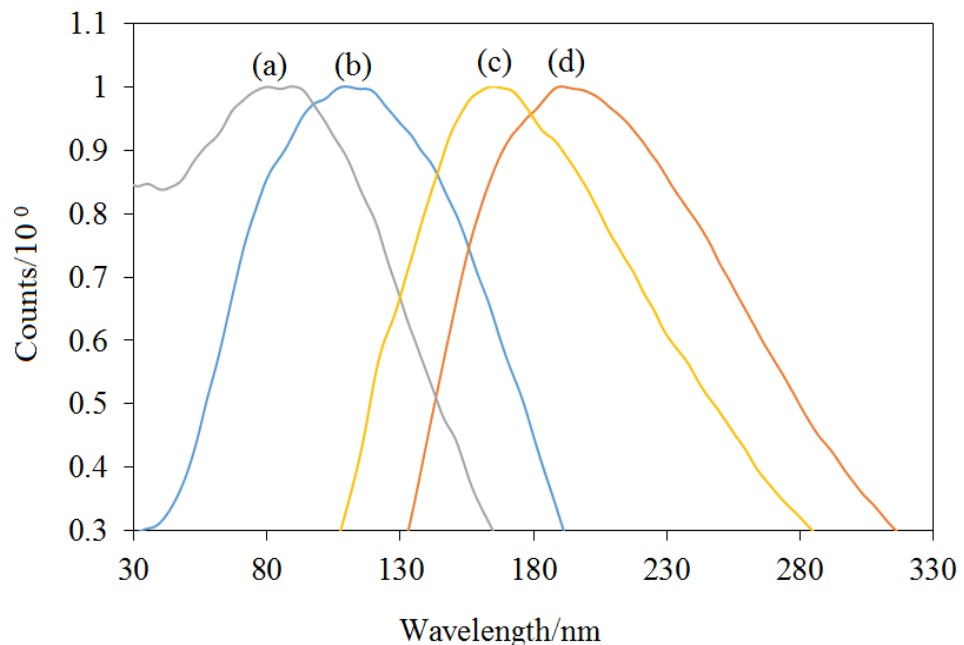


Figure 4.9: PL spectra for (a) CQDs excitation, (b) NCQDs excitation, (c) CQDs emission and (d) NCQDs emission.

This result suggested that the radiative transitions in NCQDs can be triggered at a lower wavelength compared to CQDs. The nitrogen addition to CQDs could completely alter all the electron energy states, which was also observed in literature studies (Navidfar et al., 2022; Zhang et al., 2023).

The high photoluminescence of NCQDs makes the quantum particles can be excited by UV-light irradiation with fast photocatalytic degradation capability. The luminescent behaviours may also be attributed to the sp^2 hybridization of carbon clusters with abundant trap states and small differences in the particle size distribution (Guo and Zhao, 2020). The fluorescent properties of the CQDs and NCQDs can be ascribed to the bandgap transitions, which correspond to the conjugated π -domain and surface defects that may present in the CQDs and NCQDs.

The fluorescence lifetime of NCQDs was measured using a (time-resolved photoluminescence spectroscopy (TRPL) analysis as shown in Figure 4.10. The TRPL was used to investigate the charge transfer behaviour in the electron-hole recombination process of NCQDs.

From the curve, the average carrier lifetime of the fabricated NCQDs was 2.09 ns with an emission of 459 nm at the excitation wavelength of 358 nm. The observed nanosecond lifetime of NCQDs suggests that NCQDs emission could be attributed to a singlet state. The TRPL result suggests that the lifetime of the photo-generated charge carriers in the NCQDs are significantly affected by the density of the oxygen-based functional groups. Longer lifetime shows more efficient charge transfer process, which can improve the photocatalytic activity.

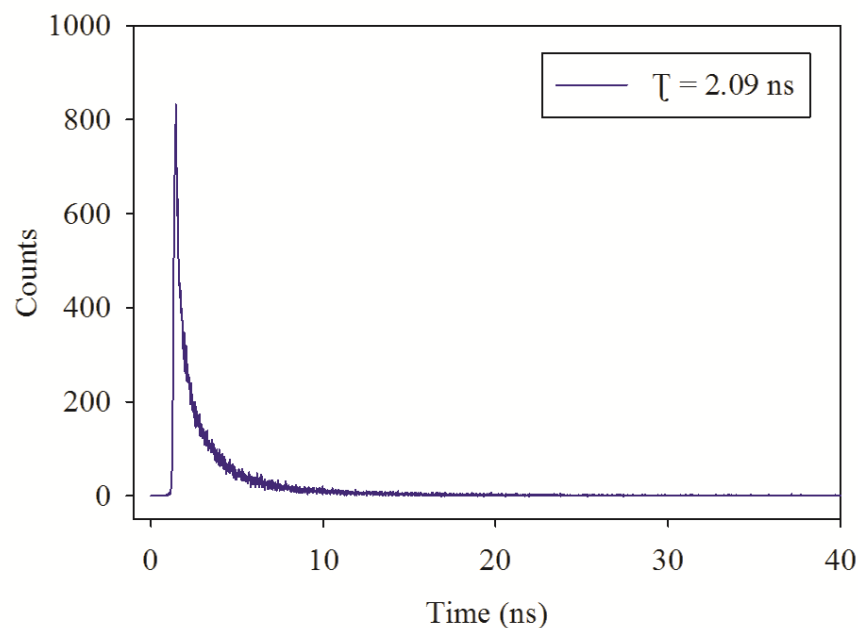


Figure 4.10: The fluorescence lifetime of the fabricated NCQDs from EFB.

4.3.5 Light absorption and optical properties

UV-Vis absorption analysis was carried out to study the optical properties of CQDs and NCQDs. Figure 4.11 shows that the UV-Vis spectra of CQDs and NCQDs exhibited characteristic transition peaks within 200 nm to 400 nm. The optical absorption peaks of CQDs and NCQDs were at 280 nm and 282 nm, respectively, which could be attributed to π - π^* transition of C=C and C-C bonds, originated from the aromatic π system and the core sp^2 carbon bonds.

The NCQDs spectrum has been slightly shifted, resulting from the addition of nitrogen atoms doped onto the CQD surfaces (Gong et al., 2019). Meanwhile, the absorbance peak for CQDs was split around the higher-energy region, which could explain the existence of some epoxides in the CQDs structure (Gao et al., 2013).

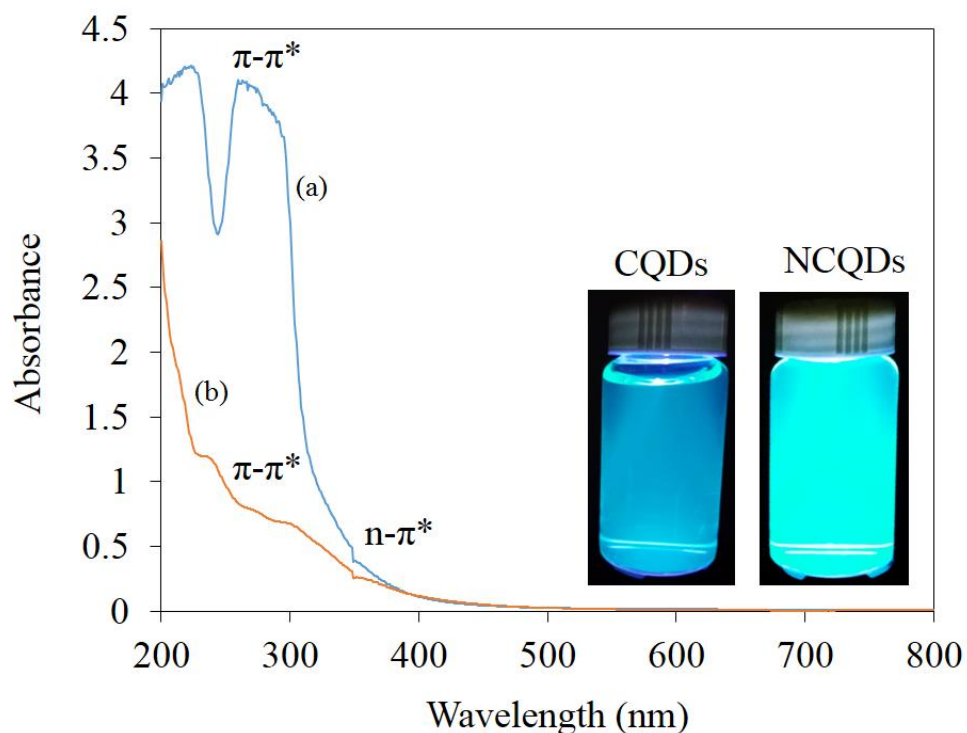


Figure 4.11: UV-Vis spectra for (a) CQDs and (b) NCQDs produced from EFB.

Another absorption peak for both CQDs and NCQDs can be observed at around 350 nm, which could be assigned to $n-\pi^*$ electron transition of C=O and C-OH groups due to the successful oxidation of carbon-based nanoparticles as well as the presence of oxygen-functionalized groups. The embedded images, as shown in Figure 4.11 are the blue fluorescence of CQDs and greenish-blue fluorescence of NCQDs.

The fabricated NCQDs can emit a strong greenish-blue luminescence when they are exposed to 395 nm UV-light irradiation. This result indicates that the hydrothermal treatment was successfully conducted on the raw materials due to the high temperature and high pressure. The high-pressure condition (up to 3 MPa) was controlled by a Teflon lined stainless steel autoclave.

Both CQDs and NCQDs exhibited fluorescent behaviours when exposed to UV-light irradiation due to the localization of electron-hole pairs. Different luminescent colours of CQDs and NCQDs were observed due to new energy levels attained by the NCQDs, which were contributed by the presence of nitrogen atoms, as well as different surface states between the CQDs and NCQDs. The fluorescent properties of quantum dots can promote the migration rates of the electrons and holes, consequently react with oxygen molecules to form radical molecules, which can improve the photocatalytic redox reaction.

4.3.6 Surface charges evaluation

Nanoparticles have surface charges that resulting in electrostatic repulsion between each particle. The strength of the electrostatic repulsion can be determined by zeta potential analysis. A relatively negative electrostatic charge for the CQDs in aqueous solution has been proven by the zeta potential analysis ($\zeta = -19.41 \pm 0.51$ mV) at a solution pH 9.3, as shown in Figure 4.12a. Meanwhile, Figure 4.12b shows the zeta potential value for NCQDs ($\zeta = -25.15 \pm 0.52$ mV) at a solution pH 9.3, in which the hydrodynamic for both CQDs and NCQDs were found to be negatively charged.

The result could indicate the presence of negatively-charged functional groups (-OH and -COOH) on the CQD and NCQD surfaces. The negatively-charged quantum dots are electron-rich species, which can easily interact with the electron-deficient species. This result made them ideal for photocatalytic degradation of organic pollutants.

The formation of oxygenated-functional groups on the CQD and NCQD surfaces are necessary for achieving a stable suspension in aqueous solution. In addition, the interactions of the similar charges on CQD and NCQD surfaces lead to the repulsive columbic forces among the particles that eventually can minimize the agglomeration of particles and hence, stabilizing them in the water dispersion (Arvind et al., 2019).

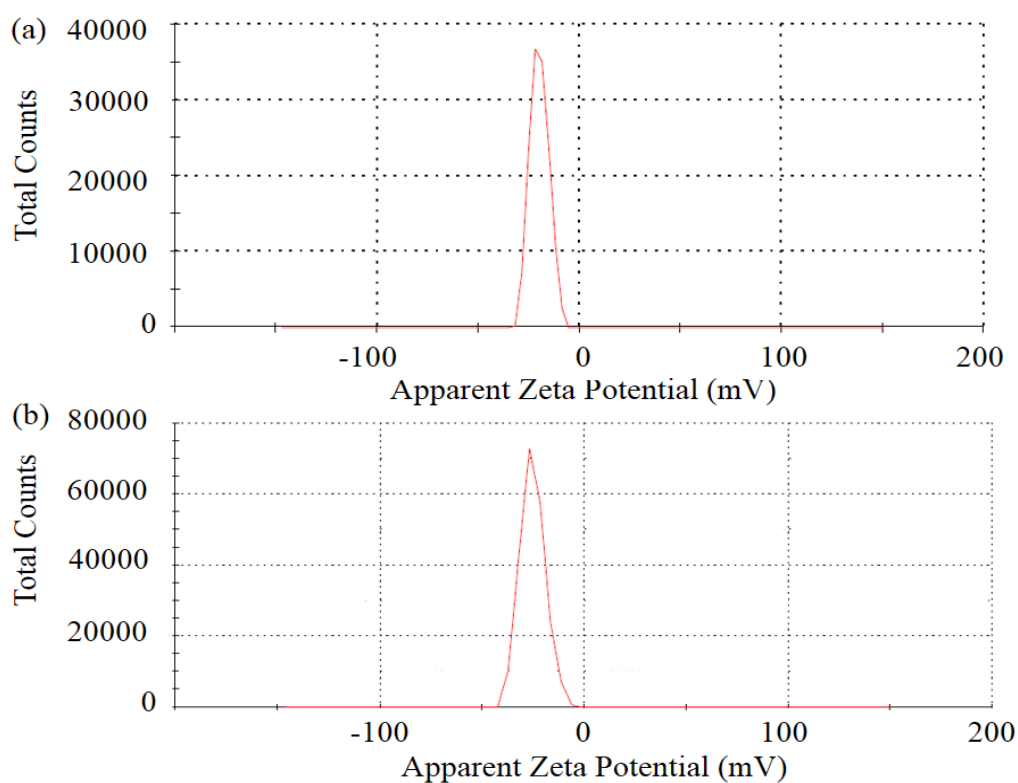


Figure 4.12: Zeta potential analysis of (a) CQDs and (b) NCQDs

4.3.7 Particle sizes distribution

Particle size distribution and surface morphology of the fabricated CQDs and NCQDs are shown in Figs. 4.13a-b and 4.14a-b, respectively. Based on the transmission electron microscopy (TEM) result, the particle sizes of CQDs and NCQDs were found to be in nanometer scale.

Figures. 4.13c and 4.14c show the histograms of CQDs and NCQDs particles diameter versus the area of particle size distribution, respectively. The particle size distribution was calculated by using Image J software (segmentation with Simple Interactive Object Extraction and Circular Selection Tool, by which the diameter of each circle was calculated by the software in the unit of nanometers) (Harris et al., 2018; V. K. Singh et al., 2019).

Histograms indicated that the average particle size distribution of CQD and NCQDs were found to be 3.5 nm and 3.4 nm, respectively. The particle sizes of both CQDs and NCQDs were observed to be in the range of 1-10 nm and in a good agreement with another work (Reshma and Mohanan, 2019).

Results showed that there was no significant difference in the particle size range, indicated that both samples (CQDs and NCQDs) were in quantum dot particle sizes, which are in good agreement with a previously reported work (Piatkowski et al., 2020).

The blazing spots and the diffuse rings in the selected area electron diffraction (SAED) pattern revealed the crystalline nature of CQDs and NCQDs (Tammina et al., 2018), as shown in Figures. 4.13d and 4.14d. Based on this observation, NCQDs could be matched to the (102) diffraction plane of the diamond-like sp^3 carbon and sp^2 graphitic carbon. Besides, NCQDs were self-assembled like a polymer matrix due to the existence of intermolecular hydrogen bond between carboxylic acid and hydroxyl functional groups.

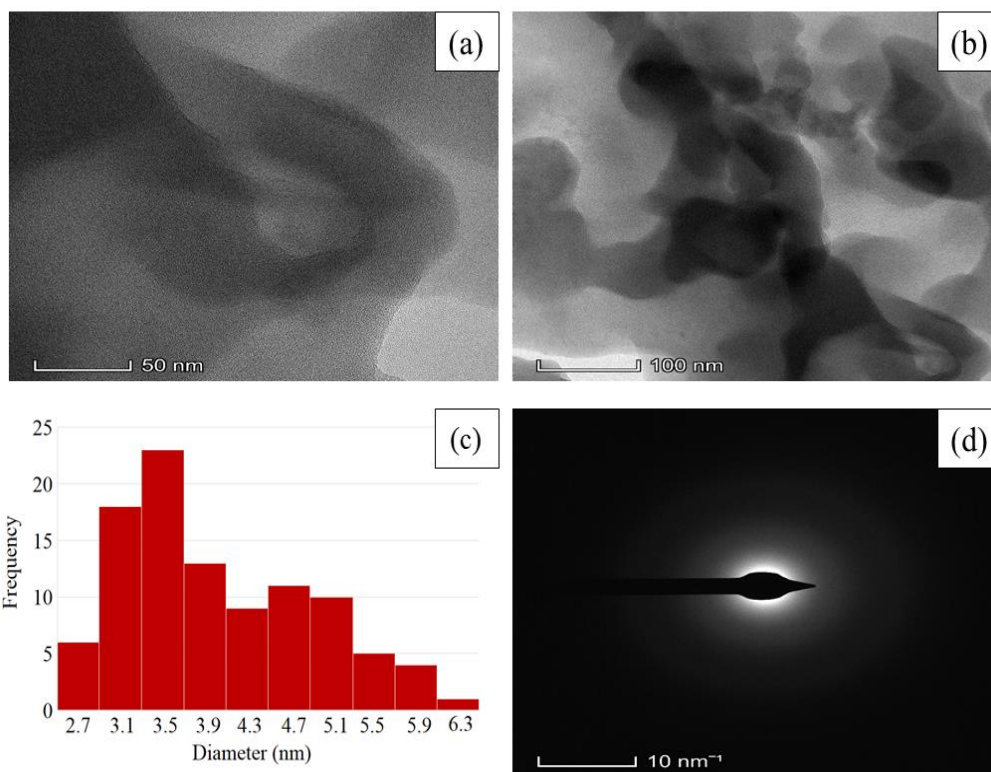


Figure 4.13: TEM images for CQDs surfaces in (a) 50 nm scale, (b) 100 nm scale, (c) a histogram of the particle size distribution of CQDs and (d) SAED pattern of CQDs.

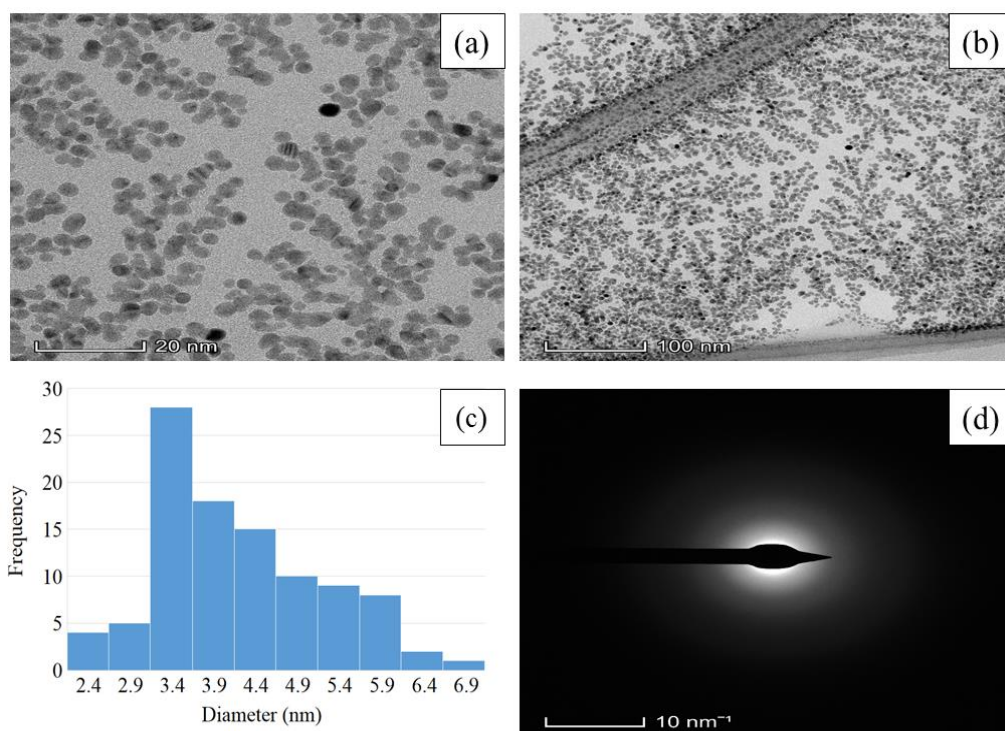


Figure 4.14: HR-TEM images for NCQDs surfaces in (a) 20 nm scale, (b) 100 nm scale, (c) a histogram of the particle size distribution of NCQDs and (d) SAED pattern of NCQDs.

4.3.8 Surface morphological studies

Figure 4.15a shows surface morphologies of CQDs. The images show that the products were composed of tiny particles with spherical surface shapes. The distribution of purified CQDs was relatively uniform and smooth. The CQD particles had high surface energy due to the nanosizes of the CQDs, which may lead to the aggregation of particles during the scanning observation.

Figure 4.15b shows surface morphologies of NCQDs. It can be observed that the NCQDs were spherical in shape. The morphology surface image of NCQDs showed unavoidable agglomerations of particles due to the high crystalline surfaces and fine particle sizes. The smaller particle sizes of the CQDs and NCQDs led to the formation of stronger interparticle attractions, which caused the formation of particle agglomerations in the dried sample (Ng et al., 2011; Seipenbusch et al., 2010).

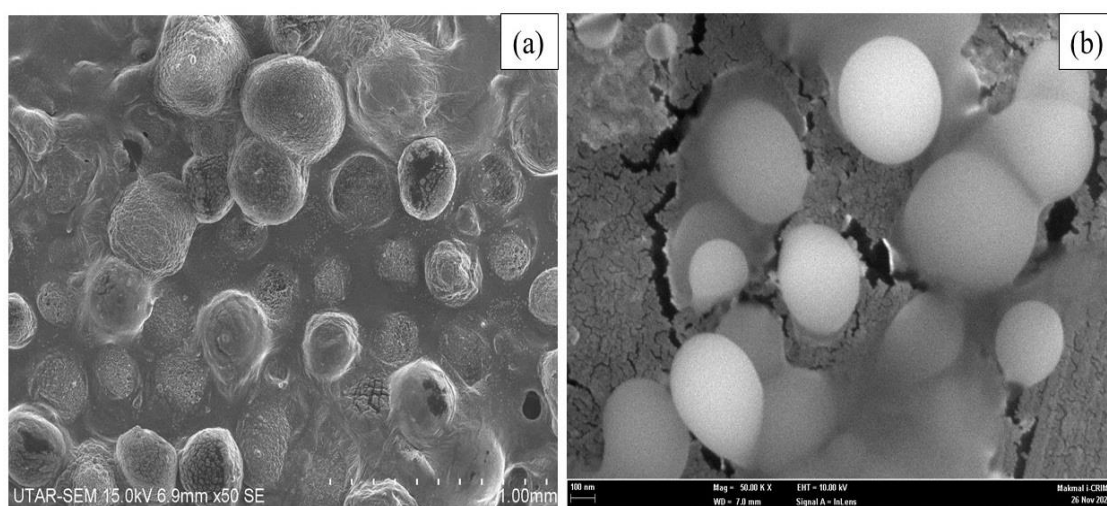


Figure 4.15: (a) SEM image at a magnification of 50.00 kx for CQDs and (b) FE-SEM image of NCQDs produced from empty fruit bunches.

4.4 Photocatalytic degradation of organic dyes by NCQDs

4.4.1 Malachite green

Malachite green (MAG) is a water-soluble triphenylmethane cationic dye which is widely used in the aquaculture industry to treat fungal and protozoa infections. It contains three aromatic rings with functional groups of C=C, C-N, C=N and a methyl group. It is an organic chloride salt, which dissolves easily in water. When MAG solution is exposed to sunlight irradiation, it can be slowly degraded due to the electrostatic attraction between positively-charged MAG and negatively-charged hydroxyl ions from water molecules. UV-light irradiation from the sunlight can generate hydroxyl radical molecules ($\text{HO}\cdot$) (Hsieh et al., 2018).

The $\text{HO}\cdot$ molecules will attack the C=C and C-C bonds that are bonded to the aromatic rings at the centre of the MAG structure to form intermediate products, as shown in Figure 4.16. MAG structure can be easily attacked by free radicals as its structure is not filled with a combination of aromatic rings like other organic dyes. Therefore, it is easily degraded once exposed to sunlight. However, the degradation efficiency rate was very slow at only about 58% within 120 min.

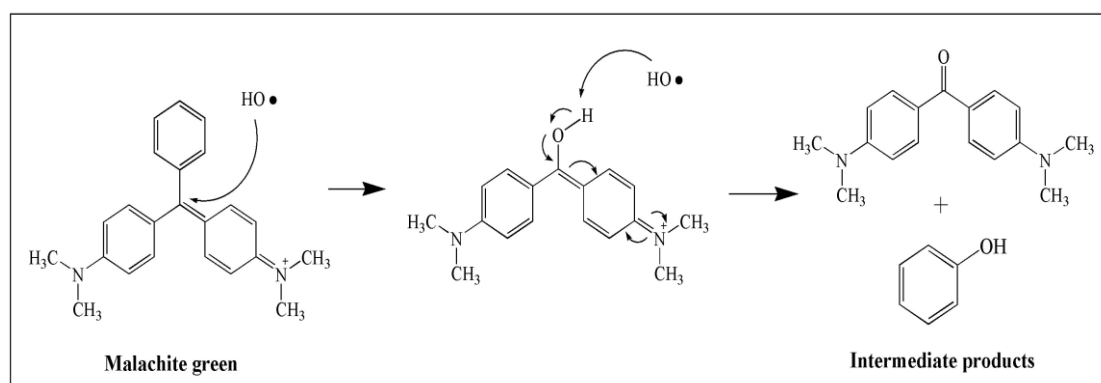


Figure 4.16: The proposed mechanism of MAG degradation without CQDs/NCQDs once exposed to sunlight.

The degradation of MAG dye was found to begin since they were in the dark after NCQDs were added. This was mainly due to the adsorption-desorption activity of MAG dye on the NCQD surfaces due to high surface contact between NCQDs and MAG dye molecules. The negative charges on the NCQDs surfaces increased due to the high NCQDs solution pH at 9.30. Therefore, it would be electrostatically attracted to the positively-charged MAG dye molecules. However, the adsorption-desorption activity in the dark was only 22%.

When the mixture was placed under sunlight irradiation, 98% of MAG could be degraded within 120 min in the presence of NCQDs. While in the absence of NCQDs, only 58% were degraded within 300 min when both sets of experiments were exposed to sunlight irradiation. This result indicated that NCQDs had a significant influence on the photocatalytic activity. Once MAG dye solution was exposed to sunlight irradiation, NCQDs particles absorbed the energy that was supplied by the sunlight. Then, the electrons were transferred from the valence band to the conduction band followed by the production of electrons-hole pairs.

The dissolved oxygen and hydroxide ions would attract electrons and holes to produce free radical molecules, which would oxidize and degrade the MAG dye molecules into non-toxic products such as carbon dioxide and water. The fabricated NCQDs could be acted as efficient photocatalysts because of their ability to absorb a decent portion of the UV-Vis region of the solar spectrum along with positive valence band, which was suitable to increase the photocatalytic redox rate.

4.4.2 Methylene blue

There was least adsorption of methylene blue (MB) dye in the dark because it is a heterocyclic aromatic chemical compound that contains three combined aromatic rings with C-S, C=N and C-N functional groups. Due to the complicated carbon-bonding in the MB structure, the adsorption of NCQDs and MB molecules was difficult.

The least significant of adsorption could be due to the repulsive interactions between the lone pair electrons from NCQDs molecules towards the lone pair electrons of nitrogen and sulphur atoms in the MB structure. Nevertheless, both MB dye solutions with NCQDs and without CQDs/NCQDs have been degraded in the presence of sunlight irradiation. The degradation of MB dye in the presence of NCQDs was found to be higher compared to the degradation without CQDs/NCQDs in which 97% of MB dye was degraded in the presence of NCQDs in comparison to 59% of MB dye degraded without CQDs/NCQDs within 180 min.

The results showed that MB dye solution could be slowly degraded under sunlight even without photocatalyst (NCQDs). This was mainly due to the lone pairs that are located at nitrogen and sulphur atoms in the MB structure. These are electron-rich regions, which became active once they were exposed to sunlight. They exhibited repulsive forces between bond pair electrons, leading to instability, and hence, they attacked the associated water molecules to form a stable bond. Therefore, a reaction between water and MB molecules occurred in which lone pairs attacked the H^+ and OH^- ions to form several intermediate products.

The proposed mechanism for MB degradation without CQDs/NCQDs is described in Figure 4.17. Nevertheless, the degradation process became faster with the aid of NCQDs as photocatalysts under the sunlight irradiation. This was due to the fact that NCQDs possessed unique lone pair states that were contributed by nitrogen atoms, which could produce special fluorescent properties. These lone pair electrons attacked the MB dye structures during the photocatalytic activity (Chengzhuang Zhou et al., 2020), which improved the degradation process.

The fabricated NCQDs in this study could improve charge separation by hindering charge recombination. Therefore, the separation and the recombination of electron-hole pairs was improved, resulting in higher performance for photocatalytic degradation activity. The result indicated that the NCQDs could provide more efficient sunlight utilization to produce more photoinduced electrons and holes (Qu et al., 2020b).

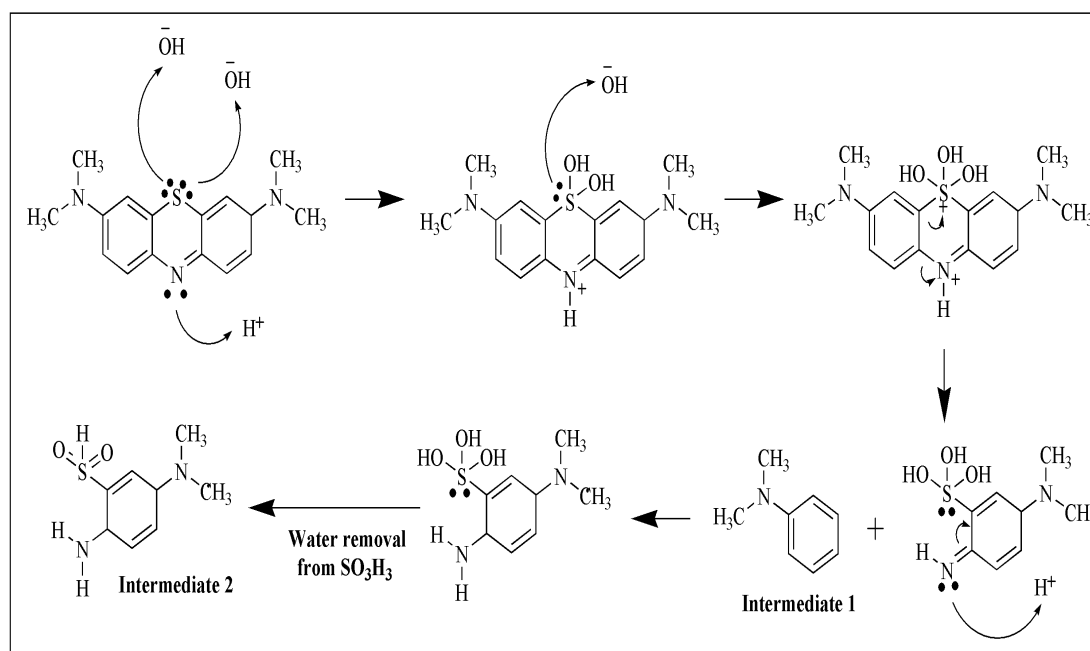


Figure 4.17: The proposed mechanism of MB degradation without CQDs/NCQDs once exposed to sunlight.

4.4.3 Methyl orange

Figure 4.18 shows the photocatalytic degradation rate of methyl orange (MO) dye obtained from UV-Vis absorbance. In the absence of NCQDs (Figure 4.18a), the degradation rate was only 11 %, while in the present of NCQDs (Figure 4.18b), 58% of MO dye molecules were degraded within 300 min when both sets of experiments were exposed to sunlight irradiation.

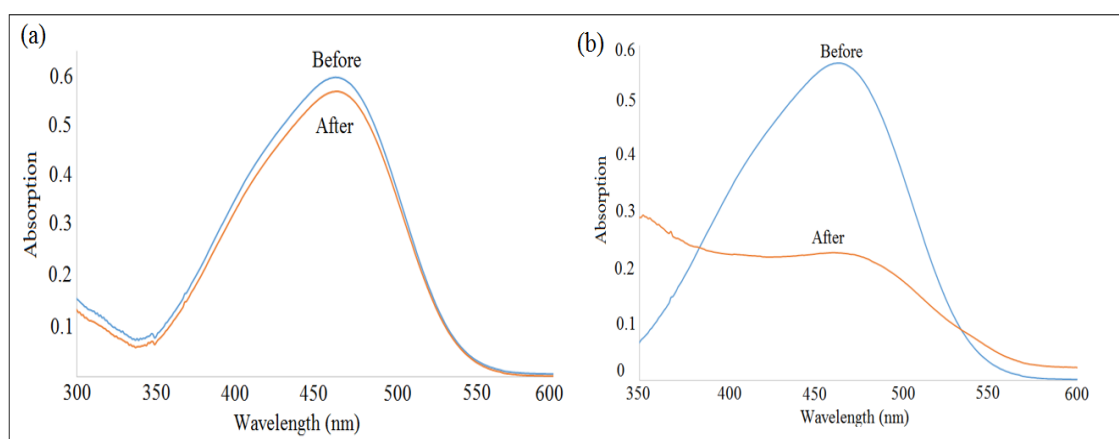


Figure 4.18: The degradation rates of MO dye solution at pH 7 (a) without CQDs/NCQDs and (b) with NCQDs under sunlight irradiation before and after 300 min of sunlight irradiation exposure.

There was no photocatalytic degradation occurred in the absence of CQDs/NCQDs due to the high stability and poor biodegradability of MO dye structure as the MO molecules consist of azo bonds ($N=N$), which are the highly stable nitrogen double bonds. At the same duration of photocatalysis in the presence of photocatalysts (NCQDs), the absorption peak decreased, showing the MO dye molecules degradation by the fabricated NCQDs. Even though the duration of exposing to sunlight was increased, the degradation rate remained constant due to some repulsion forces between the negatively charged NCQDs and MO dye. Therefore, there was no significant degradation activity towards MO dye.

4.4.4 Methyl green

In the presence of NCQDs, about 99% of methyl green (MEG) dye solution could be degraded in 30 min of UV-light irradiation. Figures 4.19 (a-b) displays plots of UV-light absorption spectra for the degradation of MEG dye under UV-light irradiation within 30 min in which the trend showed that the concentration of the MEG dye gradually decreased with increasing irradiation time at time intervals of 30 min.

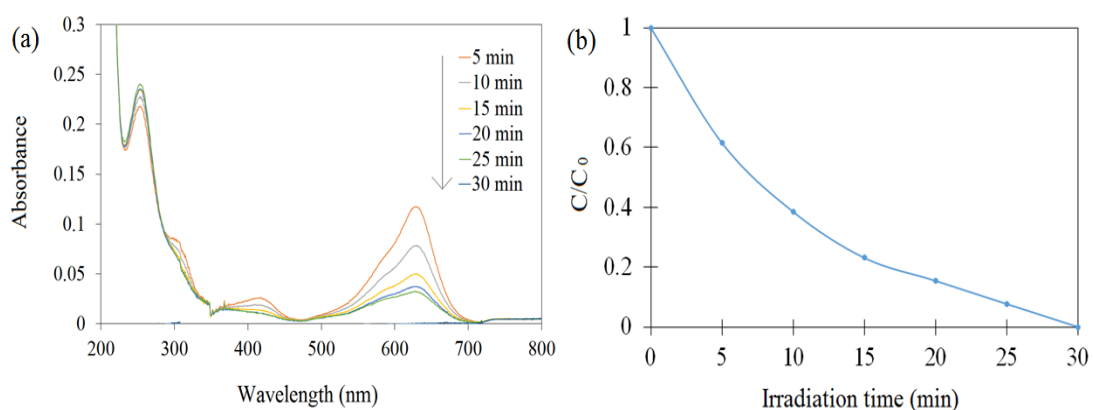


Figure 4.19: (a) Plot of UV-light absorption spectra for the degradation of MEG dye within 30 min and (b) photocatalytic degradation efficiency of MEG dye by NCQDs under UV-light irradiation within 30 min.

In the absence of NCQDs, MEG dye molecules were stable without any oxidation-reduction reactions. The excited electrons and oxidizing free radicals would not be generated in the photocatalytic system. Therefore, the degradation activity was relatively slow as only 38%. When NCQDs were added to the MEG dye solution, the excited electrons were further shuttled through the NCQDs structural framework. Therefore, the charge separation process and the generation of active radicals could be performed (Mahmood et al., 2020), bringing about a higher possibility to degrade the MEG dye, leading to remarkable photodegradation activity.

4.4.5 Mechanism of photocatalytic degradation by NCQDs

The fabricated NCQDs from EFB in this work could be an effective photocatalyst in the photocatalytic degradation of organic dyes. While in the dark condition, the adsorption rate decreased gradually until it reached the adsorption-desorption equilibrium within a duration of 60 min and remained constant up to 120 min. Figure 4.20 shows the plot of the adsorption-desorption equilibrium, indicating that the degradation activity in this work was primarily contributed by the photocatalytic degradation instead of adsorption.

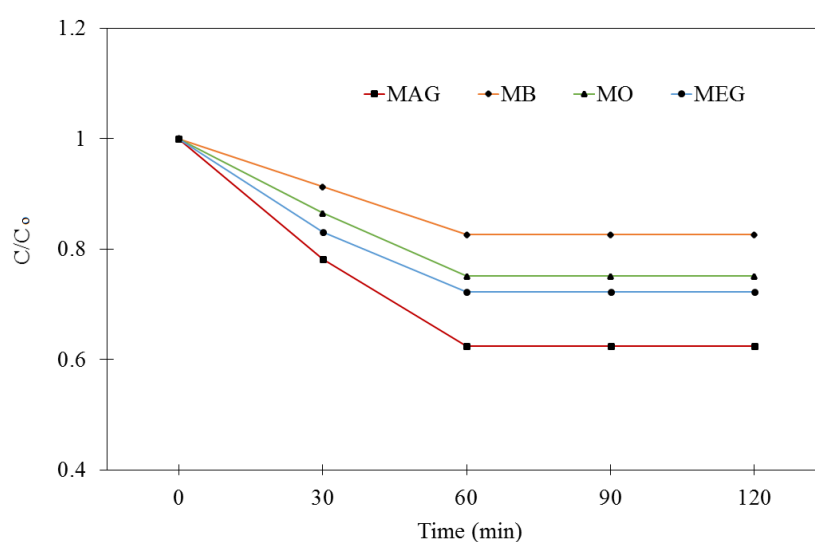


Figure 4.20: The adsorption-desorption equilibrium of different dyes using the NCQDs within 60 min in dark.

The excellent electronic conductivity of the fabricated NCQDs can improve the UV-light absorption intensity. Therefore, the NCQDs fabricated from the EFB fibers showed a lower photoluminescence excitation intensity of 386 nm, suggesting an extremely low recombination rate of photo-generated charge carriers (Hunge et al., 2021), which could contribute to the effective

photocatalytic degradation activity. Figure 4.21 shows the increasing trend in the photo-degradation activity of different dyes under sunlight irradiation.

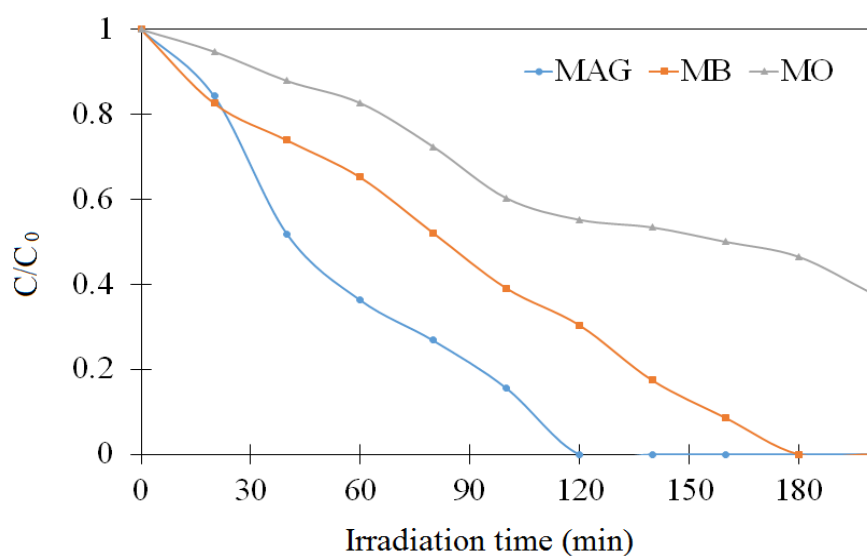


Figure 4.21: Photocatalytic degradation efficiency of MAG, MB and MO dyes by NCQDs under sunlight irradiation within 180 min.

NCQDs can serve as the electron reservoirs to trap photo-generated electrons and reduce the electron-hole recombination significantly, and thus improving the photocatalytic degradation of organic dyes. The significance of using NCQDs as photocatalysts in the photocatalytic degradation is due to the nitrogen doping to the CQDs, which affects their energy band gaps. The larger energy band gaps of NCQDs, the higher possibility in creating a new energy levels in the conduction and the valence bands, leading to the formation of new electron transfer pathways in the band regions of the fabricated NCQDs.

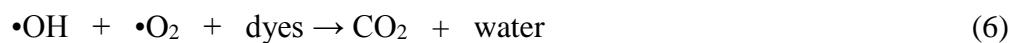
The contribution of a nitrogen atom to the CQD surfaces can significantly induce the charge delocalisation and thus, efficiently prevent the recombination of photo-excited charge carriers (Aghamali et al., 2018). Hence, the electron transfer ability of NCQDs can be more efficient because they possess high quantum yield and strong photoluminescent properties. As a

result, more photoinduced electrons and holes participate in the photocatalytic degradation of organic dyes.

Under the sunlight irradiation, NCQDs were conducive to providing more active sites and shortening the paths of electrons transportation. NCQDs can significantly promote the charge separation process during photocatalytic degradation activity, and hence, the electron-hole pairs are generated. Subsequently, the electrons (e^-) and holes (h^+) migrate to the NCQDs surfaces for oxidation and reduction reactions in order to generate free radical molecules. Due to the high oxidation ability of h^+ , it can further oxidize water molecules to form hydroxyl radicals ($\bullet OH$) while e^- can be captured by oxygen molecules to form superoxide radicals ($\bullet O_2$) (Chen et al., 2019).

Photocatalytic degradation of organic dyes in this study was induced by the excess electrons (e^-) and holes (h^+) generated. When the mixture of dye and NCQDs solution were exposed to sunlight irradiation, electrons in the NCQDs particles were excited from the valence band to the conduction band and produced electron-hole pairs. At the same time, oxygen molecules were reduced to the superoxide radicals ($\bullet O_2$), and water molecules were oxidized to the hydroxyl radicals ($\bullet OH$).

These free radical molecules were highly reactive radical species that attacked the dye molecules and degraded them. In addition, the positive holes (h^+) can also directly oxidize the organic dyes or react with water molecules to produce $\bullet OH$ radicals as h^+ is a powerful oxidizing agent. The activation of NCQDs by sunlight irradiation can be represented by the following steps (Eq. (3-6)):



The proposed photocatalytic degradation mechanism of malachite green (MAG) dye is shown in Figure 4.22. The superoxide radicals ($\bullet\text{O}_2$) and hydroxyl radicals ($\bullet\text{OH}$) can be generated on NCQD surfaces that have been activated by sunlight irradiation and consequently contribute to the decomposition of MAG dye molecules. Besides, the generated holes can directly react with hydroxyl ions to generate hydroxyl radicals, acting as strong oxidizing agents in the photocatalytic degradation activity (Jamila et al., 2020).

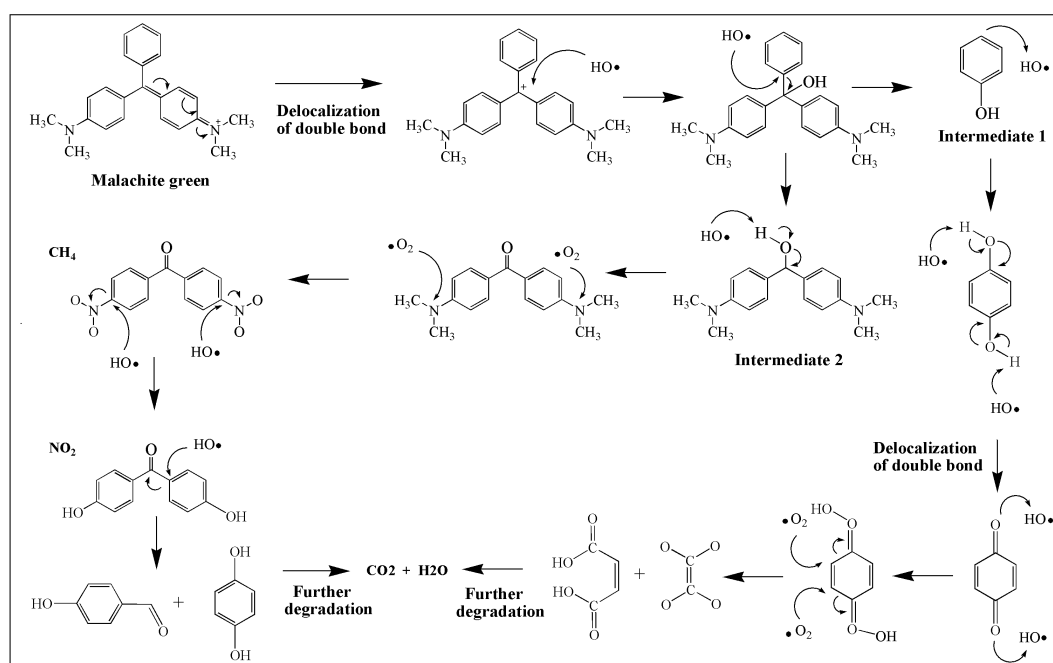


Figure 4.22: The proposed photocatalytic degradation mechanism of malachite green.

The highly reactive free radicals will react with the MAG dye molecules and hence, decompose them into various unstable intermediate products, which finally can be broken down into harmless by-products such as methane (CH₄), nitrogen dioxide (NO₂), carbon dioxide (CO₂), and water (H₂O). In addition, the reactive oxygen species ($\bullet\text{O}_2$ and $\bullet\text{OH}$) are strong oxidizing agents, which can rupture the organic bonds and oxidize most of the organic pollutants.

The photocatalytic degradation mechanism of methylene blue (MB) dye solution catalysed by NCQDs is illustrated in Figure 4.23. When NCQDs was irradiated by sunlight, the radical species ($\bullet\text{OH}$ and $\bullet\text{O}_2$) were generated. These radical species could degrade the MB dye to form several intermediate products that finally decompose into several non-toxic side products such as NH₂, CH₄, NO₂, SO₃, CO₂, and H₂O.

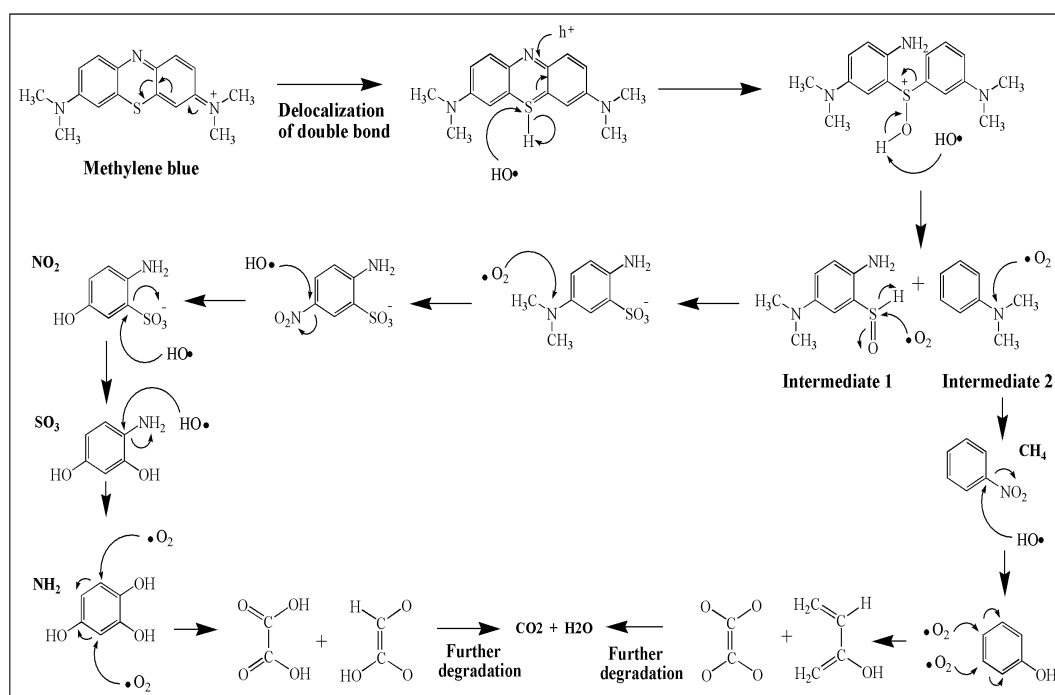


Figure 4.23: The proposed photocatalytic degradation mechanism of methylene blue

The degradation of MB dye was through the decomposition of the chromophoric structure and the destruction of the homo and heteropoly aromatic rings that presented in the MB structure (Jacob et al., 2019). The electrons in the NCQDs can be excited as the NCQDs particles have narrow band gaps, and contribute to the generation of free radical molecules. This led to the decolouration and opening-ring reactions. The improvement of electron-hole transport channels was constructed by the appropriate energy conduction or valence bands. Therefore, the highly feasible migration and separation of electrons and holes could be achieved during the photocatalytic degradation of MB dye.

The catalytic activities of NCQDs towards methyl green (MEG) dye was evaluated under sunlight and UV-light irradiation, in which the wavelength range of UV-light irradiation was within 200 to 400 nm. The degradation rate under visible light was slightly slow because the activation of NCQDs was limited to the visible light range (400 to 800 nm), and the NCQDs molecules did not have enough energy to be excited as photons. The visible light absorption can be extended by photo-sensitizers like quantum dots materials, which could suppress the charge recombination rate.

In fact, sunlight irradiation consists of both visible and UV-light irradiations. Hence, NCQDs can be greatly excited in the presence of UV-light irradiation when the wavelengths are less than 400 nm. NCQDs also can utilize visible light to increase the light absorption intensity and modify the electron density to prevent the charge carrier recombination during a photo-degradation activity.

The photocatalytic degradation mechanism of MEG dye solution catalysed by NCQDs is illustrated in Figure 4.24. The generated active radicals, such as hydroxyl and superoxide radicals, were chemically reactive and highly unstable in their radical forms. These radicals could effectively degrade the MEG dye molecules without other agents. Based on the postulated mechanism, the free radicals stimulated by the NCQD photocatalysts could contribute to the primary degradation activity. The final products of the degradation activity could be carbon dioxide and water molecules.

The presence of various oxygenated-functional groups on the NCQD surfaces could cause band bending, which provided an internal electric field that induces separation of electron-hole pairs, thus, improving photocatalytic activity (Li et al., 2018). The defective surfaces of NCQDs expanded the UV-light utilization and provided more charge carriers in redox reactions. This significantly improved the photocatalytic degradation activity on the MEG dye

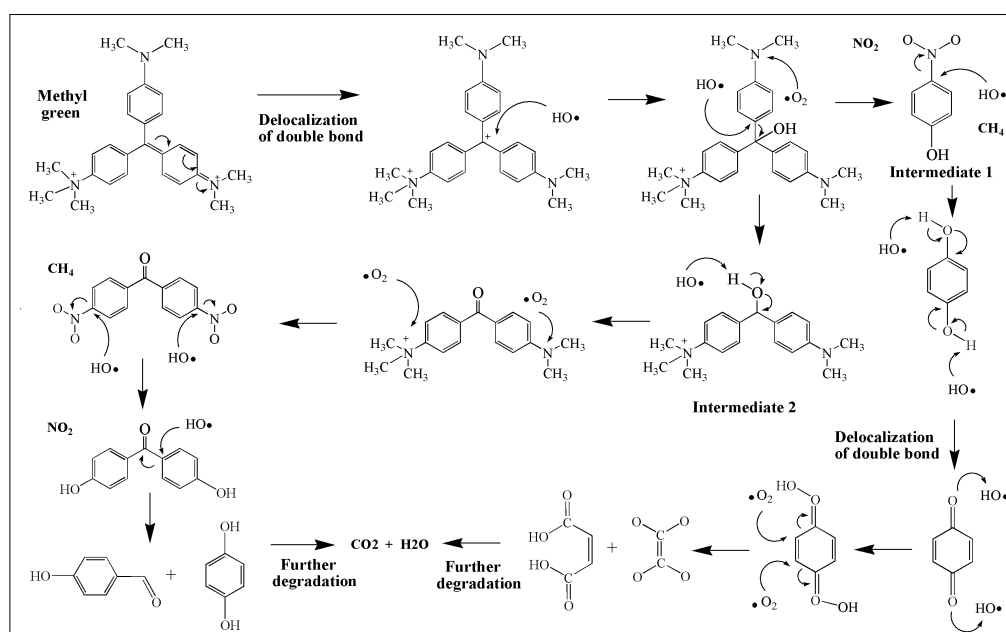


Figure 4.24: The proposed photocatalytic degradation mechanism of methyl green.

4.4.6 Determination of active species

In order to verify the heterojunction type in photocatalytic degradation activity, the contribution of reactive oxygen species was evaluated to determine the radicals that contributed to the photocatalytic degradation activity. Hydroxyl radical ($\bullet\text{OH}$) and superoxide radical ($\bullet\text{O}_2$) are the dominant reactive oxygen species in most photocatalytic processes.

Table 4.2 shows the effect of the scavengers on the photocatalytic degradation of organic dyes in the presence of NCQDs as photocatalysts. The result showed that the dye degradation efficiency became lower after the addition of scavenger agents. The IPA and BQ were the primary inhibitors in the degradation process for all dye solutions.

Table 4.2: The degradation process of organic dye solutions using the NCQDs as photocatalyst in the presence and absence of the scavenger agents.

Organic dyes	Scavenger agents	Degradation efficiency (%)
MAG	IPA	21.54
	BQ	20.08
	Without scavenger	98.54
MB	IPA	18.93
	BQ	21.32
	Without scavenger	91.50
MEG	IPA	23.43
	BQ	21.95
	Without scavenger	99.10

Theoretically, scavenger agents may react with radicals generated during the photodegradation process, decreasing the number of free radicals (Scott et al., 2019). Thus, in the presence of scavenger agents, photocatalytic degradation became ineffective. The presence of scavenger agents could also inhibit the light penetration on the NCQD surfaces during the degradation activity.

Results indicated that the photocatalytic degradation of organic dye solutions using NCQDs was mainly based on the oxidative activity of hydroxyl radicals and superoxide radicals. Moreover, NCQDs possessed highly negative charges in the solution as the pH value of NCQDs solution was 9.3. Therefore, there was a high tendency to generate reactive radicals once exposed to UV-light irradiation. The current study suggests that NCQDs is an excellent fluorescent photocatalyst in the photocatalytic degradation of organic dyes.

4.5 Optimization study by Taguchi approach

Figure 4.25 illustrates the SN ratio for different operating parameters. In general, it was found that the increase of solution pH and initial dye concentration improved the SN ratio of the system, indicating that higher degradation efficiency could be achieved. In contrast, the increase of NCQDs amount and duration only improved the system's performance up to an optimum point, in this case, 10 mL and 20 min, respectively. Among the parameters, pH of dye solution had the highest impact on the system's performance, followed by dye concentration, NCQDs amount and duration of photocatalysis, as shown in the delta analysis of SN ratio in Table 4.3.

Table 4.3: SN ratios for each factor corresponding to its level.

Factors	Mean of Means			Delta (Max-Min)	Priority
	Level 1	Level 2	Level 3		
NCQDs amount	32.32	36.90	32.47	4.57	3
pH of dye solution	24.78	37.03	39.88	15.11	1
Duration	32.52	36.66	32.52	4.15	4
Dye concentration	32.66	32.10	36.93	4.82	2

Figure 4.25 shows that the dye solution could be degraded most efficiently in an alkaline medium due to a high number of hydroxyl molecules. When NCQDs and sodium hydroxide solutions were added to the dye solution, then exposing the medium to the UV-light irradiation, electrons and holes activated by NCQDs could react with hydroxyl molecules and dissolved molecular oxygen to generate reactive hydroxyl radicals (Koohestani and Sadrnezhad, 2016; Saud et al., 2015). Thus, the MEG dye solution could be degraded.

The successful degradation of MEG dye with the addition of sodium hydroxide solution indicated that the high pH values favoured the formation of hydroxyl ions, and there was less competition on the contact between MEG dye and NCQD molecules. Therefore, the percentage of MEG dye degradation was higher in the solution with higher pH (pH 7 – 9).

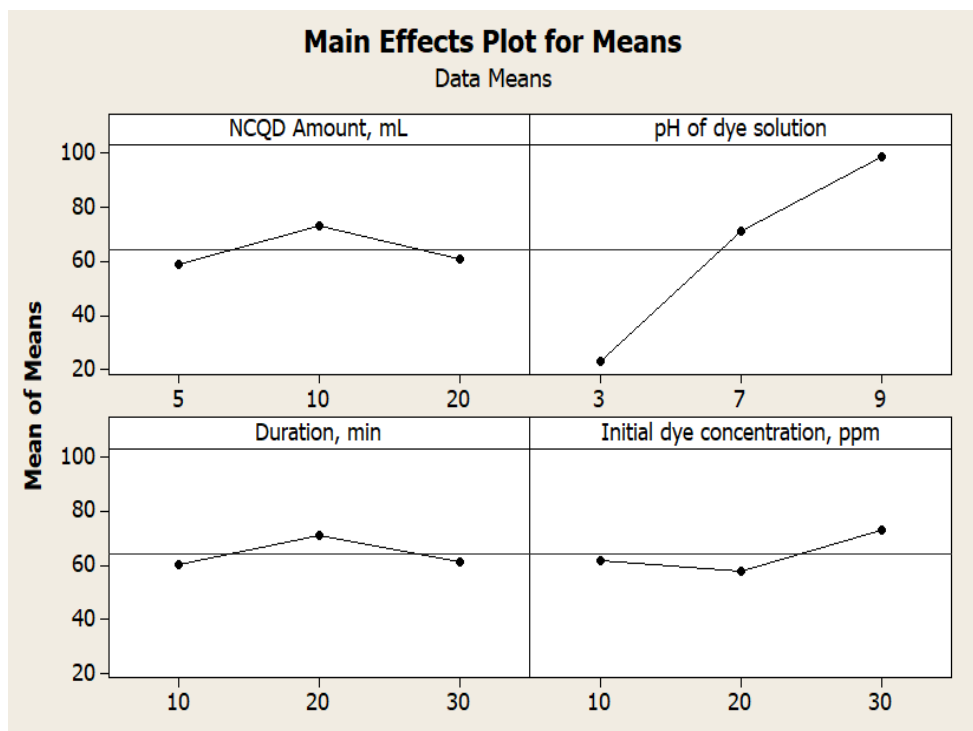


Figure 4.25: Mean of signal-to-noise ratios for four parameters in the photocatalytic degradation of MEG dye.

In contrast, the degradation activity was found to be negligible in the acidic medium, which could be due to the suppression in forming the hydroxyl radicals in acidic solution as the concentration of proton ions were higher than the hydroxyl ions. In addition, the degradation process was prolonged, probably due to the repulsion between NCQDs and cationic dye molecules, owing to the excess positive charges.

Solution at low pH conditions disrupted the NCQD surface hydroxyl groups due to the protonation process that hindered the photodegradation process. The fluorescent properties of NCQDs are slightly weaker in acidic solutions due to the deprotonation of oxygen-containing functional groups (Yang et al., 2021).

The deprotonated oxygen-containing functional groups caused lower energy to be released, which eventually decreased the photocatalytic degradation activity. The degradation activity can be maintained by photocatalysis in a neutral dye solution or at pH 7, by controlling the duration of degradation and the NCQDs amount. Photocatalytic degradation of MEG dye suggested by the Taguchi approach was carried out at pH 7 of dye solution and showed a high photodegradation rate.

Apart from pH of the dye solution, Figure 4.25 also shows that the degradation activity became faster when the initial dye concentration was increased. The higher photodegradation activity at a higher initial dye concentration was mainly due to a higher degree of attraction and reaction between NCQDs and dye molecules. The effective contacts between the oxidizing species and dye molecules were enhanced, resulting to higher degradation efficiency. In contrast, this study revealed that the sufficient amount of NCQDs was 10 mL at a concentration of 10 ppm for every 100 mL of dye solution of 10 ppm for the photocatalytic degradation activity. In addition, this amount could provide sufficient active sites in the solution in generating a higher number of radicals during photo-degradation activity.

Nevertheless, it is noteworthy that beyond this dosage, the suspension's turbidity in the mixture caused by the NCQDs could decrease UV-light penetration. The higher suspension's turbidity could reduce the UV-light irradiation from reaching the particle surfaces and caused lower degradation efficiency. Lastly, the duration for dye degradation activity was least significant according to the delta analysis ranking in Table 4.3.

The dye degradation duration was usually highly dependent on the initial dye concentration and the amount of NCQDs used in photocatalysis. Nevertheless, the results showed that the SN ratio for MEG dye degradation was preferable in 20 min. The degradation performance, in general, showed that the degradation efficiency was stable at 60-70% for the degradation duration between 10-30 min.

Based on the results as shown in Figure 4.25, the desirable levels of the parameters were concluded at: dye solution pH of 7 to 9, initial dye concentration of 30 ppm, NCQDs amount of 10 mL, and degradation duration of 20 min. Two sets of confirmation runs have been conducted, and it was found that an average value of 99.2% MEG dye degradation could be obtained from this study.

4.6 Photocatalytic kinetic study

4.6.1 First-order kinetics model

Figures 4.26 (a-b) show that the degradation of MB dye in the presence and absence of NCQDs follow first-order kinetic model, where high correlation of determination (R^2) of 0.9966 and 0.9959 are observed, respectively. Higher kinetic rate constant of $1.79 \times 10^{-2} \text{ min}^{-1}$ was observed when NCQDs are present in the process, in comparison to $1.28 \times 10^{-2} \text{ min}^{-1}$ in the experiment that was in the absence of NCQDs.

The results for degradation of MAG dye show similar trend, as shown in Figures 4.26 (c-d). High R^2 of 0.9987 and 0.9984 are observed for the experiments that are in the presence and absence of NCQDs, respectively.

The rate constant for was found to be higher ($1.92 \times 10^{-2} \text{ min}^{-1}$) when NCQDs were present in the system in comparison to the system that is without CQDs/NCQDs ($0.68 \times 10^{-2} \text{ min}^{-1}$). Based on the results, it can be concluded that the photo-kinetic degradation of MB and MAG dyes obeyed first-order kinetics model and the degradation rates of both dyes in the presence of NCQDs were higher compared to the degradation rates without CQDs/NCQDs.

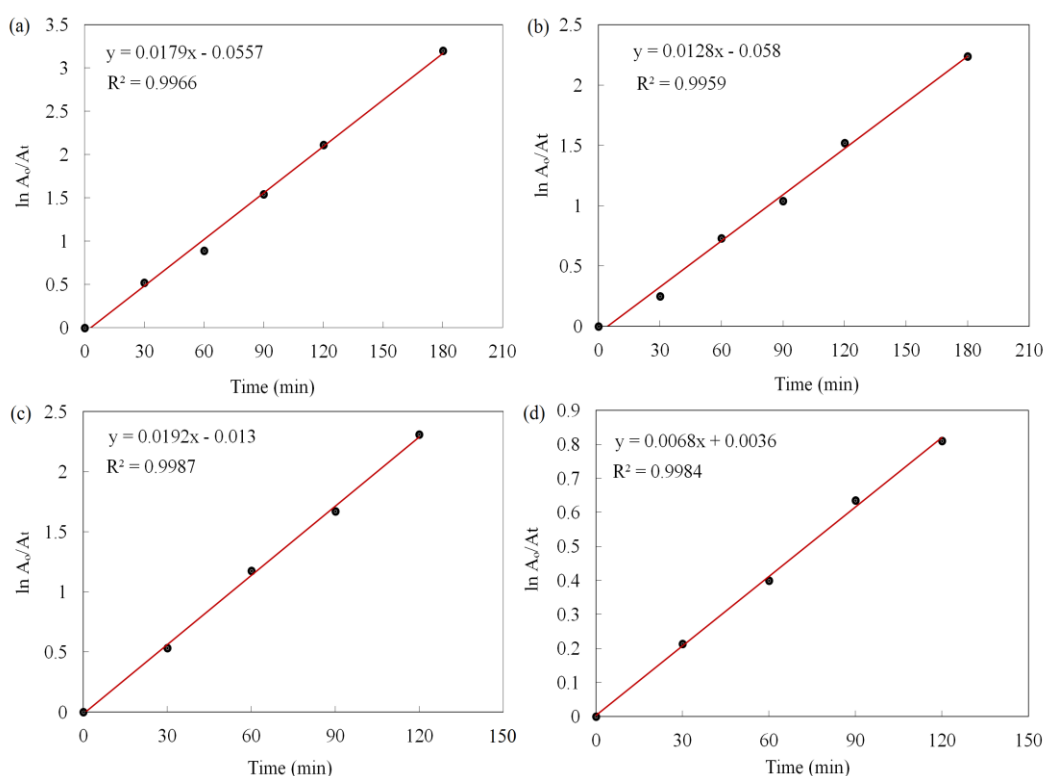


Figure 4.26: Graphs of $\ln(A_0/A_t)$ versus sunlight irradiation time for photocatalytic degradation of organic dyes: (a) MB dye in the presence of NCQDs; (b) MB dye in the absence of NCQDs; (c) MAG dye in the presence of NCQDs and (d) MAG dye in the absence of NCQDs.

4.6.2 Pseudo-second-order kinetics models

As illustrated in Figure 4.27, the kinetic study shows a linear plot of t/C_t versus irradiation time with a correlation coefficient of 0.9934, and the rate constant of photocatalytic degradation activity was 3.3386 ppm/min. The linear plot with a high correlation coefficient suggested that the pseudo-second-order model can describe the photocatalytic degradation of MEG dye by NCQDs. The photodegradation reaction might occur on the surface of the active sites of the NCQDs.

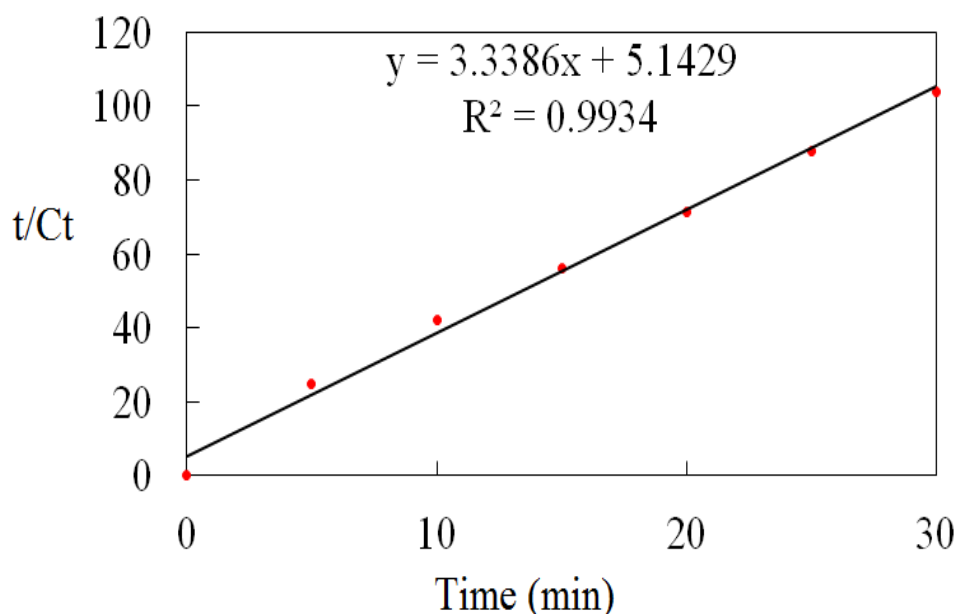


Figure 4.27: A plot of t/C_t versus UV-light irradiation time for photocatalytic degradation of MEG dye.

The negative surface charges of NCQDs favoured the electrostatic interaction with the positively charged MEG dye. Then, when the solution of MEG dye was exposed to UV-light irradiation, the NCQD particles become active in releasing electrons for excitation. More free radicals could then be generated, leading to better degradation of the MEG dye molecules.

In this study, the high kinetic rate in MEG photodegradation can be explained by nano-sized NCQDs, which possessed large surface area, high conductivity, and high capability in electron capture. NCQDs could break down the dye molecules due to ionic mobility, while the high kinetic rate indicates an enhanced ionic movement to convert them into less toxic components (Rehman et al., 2020). The results indicated that the NCQDs fabricated from empty fruit bunches are a significant photocatalyst in the photodegradation of MG dye molecules.

4.7 Stability and reactivity study

The stability of NCQDs was evaluated based on their reusability. Figure 4.28 shows that 99% MEG dye was degraded in the first cycle of NCQDs application. The degradation efficiency was slightly decreased at the subsequent cycles, which might be attributed to the surface oxidation of NCQDs that could reduce the number of reactive sites on the NCQD surfaces (Zhao et al., 2020).

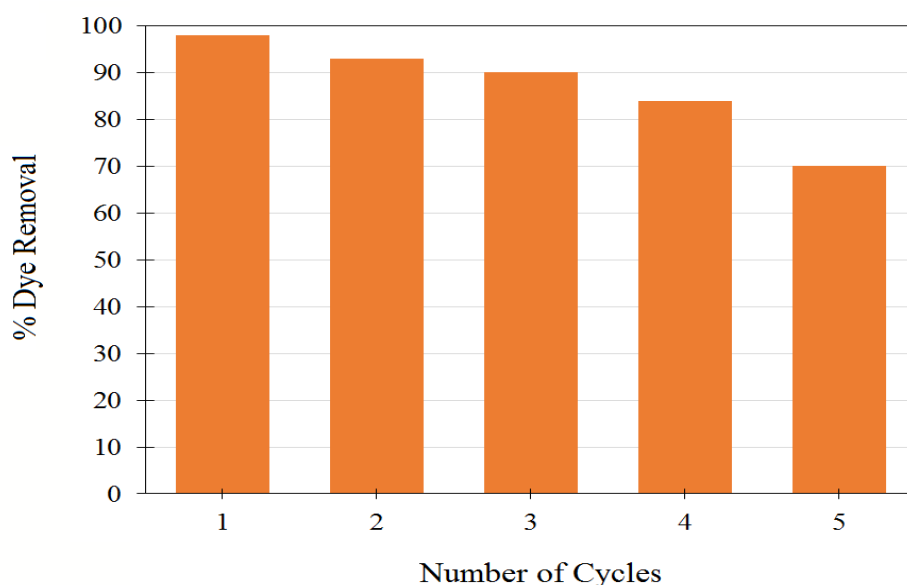


Figure 4.28: The reusability of NCQDs for at least five consecutive cycles.

The decrease in degradation efficiency in the subsequent cycle of photocatalysis could be explained by the loss of NCQDs during the separation of NCQDs from the solution by column chromatography. Nevertheless, it is noteworthy that the degradation efficiency remained above 70% for the consecutive cycles, indicating that the fabricated NCQDs possessed good reactivity and stability. The hydrophilic property of the polar functional groups on the NCQD surfaces enhanced the stability of NCQDs in aqueous systems, which could improve the electron transfer capabilities during the photodegradation activity (Seng et al., 2020).

In addition to maintaining high stability in photocatalytic behaviour during the operation, the fabricated NCQDs from empty fruit bunches were stable when stored for more than twelve months in a 5 °C refrigerator due to their strong chemical bonds and colloidal stability in distilled water.

The stability of the NCQDs in deionized water could be explained by the functional groups present in their structures. The NCQDs can form intramolecular and intermolecular hydrogen bonds with water molecules, thereby enhancing the hydrophilicity properties and preventing the corruption of chemical structure (Han et al., 2020). Since the fabricated NCQDs were prepared from agricultural waste and without toxic chemicals during the fabrication process, they are non-toxic in characteristics and convenient for long-term storage.

Figure 4.29a shows the degradation efficiency of MEG dye using the fabricated NCQDs before storage for twelve months. In order to evaluate the stability and reactivity of the fabricated NCQDs, they have been used as a photocatalyst in the degradation of MEG dye after twelve months of storage.

Figure 4.29b shows the degradation efficiency of MEG dye using the stored NCQDs. The results showed that the NCQDs maintained their fluorescent properties after being stored up to twelve months, suggesting a consistent efficiency after the long storage duration.

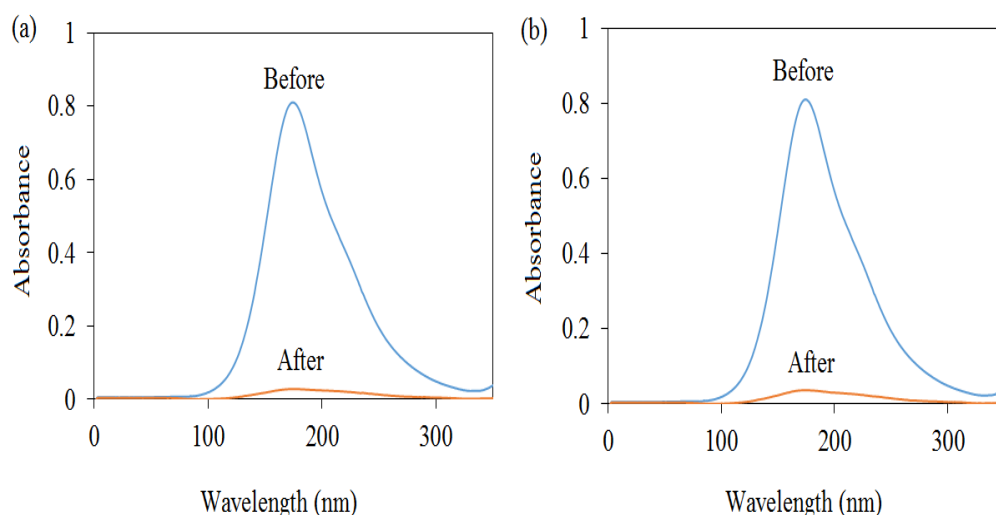


Figure 4.29: (a) The degradation rate of MEG dye using NCQDs before storage for twelve months and (b) the degradation rate of MEG dye using NCQDs that have been stored for twelve months.

The excellent stability could also be attributed to the π - π stacking interactions between the NCQD sheets, which exhibited significant tolerance against photo-bleaching under continuous UV-light irradiation. The fluorescence properties of NCQDs were also stable due to the lone pairs of electrons contributed by nitrogen atoms, which served as electron donors to supply electrons to the π -conjugated system of carbon.

Thus, the surface electrons and diffusion channels of NCQDs structure were improved, contributing to the high stability of NCQDs in the solution. Nitrogen doping can efficiently induce charge delocalization and tuning the work function of carbon, which effectively changes the electronic characteristics and energy states of NCQDs.

Moreover, the electron transfer capability of carbon materials can be efficiently promoted to enhance the desirable photocatalytic performance in degrading the MEG dyes through the fabrication of NCQDs from empty fruit bunches.

4.8 Evaluation on the degraded dyes

Total organic carbon (TOC) can be an appropriate parameter to measure organic carbon concentration in the degraded dye solution. The lower value of TOC indicated a better performance of NCQDs in the degradation of organic dye solution. Generally, the degraded dye solution consists of water and carbon dioxide molecules (Iqbal et al., 2021b). However, there is a high possibility that the degraded dye solutions contain other eliminated products, which can be estimated using the TOC analysis. Table 4.4 shows the TOC values before and after the photocatalytic degradation activity as well as the percentage of TOC removal.

Table 4.4: TOC values before and after the photocatalytic degradation by NCQDs

Organic dyes	TOC removal of the organic dyes		
	Before (mg/L)	After (mg/L)	TOC Removal (%)
Methylene blue (MB)	84.6	13.4	84.2
Malachite green (MAG)	69.5	20.8	70.1
Methyl green (MEG)	24.6	7.9	67.8

Based on the TOC results, the concentration of organic carbon in the degraded dye solutions after the photocatalytic degradation activity was slightly lower, signifying the photocatalytic degradation of organic dye solution.

This result also indicated that the degraded dye solution contained sufficient oxygen molecules and less toxic, which was less harmful to aquatic life and environment. The TOC result suggested the successful mineralization of dye solution by NCQDs to carbon dioxide and water molecules. Thus, the fabricated NCQDs from empty fruit bunches exhibited desirable mineralization ability towards dye solution. The mineralization ability of the NCQDs showed their potential for wastewater treatment, especially when dealing with organic pollutants.

4.9 Comparisons of CQDs and NCQDs performance

In this study, NCQDs fabricated from the empty fruit bunches could be a good photocatalyst in the photocatalytic degradation of organic dye solution. Due to their excitation-dependent photoluminescence behaviour, the fabricated NCQDs could be an excellent electronic conductivity to facilitate electrons transport, and hence improving the photocatalytic degradation activity. The nano-sized NCQDs possessed a large surface area with the plenty of active surfaces, improving UV-light absorption and contributing to higher redox reactions (Meghdad et al., 2018).

High electron mobility in NCQDs will improve the charge transfer ability and leads to the suppression of electron-hole recombination rate. Besides, by referring to scavenging experiments, the redox reactions could be performed to produce active radicals. In addition, the fluorescent NCQDs that was fabricated from the empty fruit bunches possessed 3.4 nm in particles sizes, indicating their high capability in emitting greenish-blue fluorescence when exposed under UV-light irradiation.

The greenish-blue fluorescence of NCQDs can be categorized as the smallest quantum dots in particle size with a larger energy band-gap, reducing the possibility of radiation recombination. This result could produce a high number of electron and hole pairs, thereby improving the photocatalytic degradation of organic dye in a sustainable reaction approach.

Figures 4.30 (a-b) show that the presence of NCQDs provides higher degradation rate for MB and MAG dyes. The rapid dye degradation could be attributed to large number of active surface sites that are processed by NCQDs for improved light harvesting capability and photocatalytic degradation reaction.

In the presence of various functional groups on the NCQD surfaces, a higher number of photo-reactive sites can be expected, which can increase the electron transfer between the catalyst and organic dye molecules. Therefore, NCQDs may be considered to be good electron transporters and acceptors, which make them good candidates for the fabrication of photocatalysts.

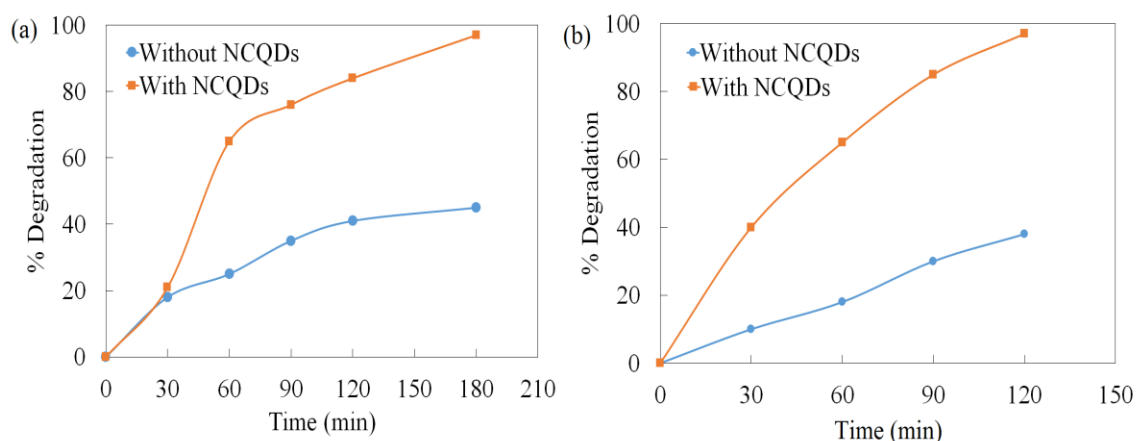


Figure 4.30: Comparison of the degradation rate of dyes in the presence and in the absence of NCQDs, versus UV-light irradiation exposure time: (a) MB dye and (b) MAG dye.

In order to evaluate the performance of NCQDs as an excellent photocatalyst, the photocatalytic degradation experiments were carried out in the presence of CQDs, NCQDs and without the presence of any photocatalyst. Table 4.5 shows the photocatalytic degradation percentage of malachite green, methylene blue, methyl green, and methyl orange dye solutions at initial concentration of 20 ppm. The NCQDs amount used in these experiments was 10 mL at a concentration of 10 ppm, and the pH solution was in pH 7.

Table 4.5: Photocatalytic degradation of dye using CQDs, NCQDs and without catalyst.

Dyes	Type of photocatalysts			Reaction Time (min)
	No catalyst (%)	CQDs (%)	NCQDs (%)	
MAG	15.25	48.32	98.54	120
MB	23.12	51.65	95.13	180
MEG	21.35	39.27	99.91	30
MO	11.23	25.67	58.32	300

Based on the Table 4.5, the NCQDs showed the highest percentage of degradation rate compared to CQDs and without the presence of photocatalyst. The molecular structure of CQDs conjugated with π electron systems increased the capability of donating and accepting electrons.

Additionally, in the presence of nitrogen (N) atom, NCQDs could induce charge delocalization efficiently, consequently enhance the fluorescent properties. The atomic size of nitrogen atom is similar to the carbon atom. Both atoms can be covalently bonded to each other, thus, induced the surface defects of CQDs (Koe et al., 2020). Besides, the electrons in the reaction system can be easily transferred since NCQDs are good electron acceptors and donors.

The surface defects of NCQDs could enhance the electronic conductivity properties in order to accelerate the transport of electrons while improving the electron concentration of NCQDs. Therefore, NCQDs that was fabricated from empty fruit bunches performed as a powerful energy-transfer component in photocatalyst material for photocatalytic degradation application.

NCQDs showed better performance compared to CQDs due to the different characteristics in terms of optical and fluorescence properties. The doping element corresponding to a relatively wide distribution of different energy levels to generate a broad UV-light absorption band. In the presence of nitrogen atoms, the electronegativity of the CQD structure could delocalize electrons, creating an electron-rich condition.

The presence of urea molecules in the fabrication of NCQDs increased the number of oxygen atoms as well, resulting in surface oxidation, which primarily serves as a capture centre for excitons, thus giving rise to surface-state-related fluorescence. As the density of the nitrogen-state increased, the quantum yield of NCQDs also improved, in which electrons can be trapped by the new surface states, contributing to the high generation of free radicals. Therefore, NCQDs were more effective in degrading organic dyes compared to CQDs. This study has proven that the fabricated NCQDs from EFB without any additional oxidizing agent or chemicals could be functionalized as an excellent photocatalyst in the photocatalytic degradation of organic dyes. Table 4.6 shows the photocatalytic degradation performance towards organic dye reported by other studies using CQDs-based photocatalyst.

Table 4.6: Photocatalytic degradation performance towards organic dyes reported from other studies.

Raw materials	Photocatalyst composites	Degradation efficiency	References
Cellulose nanofiber hydrogel and titanium dioxide	CQDs/TiO ₂	Up to 92% of methylene blue could be degraded.	(Gong et al., 2022)
Spent coffee grounds, urea and titanium dioxide	NCQDs/TiO ₂	Up to 93.1% of methylene blue could be degraded.	(Jin et al., 2023)
Carbon nitride nanosheets, bismuth tungstate, methyl alcohol, ethanol, citric acid.	CQDs-carbon nitride nanosheets/bismuth tungstate	Up to 90% of norfloxacin could be degraded	(Liu et al., 2022)
Citric acid, urea, zinc nitrate hexahydrate and trisodium citrate dehydrates.	NCQDs/ZnO	Up to 80% of norfloxacin could be degraded	(Widiyandari et al., 2023)
Polyvinyl pyrrolidone, bismuth (III) nitrate, and potassium bromide.	CQDs/BiOBr	Up to 94% of RhB dye could be degraded	(Liang et al., 2018)
Ascorbic acid, Niobium pentoxide, glycol and potassium hydroxide	CQDs/KNbO ₃	Up to 70% of crystal violet dye could be degraded	(Qu et al., 2018)
Lignin, urea and deionized water	NCQDs	Up to 99% of methylene blue, malachite green and methyl green could be degraded	This study

CHAPTER 5

CONCLUSION AND RECOMMENDATION

5.1 Summary of study

NCQDs were successfully fabricated using lignin that was extracted from the EFB biomass as raw materials through a hydrothermal treatment and nitrogen-doping procedure, due to the presence of sufficient carbon, oxygen and hydrogen content in the lignin structure.

The average particle size of NCQDs was found to be 3.4 nm. The crystallinity phases of NCQDs showed excellent interfacial charge transfer and increased light-harvesting capacity, leading to enhanced photocatalytic degradation activity.

The fabricated NCQDs is a photoluminescence material that can improve the UV-light utilization properties. The excellent electronic conductivity of NCQDs can enlarge the photon absorption region and improve the UV-light absorption intensity. Therefore, the fabricated NCQDs showed excellent performance in the photocatalytic degradation of organic dyes. They can degrade the MAG, MB, MO and MEG dyes up to 98%, 97%, 58% and 99%, respectively when exposed to sunlight or UV-light irradiation.

In contrast, in the absence of NCQDs, the photocatalytic degradation rate was very low as only 58%, 59%, 11% and 38% for MAG, MB, MO and MEG dye, respectively. From the Taguchi study, pH of dye solution had the highest impact on the system's performance, followed by dye concentration, NCQDs amount and duration of photocatalysis. The Taguchi model reported that the desirable levels of the parameters were concluded at: dye solution pH of 7 to 9, initial dye concentration of 30 ppm, NCQDs amount of 10 mL, and the duration of degradation of 20 min.

The photocatalytic reaction kinetics for MB and MAG dyes were successfully identified by the Langmuir-Hinshelwood (L-H) model, which were expressed by a first-order kinetics model. Meanwhile, the photodegradation process of MEG dye follows a pseudo-second-order kinetic model, with a 3.3386 ppm/min rate constant. NCQDs from this study were recovered using a column chromatography and reused for at least five consecutive reaction runs while maintaining their photodegradation capability towards the MEG dye solution at above 70%. The NCQDs also displayed excellent stability in photocatalytic performance in degrading the dye molecules after being stored for 12 months at 5 °C. The excellent performance of the NCQDs fabricated from EFB offers a new alternative to producing a highly efficient and non-toxic photocatalyst that could decompose a wide range of organic pollutants. This study also found that NCQDs are more efficient than CQDs as photocatalysts, which could be explained by the high fluorescent properties of NCQDs through the nitrogen-doping method. These revealed that NCQDs showed favorable photocatalytic properties for organic dye degradation.

5.2 Recommendations of future works

Future advances in the area of semiconductor photocatalysts have the potential to be developed in treating wastewater by applying the sustainable approaches. Current study has successfully used urea as a nitrogen source in the fabrication of NCQDs from EFB. In the future study, urea can be replaced with other green nitrogen sources. Besides, review study on the chemical structure of lignin that extracted from other biomass will be considered in future work in order to study the properties differences between the lignin from empty fruit bunches.

Another significant area in future research is to modify the structure of NCQDs by varying the raw materials and the doping elements used. The modification in the NCQDs structure is crucial in making the photocatalysts suitable in degrading both cationic and anionic organic dyes.

CQDs and NCQDs can appear in various fluorescent colour, which indicating the differences in their particle sizes. Therefore, the fabrication of CQDs or NCQDs possessing different fluorescent color can be developed in future research work so that the applications as photocatalysts in degrading wastewater materials can be improved. Furthermore, the discovery of the new photoluminescence CQDs and NCQDs may expand the application of carbon-based quantum dots to other fields such as optoelectronics, multi-functional fluorescent materials and nano-biotechnology. In addition to improve the photocatalytic degradation study, scavenging experiment will be improved in future research work to study the trapping of electron and hole species as well.

In addition, current study focused on the degradation of organic dye solutions. In future study, initiatives in producing photocatalyst with multifunctional properties can be suggested in degrading the real industrial effluents containing various organic contaminants, pharmaceutical and medicine wastes. These recommendations may continuously gain the interest of researchers in the area of photoluminescent CQDs.

For future study, the photoluminescence spectroscopy will be conducted at different excitation wavelength ranging from UV to NIR in order to obtain the different emission wavelength ranging from UV to NIR. Besides, UV-Vis DRS analysis could be suggested to study the absorption range of CQDs. Photocurrent analysis could also be considered in future study for determining the recombination rate of CQDs. In addition, LCMS analysis could be considered in order to determine the photocatalytic degradation pathway.

REFERENCES

- Aghamali, A., Khosravi, M., Hamishehkar, H., Modirshahla, N., Behnajady, M.A., 2018. Synthesis and characterization of high efficient photoluminescent sunlight driven photocatalyst of N-Carbon Quantum Dots. *J. Lumin.* 201, 265–274.
<https://doi.org/10.1016/j.jlumin.2018.04.061>
- Ahlawat, A., Rana, P.S., Solanki, P.R., 2021. Studies of photocatalytic and optoelectronic properties of microwave synthesized and polyethyleneimine stabilized carbon quantum dots. *Mater. Lett.* 305, 130830. <https://doi.org/10.1016/j.matlet.2021.130830>
- Ahmad Farid, M.A., Hassan, M.A., Roslan, A.M., Samsudin, M.H., Mohamad, Z.J.J., Othman, M.R., Shirai, Y., 2020. Carbon monoxide reduction in the flue gas during biochar production from oil palm empty fruit bunch. *J. Clean. Prod.* 258, 120580.
<https://doi.org/10.1016/j.jclepro.2020.120580>
- Ahmed, H.M., Ghali, M., Zahra, W., Ayad, M.M., 2021. Preparation of carbon quantum dots/polyaniline nanocomposite: Towards highly sensitive detection of picric acid. *Spectrochim. Acta Part A Mol. Biomol. Spectrosc.* 260, 119967. <https://doi.org/10.1016/j.saa.2021.119967>
- Aizat, N., Azlina, W., Abdul, W., Ghani, K., Thomas, R., Tuah, T.H., Ng, D.K.S., Syazarudin, M., 2021. Energy Conversion and Management : X Co-combustion of oil palm trunk biocoal / sub-bituminous coal fuel

blends. *Energy Convers. Manag.* X 10, 100072.

<https://doi.org/10.1016/j.ecmx.2020.100072>

Alarfaj, N., El-Tohamy, M., Oraby, H., 2018. CA 19-9 Pancreatic Tumor Marker Fluorescence Immunosensing Detection via Immobilized Carbon Quantum Dots Conjugated Gold Nanocomposite. *Int. J. Mol. Sci.* 19, 1162. <https://doi.org/10.3390/ijms19041162>

Allahbakhsh, A., Bahramian, A.R., 2018. Self-assembly of graphene quantum dots into hydrogels and cryogels: Dynamic light scattering, UV–Vis spectroscopy and structural investigations. *J. Mol. Liq.* 265, 172–180. <https://doi.org/10.1016/j.molliq.2018.05.123>

Alvandi, N., Assariha, S., Esfandiari, N., Jafari, R., 2021. Off–on sensor based on concentration-dependent multicolor fluorescent carbon dots for detecting pesticides. *Nano-Structures & Nano-Objects* 26, 100706. <https://doi.org/10.1016/j.nanoso.2021.100706>

Amal, N.M.T., Fathie, A.Z., Wan, N.F.M.F., Noorhalieza, A., Onn, H., 2008. The usage of Empty Fruit Bunch (EFB) and Palm Pressed Fibre (PPF) as substrates for the cultivation of *Pleurotus ostreatus*. *J. Teknol.* 49, 189–196.

Ansari, L., Hallaj, S., Hallaj, T., Amjadi, M., 2021. Colloids and Surfaces B : Biointerfaces Doped-carbon dots : Recent advances in their biosensing , bioimaging and therapy applications. *Colloids Surfaces B Biointerfaces* 203, 111743. <https://doi.org/10.1016/j.colsurfb.2021.111743>

Arumugam, N., Kim, J., 2018. Synthesis of carbon quantum dots from

Broccoli and their ability to detect silver ions. *Mater. Lett.* 219, 37–40.

<https://doi.org/10.1016/j.matlet.2018.02.043>

Arumugham, T., Alagumuthu, M., Amimodu, R.G., Munusamy, S., Iyer, S.K., 2020. A sustainable synthesis of green carbon quantum dot (CQD) from *Catharanthus roseus* (white flowering plant) leaves and investigation of its dual fluorescence responsive behavior in multi-ion detection and biological applications. *Sustain. Mater. Technol.* 23, e00138.

<https://doi.org/10.1016/j.susmat.2019.e00138>

Arvind, S., Mohapatra, P.K., Kalyanasundaram, D., Kumar, S., 2019. Self-functionalized ultrastable water suspension of luminescent carbon quantum dots. *Mater. Chem. Phys.* 225, 23–27.

<https://doi.org/10.1016/j.matchemphys.2018.12.031>

Azizi, B., Farhadi, K., Samadi, N., 2019. Functionalized carbon dots from zein biopolymer as a sensitive and selective fluorescent probe for determination of sumatriptan. *Microchem. J.* 146, 965–973.

<https://doi.org/10.1016/j.microc.2019.02.026>

Bai, J., He, Z., Li, L., Dang, S., Li, Y., Sun, W., 2018. The influence of side-coupled quantum dots on thermoelectric effect of parallel-coupled double quantum dot system. *Phys. B Condens. Matter.*

<https://doi.org/10.1016/j.physb.2018.06.040>

Bai, Y., Yi, X., Li, B., Chen, S., Fan, Z., 2022. Applied Surface Science Constructing porous polyimide / carbon quantum dots aerogel with efficient photocatalytic property under visible light. *Appl. Surf. Sci.* 578,

151993. <https://doi.org/10.1016/j.apsusc.2021.151993>

Bajorowicz, B., Kobyla, M.P., Go, A., Nadolna, J., Zaleska-medynska, A., Malankowska, A., 2018. Quantum dot-decorated semiconductor micro- and nanoparticles : A review of their synthesis , characterization and application in photocatalysis. *Adv. Colloid Interface Sci.* 256, 352–372. <https://doi.org/https://doi.org/10.1016/j.cis.2018.02.003>

Bakhshandeh, R., Shafiekhani, A., 2018. Ultrasonic waves and temperature effects on graphene structure fabricated by electrochemical exfoliation method. *Mater. Chem. Phys.* 212, 95–102. <https://doi.org/10.1016/j.matchemphys.2018.03.004>

Balakumar, V., Ramalingam, M., Sekar, K., Chuaicham, C., Sasaki, K., 2021. Fabrication and characterization of carbon quantum dots decorated hollow porous graphitic carbon nitride through polyaniline for photocatalysis. *Chem. Eng. J.* 426, 131739. <https://doi.org/10.1016/j.cej.2021.131739>

Basavaiah, K., Tadesse, A., RamaDevi, D., Hagos, M., Battu, G., 2018. Facile green synthesis of fluorescent carbon quantum dots from citrus lemon juice for live cell imaging. *Asian J. Nanosci. Mater.* 1, 36–46.

Brazil, T.R., Gonçalves, M., Junior, M.S.O., Rezende, M.C., 2022. Biomass and Bioenergy Sustainable process to produce activated carbon from Kraft lignin impregnated with H₃PO₄ using microwave pyrolysis. *Biomass and Bioenergy* 156, 106333. <https://doi.org/10.1016/j.biombioe.2021.106333>

- Cahino, A.M., Loureiro, R.G., Dantas, J., Madeira, V.S., Ribeiro Fernandes, P.C., 2019. Characterization and evaluation of ZnO/CuO catalyst in the degradation of methylene blue using solar radiation. *Ceram. Int.* 45, 13628–13636. <https://doi.org/10.1016/j.ceramint.2019.03.239>
- Chan, Y.J., Lee, H.W., Selvarajoo, A., 2021. Comparative study of the synergistic effect of decanter cake (DC) and empty fruit bunch (EFB) as the co-substrates in the anaerobic co-digestion (ACD) of palm oil mill effluent (POME). *Environ. Challenges* 5, 100257. <https://doi.org/10.1016/j.envc.2021.100257>
- Chang, S.H., 2014. An overview of empty fruit bunch from oil palm as feedstock for bio-oil production. *Biomass and Bioenergy* 62, 174–181. <https://doi.org/10.1016/j.biombioe.2014.01.002>
- Chaudhary, P., Verma, A., Mishra, A., Yadav, D., Pal, K., Yadav, B.C., Ranjith Kumar, E., Thapa, K.B., Mishra, S., Dwivedi, D.K., 2022a. Preparation of carbon quantum dots using bike pollutant soot: Evaluation of structural, optical and moisture sensing properties. *Phys. E Low-Dimensional Syst. Nanostructures* 139, 115174. <https://doi.org/10.1016/j.physe.2022.115174>
- Chaudhary, P., Verma, A., Mishra, A., Yadav, D., Pal, K., Yadav, B.C., Ranjith Kumar, E., Thapa, K.B., Mishra, S., Dwivedi, D.K., 2022b. Preparation of carbon quantum dots using bike pollutant soot: Evaluation of structural, optical and moisture sensing properties. *Phys. E Low-Dimensional Syst. Nanostructures* 139, 115174. <https://doi.org/10.1016/j.physe.2022.115174>

- Chellasamy, G., Arumugasamy, S.K., Govindaraju, S., Yun, K., 2022. Green synthesized carbon quantum dots from maple tree leaves for biosensing of Cesium and electrocatalytic oxidation of glycerol. *Chemosphere* 287, 131915. <https://doi.org/10.1016/j.chemosphere.2021.131915>
- Chen, H., Zhang, X., Jiang, L., Yuan, X., Liang, J., Zhang, J., Yu, H., Chu, W., Wu, Z., Li, H., Li, Y., 2021. Strategic combination of nitrogen-doped carbon quantum dots and g-C₃N₄: Efficient photocatalytic peroxydisulfate for the degradation of tetracycline hydrochloride and mechanism insight. *Sep. Purif. Technol.* 272, 118947. <https://doi.org/10.1016/j.seppur.2021.118947>
- Chen, Q., Chen, L., Qi, J., Tong, Y., Lv, Y., Xu, C., Ni, J., Liu, W., 2019. Photocatalytic degradation of amoxicillin by carbon quantum dots modified K₂Ti₆O₁₃ nanotubes: Effect of light wavelength. *Chinese Chem. Lett.* 30, 1214–1218. <https://doi.org/10.1016/j.ccllet.2019.03.002>
- Chen, W., Lv, G., Hu, W., Li, D., Chen, S., Dai, Z., 2018. Synthesis and applications of graphene quantum dots: a review. *Nanotechnol. Rev.* 7, 157–185. <https://doi.org/10.1515/ntrev-2017-0199>
- Chen, Y., Jiang, Y., Chen, B., Ye, F., Duan, H., Cui, H., 2021. Facile fabrication of N-doped carbon quantum dots modified SnO₂ composites for improved visible light photocatalytic activity. *Vacuum* 191, 110371. <https://doi.org/10.1016/j.vacuum.2021.110371>
- Cheng, J., Xu, Y., Zhou, D., Liu, K., Geng, N., Lu, J., Liu, Y., Liu, J., 2019. Novel carbon quantum dots can serve as an excellent adjuvant for the

gp85 protein vaccine against avian leukosis virus subgroup J in chickens.
Poult. Sci. 98, 5315–5320. <https://doi.org/10.3382/ps/pez313>

Cheng, Y., Bai, M., Su, J., Fang, C., Li, H., Chen, J., Jiao, J., 2019. Synthesis of fluorescent carbon quantum dots from aqua mesophase pitch and their photocatalytic degradation activity of organic dyes. *J. Mater. Sci. Technol.* 35, 1515–1522. <https://doi.org/10.1016/j.jmst.2019.03.039>

Chung Hui, K., Lun Ang, W., Soraya Sambudi, N., 2021. Nitrogen and bismuth-doped rice husk-derived carbon quantum dots for dye degradation and heavy metal removal. *J. Photochem. Photobiol. A Chem.* 418, 113411. <https://doi.org/10.1016/j.jphotochem.2021.113411>

Chung, K., Lun, W., Zaireen, W., Yahya, N., Soraya, N., 2022. Chemosphere Effects of nitrogen / bismuth-doping on the photocatalyst composite of carbon dots / titanium dioxide nanoparticles (CDs / TNP) for enhanced visible light-driven removal of diclofenac 290.

Coral Medina, J.D., Woiciechowski, A., Zandona Filho, A., Nosedá, M.D., Kaur, B.S., Soccol, C.R., 2015. Lignin preparation from oil palm empty fruit bunches by sequential acid/alkaline treatment – A biorefinery approach. *Bioresour. Technol.* 194, 172–178.
<https://doi.org/10.1016/j.biortech.2015.07.018>

Cui, L., Ren, X., Wang, J., Sun, M., 2020. Synthesis of homogeneous carbon quantum dots by ultrafast dual-beam pulsed laser ablation for bioimaging. *Mater. Today Nano* 12, 100091.
<https://doi.org/10.1016/j.mtnano.2020.100091>

- Cui, P., Kuai, Y., Wu, Q., Zheng, Y., Liu, X., 2019. Synthesis of a fluorescent cation surfactant derived from carbon quantum dots. *Mater. Lett.* 235, 161–163. <https://doi.org/10.1016/j.matlet.2018.10.018>
- Cui, P., Xue, Y., 2022. The role of center-N-doping in non-radiative recombination loss of nitrogen-doped graphene quantum dots. *Mater. Sci. Semicond. Process.* 139, 106323. <https://doi.org/10.1016/j.mssp.2021.106323>
- Cui, Y., Lin, C., Li, M., Zhu, N., Meng, J., Zhao, J., 2022. CuWO₄/CuS heterojunction photocatalyst for the application of visible-light-driven photodegradation of dye pollutions. *J. Alloys Compd.* 893, 162181. <https://doi.org/10.1016/j.jallcom.2021.162181>
- Cui, Y., Wang, T., Liu, J., Hu, L., Nie, Q., Tan, Z., Yu, H., 2021. Enhanced solar photocatalytic degradation of nitric oxide using graphene quantum dots / bismuth tungstate composite catalysts. *Chem. Eng. J.* 420, 129595. <https://doi.org/10.1016/j.cej.2021.129595>
- Das, R., Bandyopadhyay, R., Pramanik, P., 2018. Carbon quantum dots from natural resource: A review. *Mater. Today Chem.* 8, 96–109. <https://doi.org/10.1016/j.mtchem.2018.03.003>
- Das, S.K., Chakrabarty, S., Gawas, R., Jasuja, K., 2022. Serendipitous formation of photoluminescent carbon quantum dots by mere immersion of a polymer in an organic solvent. *Carbon Trends* 8, 100183. <https://doi.org/10.1016/j.cartre.2022.100183>
- Deng, X., Feng, Y., Li, H., Du, Z., Teng, Q., Wang, H., 2018. N-doped carbon

quantum dots as fluorescent probes for highly selective and sensitive detection of Fe³⁺ ions. *Particuology* 41, 94–100.

<https://doi.org/10.1016/j.partic.2017.12.009>

Derman, E., Abdulla, R., Marbawi, H., Sabullah, M.K., 2018. Oil palm empty fruit bunches as a promising feedstock for bioethanol production in Malaysia. *Renew. Energy* 129, 285–298.

<https://doi.org/10.1016/j.renene.2018.06.003>

Dhandapani, E., Duraisamy, N., Periasamy, P., T., P.V., 2020. Highly green fluorescent carbon quantum dots synthesis via hydrothermal method from fish scale. *Mater. Today Proc.* 26, A1–A5.

<https://doi.org/10.1016/j.matpr.2021.04.396>

Dong, Y., Shao, J., Chen, C., Li, H., Wang, R., Chi, Y., Lin, X., Chen, G., 2012. Blue luminescent graphene quantum dots and graphene oxide prepared by tuning the carbonization degree of citric acid. *Carbon N. Y.*

50, 4738–4743. <https://doi.org/10.1016/j.carbon.2012.06.002>

Duan, C., Xie, L., Wang, S., Dai, Y., Yin, L., 2022a. Chemosphere Photocatalytic hydrogen evolution by degradation of organic pollutants over quantum dots doped nitrogen carbide. *Chemosphere* 291, 132873.

<https://doi.org/10.1016/j.chemosphere.2021.132873>

Duan, C., Xie, L., Wang, S., Dai, Y., Yin, L., 2022b. Photocatalytic hydrogen evolution by degradation of organic pollutants over quantum dots doped nitrogen carbide. *Chemosphere* 291, 132873.

<https://doi.org/10.1016/j.chemosphere.2021.132873>

- Elango, D., Packialakshmi, J.S., Manikandan, V., Jayanthi, P., 2022. Sustainable synthesis of carbon quantum dots from shrimp shell and its emerging applications. *Mater. Lett.* 312, 131667. <https://doi.org/10.1016/j.matlet.2022.131667>
- Eskalen, H., Uru, S., Cömertpay, S., Hakan, A., Özgan, Ş., 2020. Industrial Crops & Products Microwave-assisted ultra-fast synthesis of carbon quantum dots from linter : Fluorescence cancer imaging and human cell growth inhibition properties 147. <https://doi.org/10.1016/j.indcrop.2020.112209>
- Fadhil, Z., Shamikh, D., Hasan, A., Al-mashhadani, M.H., Ahmed, A., Hashim, H., Yousif, E., 2022. Materials Science for Energy Technologies Extracted lignin from oil palm empty fruit bunch as natural eco-friendly poly (vinyl chloride) photo-stabilizer. *Mater. Sci. Energy Technol.* 5, 15–21. <https://doi.org/10.1016/j.mset.2021.10.003>
- Fang, L., Zheng, J., 2021. Carbon quantum dots : Synthesis and correlation of luminescence behavior with microstructure. *New Carbon Mater.* 36, 625–631. [https://doi.org/10.1016/S1872-5805\(21\)60031-8](https://doi.org/10.1016/S1872-5805(21)60031-8)
- Fang, L.Y., Zheng, J.T., 2021. Carbon quantum dots: Synthesis and correlation of luminescence behavior with microstructure. *Xinxing Tan Cailiao/New Carbon Mater.* 36, 625–631. [https://doi.org/10.1016/S1872-5805\(21\)60031-8](https://doi.org/10.1016/S1872-5805(21)60031-8)
- Faraji, M., Moradi Dehaghi, S., 2021. Pd-doped g-C₃N₄ decorated by nitrogen-doped carbon quantum dot as a high performance electrocatalyst

with superior durability and methanol tolerance for oxygen reduction reaction. *Inorg. Chem. Commun.* 123, 108328.

<https://doi.org/10.1016/j.inoche.2020.108328>

Fauzi, A.A., Jalil, A.A., Hassan, N.S., Aziz, F.F.A., Azami, M.S., Hussain, I., Saravanan, R., Vo, D.-V.N., 2022. A critical review on relationship of CeO₂-based photocatalyst towards mechanistic degradation of organic pollutant. *Chemosphere* 286, 131651.

<https://doi.org/10.1016/j.chemosphere.2021.131651>

Flihh, S.M., Ammar, S.H., 2021. Fabrication and photocatalytic degradation activity of core/shell ZIF-67@CoWO₄@CoS heterostructure photocatalysts under visible light. *Environ. Nanotechnology, Monit. Manag.* 16, 100595. <https://doi.org/10.1016/j.enmm.2021.100595>

Foo, M.L., Ooi, C.W., Tan, K.W., Chew, I.M.L., 2022. Preparation of black cumin seed oil Pickering nanoemulsion with enhanced stability and antioxidant potential using nanocrystalline cellulose from oil palm empty fruit bunch. *Chemosphere* 287, 132108.

<https://doi.org/10.1016/j.chemosphere.2021.132108>

Ganesan, S., Kalimuthu, R., Kanagaraj, T., Kulandaivelu, R., Nagappan, R., Pragasan, L.A., Ponnusamy, V.K., 2022. Microwave-assisted green synthesis of multi-functional carbon quantum dots as efficient fluorescence sensor for ultra-trace level monitoring of ammonia in environmental water. *Environ. Res.* 206, 112589.

<https://doi.org/10.1016/j.envres.2021.112589>

- Gao, M.X., Liu, C.F., Wu, Z.L., Zeng, Q.L., Yang, X.X., Wu, W.B., Li, Y.F., Huang, C.Z., 2013. A surfactant-assisted redox hydrothermal route to prepare highly photoluminescent carbon quantum dots with aggregation-induced emission enhancement properties. *Chem. Commun.* 49, 8015. <https://doi.org/10.1039/c3cc44624g>
- Gao, X., Li, H., Niu, X., Zhang, D., Wang, Y., Fan, H., Wang, K., 2021. Carbon quantum dots modified Ag₂S / CS nanocomposite as effective antibacterial agents. *J. Inorg. Biochem.* 220, 111456. <https://doi.org/10.1016/j.jinorgbio.2021.111456>
- Gong, J., Guo, Y., Lu, J., Cheng, Y., Wang, H., 2022. TEMPO oxidized nanofiber carbon quantum dots / TiO₂ composites with enhanced photocatalytic activity for degradation of methylene blue. *Chem. Phys. Lett.* 788, 139297. <https://doi.org/10.1016/j.cplett.2021.139297>
- Gong, X., Gao, X., Du, W., Zhang, H., Zhang, S., Nguyen, T.T., Guo, M., 2019. Wood powder-derived quantum dots for CeO₂ photocatalytic and anti-counterfeit applications. *Opt. Mater. (Amst)*. 96, 109302. <https://doi.org/10.1016/j.optmat.2019.109302>
- Goudarzi, A., Lin, L.-T., Ko, F.K., 2014. X-Ray Diffraction Analysis of Kraft Lignins and Lignin-Derived Carbon Nanofibers. *J. Nanotechnol. Eng. Med.* 5, 021006. <https://doi.org/10.1115/1.4028300>
- Guo, Y., Cao, F., Li, Y., 2018. Solid phase synthesis of nitrogen and phosphor co-doped carbon quantum dots for sensing Fe³⁺ and the enhanced photocatalytic degradation of dyes. *Sensors Actuators B Chem.* 255,

1105–1111. <https://doi.org/10.1016/j.snb.2017.08.104>

Guo, Y., Zhao, W., 2020. Hydrothermal synthesis of highly fluorescent nitrogen-doped carbon quantum dots with good biocompatibility and the application for sensing ellagic acid. *Spectrochim. Acta - Part A Mol. Biomol. Spectrosc.* 240, 118580.
<https://doi.org/10.1016/j.saa.2020.118580>

Haan, Y., Norashiqin, S., Chun, K., 2020. *Journal of Water Process Engineering Sustainable approach to the synthesis of cellulose membrane from oil palm empty fruit bunch for dye wastewater treatment. J. Water Process Eng.* 34, 101182. <https://doi.org/10.1016/j.jwpe.2020.101182>

Hagiwara, K., Horikoshi, S., Serpone, N., 2021a. *Journal of Photochemistry & Photobiology , A : Chemistry Luminescent monodispersed carbon quantum dots by a microwave solvothermal method toward bioimaging applications. J. Photochem. Photobiol. A Chem.* 415, 113310.
<https://doi.org/10.1016/j.jphotochem.2021.113310>

Hagiwara, K., Horikoshi, S., Serpone, N., 2021b. Luminescent monodispersed carbon quantum dots by a microwave solvothermal method toward bioimaging applications. *J. Photochem. Photobiol. A Chem.* 415, 113310.
<https://doi.org/10.1016/j.jphotochem.2021.113310>

Han, W., Li, D., Zhang, M., Ximin, H., Duan, X., Liu, S., Wang, S., 2020. Photocatalytic activation of peroxymonosulfate by surface-tailored carbon quantum dots. *J. Hazard. Mater.* 395.
<https://doi.org/10.1016/j.jhazmat.2020.122695>

Harris, C., Alcock, A., Trefan, L., Nuttall, D., Evans, S.T., Maguire, S., Kemp, A.M., 2018. Optimising the measurement of bruises in children across conventional and cross polarized images using segmentation analysis techniques in Image J, Photoshop and circle diameter measurements. *J. Forensic Leg. Med.* 54, 114–120.
<https://doi.org/10.1016/j.jflm.2017.12.020>

Hemmateenejad, B., Shadabipour, P., Khosousi, T., Shamsipur, M., 2015. Chemometrics investigation of the light-free degradation of methyl green and malachite green by starch-coated CdSe quantum dots. *J. Ind. Eng. Chem.* 27, 384–390. <https://doi.org/10.1016/j.jiec.2015.01.018>

Hidayati, S., Satyajaya, W., Fudholi, A., 2020a. Lignin isolation from black liquor from oil palm empty fruit bunch using acid. *J. Mater. Res. Technol.* 9, 11382–11391. <https://doi.org/10.1016/j.jmrt.2020.08.023>

Hidayati, S., Satyajaya, W., Fudholi, A., 2020b. Lignin isolation from black liquor from oil palm empty fruit bunch using acid. *J. Mater. Res. Technol.* 9, 11382–11391. <https://doi.org/10.1016/j.jmrt.2020.08.023>

Hsieh, M., Juang, R., Ashraf, Y., Fu, C., 2022. Journal of the Taiwan Institute of Chemical Engineers Synthesis and characterization of high-performance ZnO / graphene quantum dot composites for photocatalytic degradation of metronidazole 131.
<https://doi.org/10.1016/j.jtice.2021.104180>

Hsieh, M.C., Panchangam, S.C., Lai, W.W.P., Lin, A.Y.C., 2018. Degradation of methadone by the sunlight/FC process: Kinetics, radical species

participation and influence of the water matrix. *Chemosphere* 209, 104–112. <https://doi.org/10.1016/j.chemosphere.2018.06.076>

Huang, J., Wang, B., Hao, Z., Zhou, Z., Qu, Y., 2021. Boosting charge separation and broadening NIR light response over defected WO₃ quantum dots coupled g-C₃N₄ nanosheets for photocatalytic degrading antibiotics. *Chem. Eng. J.* 416, 129109. <https://doi.org/10.1016/j.cej.2021.129109>

Hunge, Y.M., Yadav, A.A., Khan, S., Takagi, K., Suzuki, N., Teshima, K., Terashima, C., Fujishima, A., 2021. Photocatalytic degradation of bisphenol A using titanium dioxide@nanodiamond composites under UV light illumination. *J. Colloid Interface Sci.* 582, 1058–1066. <https://doi.org/10.1016/j.jcis.2020.08.102>

Huynh, M.H. V, White, P.S., John, K.D., Meyer, T.J., 2001. Isolation and Characterization of the Osmium(V)–Imido Complex [OsV(Tp)(Cl)₂(NH)] We are grateful to the National Science Foundation under Grant number CHE-9503738, the Los Alamos National Laboratory (DOE) under Grant Number 10730-001-00-2C, and the Labora. *Angew. Chemie Int. Ed.* 40, 4049. [https://doi.org/10.1002/1521-3773\(20011105\)40:21<4049::AID-ANIE4049>3.0.CO;2-W](https://doi.org/10.1002/1521-3773(20011105)40:21<4049::AID-ANIE4049>3.0.CO;2-W)

Iqbal, Mahwish, Bhatti, H.N., Younis, S., Rehmat, S., Alwadai, N., Almuqrin, A.H., Iqbal, Munawar, 2021a. Graphene oxide nanocomposite with CuSe and photocatalytic removal of methyl green dye under visible light irradiation. *Diam. Relat. Mater.* 113, 108254. <https://doi.org/10.1016/j.diamond.2021.108254>

- Iqbal, Mahwish, Bhatti, H.N., Younis, S., Rehmat, S., Alwadai, N., Almuqrin, A.H., Iqbal, Munawar, 2021b. Graphene oxide nanocomposite with CuSe and photocatalytic removal of methyl green dye under visible light irradiation. *Diam. Relat. Mater.* 113, 108254.
<https://doi.org/10.1016/j.diamond.2021.108254>
- Issa, M.A., Abidin, Z.Z., Sobri, S., Abdul-rashid, S., Mahdi, M.A., Ibrahim, N.A., Pudza, M.Y., 2020. Chinese Journal of Chemical Engineering Fabrication , characterization and response surface method optimization for quantum efficiency of fluorescent nitrogen-doped carbon dots obtained from carboxymethylcellulose of oil palms empty fruit bunch. *Chinese J. Chem. Eng.* 28, 584–592.
<https://doi.org/10.1016/j.cjche.2019.04.003>
- Izadyar, N., Ong, H.C., Chong, W.T., Mojumder, J.C., Leong, K.Y., 2016. Investigation of potential hybrid renewable energy at various rural areas in Malaysia. *J. Clean. Prod.* 139, 61–73.
<https://doi.org/10.1016/j.jclepro.2016.07.167>
- Jabar, J.M., Odusote, Y.A., 2020. Removal of cibacron blue 3G-A (CB) dye from aqueous solution using chemo-physically activated biochar from oil palm empty fruit bunch fiber. *Arab. J. Chem.* 13, 5417–5429.
<https://doi.org/10.1016/j.arabjc.2020.03.020>
- Jacob, J.M., Rajan, R., Aji, M., Kurup, G.G., Pugazhendhi, A., 2019. Bio-inspired ZnS quantum dots as efficient photo catalysts for the degradation of methylene blue in aqueous phase. *Ceram. Int.* 45, 4857–4862.
<https://doi.org/10.1016/j.ceramint.2018.11.182>

- Jamila, G.S., Sajjad, S., Leghari, S.A.K., Long, M., 2020. Nitrogen doped carbon quantum dots and GO modified WO₃ nanosheets combination as an effective visible photo catalyst. *J. Hazard. Mater.* 382, 121087. <https://doi.org/10.1016/j.jhazmat.2019.121087>
- Javed, M., Saqib, A.N.S., Ata-ur-Rehman, Ali, B., Faizan, M., Anang, D.A., Iqbal, Z., Abbas, S.M., 2019. Carbon quantum dots from glucose oxidation as a highly competent anode material for lithium and sodium-ion batteries. *Electrochim. Acta* 297, 250–257. <https://doi.org/10.1016/j.electacta.2018.11.167>
- Jia, J., Zhang, X., Jiang, C., Huang, W., Wang, Y., 2020. Visible-light-driven nitrogen-doped carbon quantum dots decorated g-C₃N₄/Bi₂WO₆ Z-scheme composite with enhanced photocatalytic activity and mechanism insight. *J. Alloys Compd.* 835, 155180. <https://doi.org/10.1016/j.jallcom.2020.155180>
- Jian, H.-J., Wu, R.-S., Lin, T.-Y., Li, Y.-J., Lin, H.-J., Harroun, S.G., Lai, J.-Y., Huang, C.-C., 2017. Super-Cationic Carbon Quantum Dots Synthesized from Spermidine as an Eye Drop Formulation for Topical Treatment of Bacterial Keratitis. *ACS Nano* 11, 6703–6716. <https://doi.org/10.1021/acsnano.7b01023>
- Jiang, X., Qin, D., Mo, G., Feng, J., Yu, C., Mo, W., Deng, B., 2019. Ginkgo leaf-based synthesis of nitrogen-doped carbon quantum dots for highly sensitive detection of salazosulfapyridine in mouse plasma. *J. Pharm. Biomed. Anal.* 164, 514–519. <https://doi.org/10.1016/j.jpba.2018.11.025>

- Jin, Y., Tang, W., Wang, J., Ren, F., Chen, Z., Sun, Z., Ren, P.-G., 2023. Construction of biomass derived carbon quantum dots modified TiO₂ photocatalysts with superior photocatalytic activity for methylene blue degradation. *J. Alloys Compd.* 932, 167627.
<https://doi.org/10.1016/j.jallcom.2022.167627>
- Jindal, S., Giripunje, S.M., 2018. An insight into electronic and optical properties of multilayer graphene quantum dots synthesized by hydrothermal approach. *Synth. Met.* 239, 36–42.
<https://doi.org/10.1016/j.synthmet.2018.03.005>
- Joseph, C.G., Quek, K.S., Daud, W.M.A.W., Moh, P.Y., 2017. Physical Activation of Oil Palm Empty Fruit Bunch via CO₂ Activation Gas for CO₂ Adsorption. *IOP Conf. Ser. Mater. Sci. Eng.* 206, 012003.
<https://doi.org/10.1088/1757-899X/206/1/012003>
- Joshi, P.N., Mathias, A., Mishra, A., Mathias, A., 2018. Synthesis of ecofriendly fluorescent carbon dots and their biomedical and environmental applications. *Mater. Technol.* 33, 672–680.
<https://doi.org/10.1080/10667857.2018.1492683>
- Jusuf, B.N., Sambudi, N.S., Isnaeni, Samsuri, S., 2018. Microwave-assisted synthesis of carbon dots from eggshell membrane ashes by using sodium hydroxide and their usage for degradation of methylene blue. *J. Environ. Chem. Eng.* 6, 7426–7433. <https://doi.org/10.1016/j.jece.2018.10.032>
- Kaczmarek, A., Hoffman, J., Morgiel, J., Mościcki, T., Stobiński, L., Szymański, Z., Małolepszy, A., 2021. Luminescent Carbon Dots

Synthesized by the Laser Ablation of Graphite in Polyethylenimine and Ethylenediamine. *Materials* (Basel). 14, 729.

<https://doi.org/10.3390/ma14040729>

Kalaiyarasan, G., Joseph, J., 2019. Cholesterol derived carbon quantum dots as fluorescence probe for the specific detection of hemoglobin in diluted human blood samples. *Mater. Sci. Eng. C* 94, 580–586.

<https://doi.org/10.1016/j.msec.2018.10.007>

Kamarol Zaman, A.S., Tan, T.L., A/P Chowmasundaram, Y., Jamaludin, N., Sadrolhosseini, A.R., Rashid, U., Rashid, S.A., 2021. Properties and molecular structure of carbon quantum dots derived from empty fruit bunch biochar using a facile microwave-assisted method for the detection of Cu²⁺ ions. *Opt. Mater. (Amst)*. 112, 110801.

<https://doi.org/10.1016/j.optmat.2021.110801>

Karunakaran, V., Abd-Talib, N., Kelly Yong, T.L., 2019. Lignin from oil palm empty fruit bunches (EFB) under subcritical phenol conditions as a precursor for carbon fiber production. *Mater. Today Proc.* 31, 100–105.

<https://doi.org/10.1016/j.matpr.2020.01.252>

Karunakaran, V., Abd-talib, N., Yong, T.K., 2020. *Materials Today : Proceedings* Lignin from oil palm empty fruit bunches (EFB) under subcritical phenol conditions as a precursor for carbon fiber production.

Mater. Today Proc. 31, 100–105.

<https://doi.org/10.1016/j.matpr.2020.01.252>

Kaur, Manpreet, Kaur, Manmeet, Sharma, V.K., 2018. Nitrogen-doped

graphene and graphene quantum dots: A review on synthesis and applications in energy, sensors and environment. *Adv. Colloid Interface Sci.* 259, 44–64. <https://doi.org/10.1016/j.cis.2018.07.001>

Khan, Z.M.S.H., Rahman, R.S., Shumaila, Islam, S., Zulfequar, M., 2019. Hydrothermal treatment of red lentils for the synthesis of fluorescent carbon quantum dots and its application for sensing Fe³⁺. *Opt. Mater. (Amst)*. 91, 386–395. <https://doi.org/10.1016/j.optmat.2019.03.054>

Khan, Z.M.S.H., Saifi, S., Shumaila, Aslam, Z., Khan, S.A., Zulfequar, M., 2020. A facile one step hydrothermal synthesis of carbon quantum dots for label -free fluorescence sensing approach to detect picric acid in aqueous solution. *J. Photochem. Photobiol. A Chem.* 388. <https://doi.org/10.1016/j.jphotochem.2019.112201>

Koe, W.S., Chong, W.C., Pang, Y.L., Koo, C.H., Ebrahim, M., Mohammad, A.W., 2020. Novel nitrogen and sulphur co-doped carbon quantum dots/titanium oxide photocatalytic membrane for in-situ degradation and removal of pharmaceutical compound. *J. Water Process Eng.* 33, 101068. <https://doi.org/10.1016/j.jwpe.2019.101068>

Kondee, S., Arayawut, O., Pon-On, W., Wongchoosuk, C., 2022. Nitrogen-doped carbon oxide quantum dots for flexible humidity sensor: Experimental and SCC-DFTB study. *Vacuum* 195, 110648. <https://doi.org/10.1016/j.vacuum.2021.110648>

Koohestani, H., Sadrnezhad, S.K., 2016. Photocatalytic degradation of methyl orange and cyanide by using TiO₂/CuO composite. *Desalin.*

Water Treat. 57, 22029–22038.

<https://doi.org/10.1080/19443994.2015.1132395>

Kumar, G., Cilamkoti, V., Dutta, R.K., 2022. Sunlight mediated enhanced photocatalytic degradation of antibiotics in aqueous medium using silicon doped carbon quantum dots decorated Bi₂MoO₆ nanoflakes. *Colloids Surfaces A Physicochem. Eng. Asp.* 639, 128368.

<https://doi.org/10.1016/j.colsurfa.2022.128368>

Kumar, N., Abubakar Sadique, M., Khan, R., 2021. Electrochemical exfoliation of graphene quantum dots from waste dry cell battery for biosensor applications. *Mater. Lett.* 305, 130829.

<https://doi.org/10.1016/j.matlet.2021.130829>

Kumari, B., Kumari, R., Das, P., 2018. Visual detection of G-quadruplex with mushroom derived highly fluorescent carbon quantum dots. *J. Pharm. Biomed. Anal.* 157, 137–144. <https://doi.org/10.1016/j.jpba.2018.05.013>

Latief, U., Islam, S., Zubair, M.S.H., Khan, M.S., 2021. Spectrochimica Acta Part A : Molecular and Biomolecular Spectroscopy A facile green synthesis of functionalized carbon quantum dots as fluorescent probes for a highly selective and sensitive detection of Fe³⁺ ions. *Spectrochim. Acta Part A Mol. Biomol. Spectrosc.* 262, 120132.

<https://doi.org/10.1016/j.saa.2021.120132>

Li, H., He, X., Kang, Z., Huang, H., Liu, Y., Liu, J., Lian, S., Tsang, C.H.A., Yang, X., Lee, S.-T., 2010. Water-Soluble Fluorescent Carbon Quantum Dots and Photocatalyst Design. *Angew. Chemie Int. Ed.* 49, 4430–4434.

<https://doi.org/10.1002/anie.200906154>

Li, H., Zhang, Y., Ding, J., Wu, T., Cai, S., Zhang, W., Cai, R., Chen, C., Yang, R., 2022. Synthesis of Carbon Quantum Dots for Application of Alleviating Amyloid- β Mediated Neurotoxicity. *Colloids Surfaces B Biointerfaces* 212, 112373.

<https://doi.org/10.1016/j.colsurfb.2022.112373>

Li, R., Zhu, Z., Pan, P., Liu, J., Zhou, B., Liu, C., Yang, Z., Wang, J., Li, X., Yang, X., Chang, J., Niu, H., 2022. One-step synthesis of nitrogen-doped carbon quantum dots for paper-based electrochemiluminescence detection of Cu^{2+} ions. *Microchem. J.* 174, 107057.

<https://doi.org/10.1016/j.microc.2021.107057>

Li, Xuehua, Ge, F., Li, Xiaobing, Zhou, X., Qian, J., Fu, G., Shi, L., Xu, Y., 2019. Rapid and large-scale production of carbon dots by salt-assisted electrochemical exfoliation of graphite rods. *J. Electroanal. Chem.* 851, 113390. <https://doi.org/10.1016/j.jelechem.2019.113390>

Li, Y., Sun, Y., Ho, W., Zhang, Y., Huang, H., Cai, Q., Dong, F., 2018. Highly enhanced visible-light photocatalytic NO_x purification and conversion pathway on self-structurally modified g-C₃N₄ nanosheets. *Sci. Bull.* 63, 609–620. <https://doi.org/10.1016/j.scib.2018.04.009>

Liang, Y., Liu, Y., Li, S., Lu, B., Liu, C., Yang, H., Ren, X., Hou, Y., 2019. Hydrothermal growth of nitrogen-rich carbon dots as a precise multifunctional probe for both Fe^{3+} detection and cellular bio-imaging. *Opt. Mater. (Amst.)* 89, 92–99.

<https://doi.org/10.1016/j.optmat.2019.01.008>

Liang, Z., Yang, J., Zhou, C., Mo, Q., Zhang, Y., 2018. Carbon quantum dots modified BiOBr microspheres with enhanced visible light photocatalytic performance. *Inorg. Chem. Commun.* 90, 97–100.

<https://doi.org/10.1016/j.inoche.2018.02.013>

Liu, G., Jia, H., Li, N., Li, X., Yu, Z., Wang, J., Song, Y., 2019. High-fluorescent carbon dots (CDs) originated from China grass carp scales (CGCS) for effective detection of Hg(II) ions. *Microchem. J.* 145, 718–728. <https://doi.org/10.1016/j.microc.2018.11.044>

Liu, G., Pan, X., Li, J., Li, C., Ji, C., 2021. Facile preparation and characterization of anatase TiO₂/nanocellulose composite for photocatalytic degradation of methyl orange. *J. Saudi Chem. Soc.* 25, 101383. <https://doi.org/10.1016/j.jscs.2021.101383>

Liu, H., Liang, J., Fu, S., Li, L., Cui, J., Gao, P., Zhao, F., Zhou, J., 2020. N doped carbon quantum dots modified defect-rich g-C₃N₄ for enhanced photocatalytic combined pollutions degradation and hydrogen evolution. *Colloids Surfaces A Physicochem. Eng. Asp.* 591.

<https://doi.org/10.1016/j.colsurfa.2020.124552>

Liu, W., Zhang, R., Kang, Y., Zhang, X., Wang, H., Li, L., Diao, H., Wei, W., 2019. Preparation of nitrogen-doped carbon dots with a high fluorescence quantum yield for the highly sensitive detection of Cu²⁺ ions, drawing anti-counterfeit patterns and imaging live cells. *New Carbon Mater.* 34, 390–402. [https://doi.org/10.1016/S1872-5805\(19\)30024-1](https://doi.org/10.1016/S1872-5805(19)30024-1)

- Liu, X., Yang, Z., Yang, Y., Li, H., 2022. Chemosphere Carbon quantum dots sensitized 2D / 2D carbon nitride nanosheets / bismuth tungstate for visible light photocatalytic degradation norfloxacin. *Chemosphere* 287, 132126. <https://doi.org/10.1016/j.chemosphere.2021.132126>
- Liu, Y., Li, W., Wu, P., Ma, C., Wu, X., Xu, M., Luo, S., Xu, Z., Liu, S., 2019. Hydrothermal synthesis of nitrogen and boron co-doped carbon quantum dots for application in acetone and dopamine sensors and multicolor cellular imaging. *Sensors Actuators, B Chem.* 281, 34–43. <https://doi.org/10.1016/j.snb.2018.10.075>
- Loo, W.W., Pang, Y.L., Lim, S., Wong, K.H., Lai, C.W., Abdullah, A.Z., 2021. Enhancement of photocatalytic degradation of Malachite Green using iron doped titanium dioxide loaded on oil palm empty fruit bunch-derived activated carbon. *Chemosphere* 272, 129588. <https://doi.org/10.1016/j.chemosphere.2021.129588>
- Mahmood, A., Wang, X., Shi, G., Wang, Z., Xie, X., Sun, J., 2020. Revealing adsorption and the photodegradation mechanism of gas phase o-xylene on carbon quantum dots modified TiO₂ nanoparticles. *J. Hazard. Mater.* 386, 121962. <https://doi.org/10.1016/j.jhazmat.2019.121962>
- Makkar, M., Viswanatha, R., 2018. Frontier challenges in doping quantum dots: synthesis and characterization. *RSC Adv.* 8, 22103–22112. <https://doi.org/10.1039/C8RA03530J>
- Martins, N.C.T., Ângelo, J., Girão, A.V., Trindade, T., Andrade, L., Mendes, A., 2016. N-doped carbon quantum dots/TiO₂ composite with improved

photocatalytic activity. *Appl. Catal. B Environ.* 193, 67–74.

<https://doi.org/10.1016/j.apcatb.2016.04.016>

Meghdad, P., Moradi, S., Shahlaei, M., Farhadian, N., 2018. Application of carbon dots as efficient catalyst for the green oxidation of phenol: Kinetic study of the degradation and optimization using response surface methodology. *J. Hazard. Mater.* 353, 444–453.

<https://doi.org/10.1016/j.jhazmat.2018.04.038>

Ming, H., Wei, D., Yang, Y., Chen, B., Yang, C., Zhang, J., Hou, Y., 2021a. Photocatalytic activation of peroxymonosulfate by carbon quantum dots functionalized carbon nitride for efficient degradation of bisphenol A under visible-light irradiation. *Chem. Eng. J.* 424, 130296.

<https://doi.org/10.1016/j.cej.2021.130296>

Ming, H., Wei, D., Yang, Y., Chen, B., Yang, C., Zhang, J., Hou, Y., 2021b. Photocatalytic activation of peroxymonosulfate by carbon quantum dots functionalized carbon nitride for efficient degradation of bisphenol A under visible-light irradiation. *Chem. Eng. J.* 424, 130296.

<https://doi.org/10.1016/j.cej.2021.130296>

Monte, S.S., Andrade, S.I.E., Lima, M.B., Araujo, M.C.U., 2019. Synthesis of highly fluorescent carbon dots from lemon and onion juices for determination of riboflavin in multivitamin/mineral supplements. *J. Pharm. Anal.* 9, 209–216. <https://doi.org/10.1016/j.jpha.2019.02.003>

<https://doi.org/10.1016/j.jpha.2019.02.003>

Mukthar Ali, M., Arya Nair, J.S., Sandhya, K.Y., 2019. Role of reactive oxygen species in the visible light photocatalytic mineralization of

rhodamine B dye by P25–carbon dot photocatalyst. *Dye. Pigment.* 163, 274–284. <https://doi.org/10.1016/j.dyepig.2018.11.057>

Munishwar, S.R., Pawar, P.P., Janbandhu, S.Y., Gedam, R.S., 2018. Growth of CdSSe quantum dots in borosilicate glass by controlled heat treatment for band gap engineering. *Opt. Mater. (Amst).* 86, 424–432. <https://doi.org/10.1016/j.optmat.2018.10.040>

Myint, A.A., Rhim, W.K., Nam, J.M., Kim, J., Lee, Y.W., 2018. Water-soluble, lignin-derived carbon dots with high fluorescent emissions and their applications in bioimaging. *J. Ind. Eng. Chem.* 66, 387–395. <https://doi.org/10.1016/j.jiec.2018.06.005>

Narapakdeesakul, D., Sridach, W., Wittaya, T., 2013. Recovery, characteristics and potential use as linerboard coatings material of lignin from oil palm empty fruit bunches' black liquor. *Ind. Crops Prod.* 50, 8–14. <https://doi.org/10.1016/j.indcrop.2013.07.011>

Naushad, M., Ahamad, T., Ubaidullah, M., Ahmed, J., Ghafar, A.A., Al-Sheetan, K.M., Arunachalam, P., 2021. Nitrogen-doped carbon quantum dots (N-CQDs)/Co₃O₄ nanocomposite for high performance supercapacitor. *J. King Saud Univ. - Sci.* 33, 101252. <https://doi.org/10.1016/j.jksus.2020.101252>

Navidfar, A., Peker, M.I., Budak, E., Unlu, C., Trabzon, L., 2022. Carbon quantum dots enhanced graphene/carbon nanotubes polyurethane hybrid nanocomposites. *Compos. Part B Eng.* 247, 110310. <https://doi.org/10.1016/j.compositesb.2022.110310>

- Ng, L.Y., Leo, C.P., Mohammad, A.W., 2011. Optimizing the incorporation of silica nanoparticles in polysulfone/poly(vinyl alcohol) membranes with response surface methodology. *J. Appl. Polym. Sci.* 121, 1804–1814. <https://doi.org/10.1002/app.33628>
- Or, K.H., Putra, A., Selamat, M.Z., 2017. Oil palm empty fruit bunch fibres as sustainable acoustic absorber. *Appl. Acoust.* 119, 9–16. <https://doi.org/10.1016/j.apacoust.2016.12.002>
- Pan, D., Wang, Lijun, Li, Z., Geng, B., Zhang, C., Zhan, J., Yin, L., Wang, Liang, 2018. Synthesis of graphene quantum dot/metal-organic framework nanocomposites as yellow phosphors for white light-emitting diodes. *New J. Chem.* 42, 5083–5089. <https://doi.org/10.1039/c7nj04909a>
- Pan, D., Zhang, J., Li, Z., Wu, M., 2010. Hydrothermal route for cutting graphene sheets into blue-luminescent graphene quantum dots. *Adv. Mater.* 22, 734–738. <https://doi.org/10.1002/adma.200902825>
- Papaoannou, N., Marinovic, A., Yoshizawa, N., Goode, A.E., Fay, M., Khlobystov, A., Titirici, M.M., Sapelkin, A., 2018. Structure and solvents effects on the optical properties of sugar-derived carbon nanodots. *Sci. Rep.* 8, 1–10. <https://doi.org/10.1038/s41598-018-25012-8>
- Piatkowski, P., Masi, S., Galar, P., Gutiérrez, M., Ngo, T.T., Mora-Seró, I., Douhal, A., 2020. Deciphering the role of quantum dot size in the ultrafast charge carrier dynamics at the perovskite–quantum dot interface. *J. Mater. Chem. C.* <https://doi.org/10.1039/D0TC03835K>

- Piri, M., Sepehr, E., Rengel, Z., 2019. Citric acid decreased and humic acid increased Zn sorption in soils. *Geoderma* 341, 39–45.
<https://doi.org/10.1016/j.geoderma.2018.12.027>
- Pirsaheb, M., Asadi, A., Sillanpää, M., Farhadian, N., 2018. Application of carbon quantum dots to increase the activity of conventional photocatalysts: A systematic review. *J. Mol. Liq.* 271, 857–871.
<https://doi.org/10.1016/j.molliq.2018.09.064>
- Qi, C., Wang, H., Yang, A., Wang, X., Xu, J., 2021. Facile Fabrication of Highly Fluorescent N - Doped Carbon Quantum Dots Using an Ultrasonic-Assisted Hydrothermal Method : Optical Properties and Cell Imaging. <https://doi.org/10.1021/acsomega.1c04903>
- Qi, H., Zhai, Z., Dong, X., Zhang, P., 2022. Nitrogen doped carbon quantum dots (N-CQDs) with high luminescence for sensitive and selective detection of hypochlorite ions by fluorescence quenching. *Spectrochim. Acta - Part A Mol. Biomol. Spectrosc.* 279, 121456.
<https://doi.org/10.1016/j.saa.2022.121456>
- Qiankun, C., Chen, L., Qi, J., Tong, Y., Lv, Y., Xu, C., Ni, J., Liu, W., 2019. Photocatalytic degradation of amoxicillin by carbon quantum dots modified K₂Ti₆O₁₃ nanotubes: Effect of light wavelength. *Chinese Chem. Lett.* 30, 1214–1218. <https://doi.org/10.1016/j.ccllet.2019.03.002>
- Qu, Y., Xu, X., Huang, R., Qi, W., Su, R., He, Z., 2020a. Enhanced photocatalytic degradation of antibiotics in water over functionalized N,S-doped carbon quantum dots embedded ZnO nanoflowers under

sunlight irradiation. *Chem. Eng. J.* 382, 123016.

<https://doi.org/10.1016/j.cej.2019.123016>

Qu, Y., Xu, X., Huang, R., Qi, W., Su, R., He, Z., 2020b. Enhanced photocatalytic degradation of antibiotics in water over functionalized N,S-doped carbon quantum dots embedded ZnO nanoflowers under sunlight irradiation. *Chem. Eng. J.* 382, 123016.

<https://doi.org/10.1016/j.cej.2019.123016>

Qu, Z., Wang, Jing, Tang, J., Shu, X., Liu, X., Zhang, Z., Wang, Jun, 2018. Carbon quantum dots/KNbO₃ hybrid composites with enhanced visible-light driven photocatalytic activity toward dye waste-water degradation and hydrogen production. *Mol. Catal.* 445, 1–11.

<https://doi.org/10.1016/j.mcat.2017.11.002>

Rahmi, Iqhrammullah, M., Audina, U., Husin, H., Fathana, H., 2021. Adsorptive removal of Cd (II) using oil palm empty fruit bunch-based charcoal/chitosan-EDTA film composite. *Sustain. Chem. Pharm.* 21, 100449. <https://doi.org/10.1016/j.scp.2021.100449>

Rajabi, H.R., Khani, O., Shamsipur, M., Vatanpour, V., 2013. High-performance pure and Fe³⁺-ion doped ZnS quantum dots as green nanophotocatalysts for the removal of malachite green under UV-light irradiation. *J. Hazard. Mater.* 250–251, 370–378.

<https://doi.org/10.1016/j.jhazmat.2013.02.007>

Rambabu, K., Bharath, G., Banat, F., Loke, P., 2020. Biosorption performance of date palm empty fruit bunch wastes for toxic hexavalent chromium

removal. *Environ. Res.* 187, 109694.

<https://doi.org/10.1016/j.envres.2020.109694>

Ramlee, N.A., Naveen, J., Jawaid, M., 2021. Potential of oil palm empty fruit bunch (OPEFB) and sugarcane bagasse fibers for thermal insulation application – A review. *Constr. Build. Mater.* 271, 121519.

<https://doi.org/10.1016/j.conbuildmat.2020.121519>

Rehman, A., Daud, A., Warsi, M.F., Shakir, I., Agboola, P.O., Sarwar, M.I., Zulfiqar, S., 2020. Nanostructured maghemite and magnetite and their nanocomposites with graphene oxide for photocatalytic degradation of methylene blue. *Mater. Chem. Phys.* 256, 123752.

<https://doi.org/10.1016/j.matchemphys.2020.123752>

Ren, X., Zhang, F., Guo, B., Gao, N., Zhang, X., 2019. Synthesis of N-Doped Micropore Carbon Quantum Dots with High Quantum Yield and Dual-Wavelength Photoluminescence Emission from Biomass for Cellular Imaging. *Nanomaterials* 9, 495. <https://doi.org/10.3390/nano9040495>

Reshma, V.G., Mohanan, P.V., 2019. Quantum dots: Applications and safety consequences. *J. Lumin.* 205, 287–298.

<https://doi.org/10.1016/j.jlumin.2018.09.015>

Riahi, Z., Rhim, J.-W., Bagheri, R., Pircheraghi, G., Lotfali, E., 2022.

Carboxymethyl cellulose-based functional film integrated with chitosan-based carbon quantum dots for active food packaging applications. *Prog. Org. Coatings* 166, 106794.

<https://doi.org/10.1016/j.porgcoat.2022.106794>

- Riaz, R., Ali, M., Maiyalagan, T., Anjum, A.S., Lee, S., Ko, M.J., Jeong, S.H., 2019. Dye-sensitized solar cell (DSSC) coated with energy down shift layer of nitrogen-doped carbon quantum dots (N-CQDs) for enhanced current density and stability. *Appl. Surf. Sci.* 483, 425–431.
<https://doi.org/10.1016/j.apsusc.2019.03.236>
- Rosli, S., Harun, S., Jahim, J.M., Othaman, R., 2017. CHEMICAL AND PHYSICAL CHARACTERIZATION OF OIL PALM EMPTY FRUIT BUNCH. *Malaysian J. Anal. Sci.* 21, 188–196.
<https://doi.org/10.17576/mjas-2017-2101-22>
- SA, S., MN, E., AE, T., AN, K., 2017. Synthesis of Carbon Dots with Tunable Luminescence. *J. Mater. Sci. Eng.* 06. <https://doi.org/10.4172/2169-0022.1000376>
- Sabet, M., Mahdavi, K., 2019. Green synthesis of high photoluminescence nitrogen-doped carbon quantum dots from grass via a simple hydrothermal method for removing organic and inorganic water pollutions. *Appl. Surf. Sci.* 463, 283–291.
<https://doi.org/10.1016/j.apsusc.2018.08.223>
- Saboorizadeh, B., Zare-dorabei, R., Shahbazi, N., 2021a. Journal of the Taiwan Institute of Chemical Engineers Green synthesis of carbon quantum dots and their application as a fluorometric sensor for highly selective determination of 6- mercaptopurine in biological samples. *J. Taiwan Inst. Chem. Eng.* 129, 389–395.
<https://doi.org/10.1016/j.jtice.2021.09.015>

- Saboorizadeh, B., Zare-Dorabei, R., Shahbazi, N., 2021b. Green synthesis of carbon quantum dots and their application as a fluorometric sensor for highly selective determination of 6-mercaptopurine in biological samples. *J. Taiwan Inst. Chem. Eng.* 129, 389–395.
<https://doi.org/10.1016/j.jtice.2021.09.015>
- Saikia, M., Hower, J.C., Das, T., Dutta, T., Saikia, B.K., 2019. Feasibility study of preparation of carbon quantum dots from Pennsylvania anthracite and Kentucky bituminous coals. *Fuel* 243, 433–440.
<https://doi.org/10.1016/j.fuel.2019.01.151>
- Saikia, M., Singh, A., Dihingia, A., Khare, P., Kalita, J., Saikia, B.K., 2022. Scalable production, cell toxicity assessment, and plant growth promotion activities of carbon quantum dots derived from low-quality coal feedstock. *Chem. Eng. J.* 433, 133633.
<https://doi.org/10.1016/j.cej.2021.133633>
- Salifairus, M.J., Abd Hamid, S.B., Soga, T., A.H. Alrokayan, S., A. Khan, H., Rusop, M., 2016. Structural and optical properties of graphene from green carbon source via thermal chemical vapor deposition. *J. Mater. Res.* 31, 1947–1956. <https://doi.org/10.1557/jmr.2016.200>
- Saud, P.S., Pant, B., Alam, A.-M., Ghouri, Z.K., Park, M., Kim, H.-Y., 2015. Carbon quantum dots anchored TiO₂ nanofibers: Effective photocatalyst for waste water treatment. *Ceram. Int.* 41, 11953–11959.
<https://doi.org/10.1016/j.ceramint.2015.06.007>
- Scott, T., Zhao, H., Deng, W., Feng, X., Li, Y., 2019. Photocatalytic

degradation of phenol in water under simulated sunlight by an ultrathin MgO coated Ag/TiO₂ nanocomposite. *Chemosphere* 216, 1–8.

<https://doi.org/10.1016/j.chemosphere.2018.10.083>

Seipenbusch, M., Rothenbacher, S., Kirchhoff, M., Schmid, H.-J., Kasper, G., Weber, A.P., 2010. Interparticle forces in silica nanoparticle agglomerates. *J. Nanoparticle Res.* 12, 2037–2044.

<https://doi.org/10.1007/s11051-009-9760-5>

Seng, R.X., Tan, L.L., Lee, W.P.C., Ong, W.J., Chai, S.P., 2020. Nitrogen-doped carbon quantum dots-decorated 2D graphitic carbon nitride as a promising photocatalyst for environmental remediation: A study on the importance of hybridization approach. *J. Environ. Manage.* 255, 109936.

<https://doi.org/10.1016/j.jenvman.2019.109936>

Septevani, A.A., Rifathin, A., Sari, A.A., Sampora, Y., Ariani, G.N., Sudiarmanto, Sondari, D., 2020. Oil palm empty fruit bunch-based nanocellulose as a super-adsorbent for water remediation. *Carbohydr. Polym.* 229, 115433.

<https://doi.org/10.1016/j.carbpol.2019.115433>

Shaik, S.A., Sengupta, S., Varma, R.S., Gawande, M.B., Goswami, A., 2021. Syntheses of N-Doped Carbon Quantum Dots (NCQDs) from Bioderived Precursors: A Timely Update. *ACS Sustain. Chem. Eng.* 9, 3–49.

<https://doi.org/10.1021/acssuschemeng.0c04727>

Shen, T., Wang, Q., Guo, Z., Kuang, J., Cao, W., 2018. Hydrothermal synthesis of carbon quantum dots using different precursors and their combination with TiO₂ for enhanced photocatalytic activity. *Ceram. Int.*

44, 11828–11834. <https://doi.org/10.1016/j.ceramint.2018.03.271>

Shi, X., Yan, L., Fan, S., Huang, Y., Xu, H., Lai, N., 2022. Indoor synthesis of carbon quantum dots and its potential applications study as tracers in oilfields. *J. Pet. Sci. Eng.* 213, 110325.

<https://doi.org/10.1016/j.petrol.2022.110325>

Shi, Y., Liu, X., Wang, M., Huang, J., Jiang, X., Pang, J., Xu, F., Zhang, X., 2019a. Synthesis of N-doped carbon quantum dots from bio-waste lignin for selective irons detection and cellular imaging. *Int. J. Biol. Macromol.* 128, 537–545. <https://doi.org/10.1016/j.ijbiomac.2019.01.146>

Shi, Y., Liu, X., Wang, M., Huang, J., Jiang, X., Pang, J., Xu, F., Zhang, X., 2019b. Synthesis of N-doped carbon quantum dots from bio-waste lignin for selective irons detection and cellular imaging. *Int. J. Biol. Macromol.* 128, 537–545. <https://doi.org/10.1016/j.ijbiomac.2019.01.146>

Singh, R.K., Kumar, R., Singh, D.P., Savu, R., Moshkalev, S.A., 2019.

Progress in microwave-assisted synthesis of quantum dots (graphene/carbon/semiconducting) for bioapplications: a review. *Mater. Today Chem.* 12, 282–314.

<https://doi.org/10.1016/j.mtchem.2019.03.001>

Singh, V.K., Singh, V., Yadav, P.K., Chandra, S., Bano, D., Koch, B., Talat, M., Hasan, S.H., 2019. Nitrogen doped fluorescent carbon quantum dots for on-off-on detection of Hg²⁺ and glutathione in aqueous medium:

Live cell imaging and IMPLICATION logic gate operation. *J.*

Photochem. Photobiol. A Chem. 384, 112042.

<https://doi.org/10.1016/j.jphotochem.2019.112042>

Sistani, S., Shekarchizadeh, H., 2021a. *Analytica Chimica Acta* Fabrication of fluorescence sensor based on molecularly imprinted polymer on amine-modified carbon quantum dots for fast and highly sensitive and selective detection of tannic acid in food samples 1186.

<https://doi.org/10.1016/j.aca.2021.339122>

Sistani, S., Shekarchizadeh, H., 2021b. Fabrication of fluorescence sensor based on molecularly imprinted polymer on amine-modified carbon quantum dots for fast and highly sensitive and selective detection of tannic acid in food samples. *Anal. Chim. Acta* 1186, 339122.

<https://doi.org/10.1016/j.aca.2021.339122>

Söderström, M.T., Ketola, R.A., 1994. Identification of nerve agents and their homologues and dialkyl methylphosphonates by gas chromatography/fourier transform infrared spectrometry (GC-FTIR) - Part I: Spectral interpretation. *Fresenius. J. Anal. Chem.* 350, 162–167.

<https://doi.org/10.1007/BF00323181>

Sohrabi, M.R., Khavaran, A., Shariati, Shahab, Shariati, Shayan, 2017.

Removal of Carmoisine edible dye by Fenton and photo Fenton processes using Taguchi orthogonal array design. *Arab. J. Chem.* 10, S3523–S3531.

<https://doi.org/10.1016/j.arabjc.2014.02.019>

Sui, Y., Wu, L., Zhong, S., Liu, Q., 2019. Carbon quantum dots/TiO₂ nanosheets with dominant (001) facets for enhanced photocatalytic hydrogen evolution. *Appl. Surf. Sci.* 480, 810–816.

<https://doi.org/10.1016/j.apsusc.2019.03.028>

Tammina, S.K., Mandal, B.K., Kadiyala, N.K., 2018. Photocatalytic degradation of methylene blue dye by nonconventional synthesized SnO₂ nanoparticles. *Environ. Nanotechnology, Monit. Manag.* 10, 339–350.
<https://doi.org/10.1016/j.enmm.2018.07.006>

Tan, A., Yang, G., Wan, X., 2021. Ultra-high quantum yield nitrogen-doped carbon quantum dots and their versatile application in fluorescence sensing, bioimaging and anti-counterfeiting. *Spectrochim. Acta - Part A Mol. Biomol. Spectrosc.* 253, 119583.
<https://doi.org/10.1016/j.saa.2021.119583>

Tan, Y., Wang, X., Xiong, F., Ding, J., Qing, Y., Wu, Y., 2021. Industrial Crops & Products Preparation of lignin-based porous carbon as an efficient absorbent for the removal of methylene blue. *Ind. Crop. Prod.* 171, 113980. <https://doi.org/10.1016/j.indcrop.2021.113980>

Tian, L., Chen, F., Ding, H., Li, Xuehua, Li, Xiaobing, 2020. The influence of inorganic electrolyte on the properties of carbon quantum dots in electrochemical exfoliation. *J. Electroanal. Chem.* 878, 114673.
<https://doi.org/10.1016/j.jelechem.2020.114673>

Tian, P., Tang, L., Teng, K.S., Lau, S.P., 2018. Graphene quantum dots from chemistry to applications. *Mater. Today Chem.* 10, 221–258.
<https://doi.org/10.1016/j.mtchem.2018.09.007>

Wang, C., Wang, Y., Shi, H., Yan, Y., Liu, E., Hu, X., Fan, J., 2019. A strong blue fluorescent nanoprobe for highly sensitive and selective detection of

mercury(II) based on sulfur doped carbon quantum dots. *Mater. Chem. Phys.* 232, 145–151. <https://doi.org/10.1016/j.matchemphys.2019.04.071>

Wang, F., Chen, P., Feng, Y., Xie, Z., Liu, Y., Su, Y., Zhang, Q., Wang, Y., Yao, K., Lv, W., Liu, G., 2017a. Facile synthesis of N-doped carbon dots/g-C₃N₄ photocatalyst with enhanced visible-light photocatalytic activity for the degradation of indomethacin. *Appl. Catal. B Environ.* 207, 103–113. <https://doi.org/10.1016/j.apcatb.2017.02.024>

Wang, F., Chen, P., Feng, Y., Xie, Z., Liu, Y., Su, Y., Zhang, Q., Wang, Y., Yao, K., Lv, W., Liu, G., 2017b. Facile synthesis of N-doped carbon dots/g-C₃N₄ photocatalyst with enhanced visible-light photocatalytic activity for the degradation of indomethacin. *Appl. Catal. B Environ.* 207, 103–113. <https://doi.org/10.1016/j.apcatb.2017.02.024>

Wang, G., Wang, F., Liu, S., Li, M., Xie, M., Yang, Z., Xiang, Y., Lv, S., Han, W., 2021. Construction of heterojuncted photocatalyst with TiO₂ quantum dots and graphene oxide nanosheets for highly efficient photocatalysis. *Scr. Mater.* 199, 113862. <https://doi.org/10.1016/j.scriptamat.2021.113862>

Wang, G., Zhang, S., Cui, J., Gao, W., Rong, X., Lu, Y., Gao, C., 2022a. Preparation of nitrogen-doped carbon quantum dots from chelating agent and used as fluorescent probes for accurate detection of ClO⁻ and Cr(VI). *Anal. Chim. Acta* 1195, 339478. <https://doi.org/10.1016/j.aca.2022.339478>

Wang, G., Zhang, S., Cui, J., Gao, W., Rong, X., Lu, Y., Gao, C., 2022b.

Preparation of nitrogen-doped carbon quantum dots from chelating agent and used as fluorescent probes for accurate detection of ClO⁻ and Cr(VI).

Anal. Chim. Acta 1195, 339478.

<https://doi.org/10.1016/j.aca.2022.339478>

Wang, L., Li, W., Wu, B., Li, Z., Wang, S., Liu, Y., Pan, D., Wu, M., 2016.

Facile synthesis of fluorescent graphene quantum dots from coffee grounds for bioimaging and sensing. *Chem. Eng. J.* 300, 75–82.

<https://doi.org/10.1016/j.cej.2016.04.123>

Wang, Q., Wang, G., Liang, X., Dong, X., Zhang, X., 2019. Supporting

carbon quantum dots on NH₂-MIL-125 for enhanced photocatalytic degradation of organic pollutants under a broad spectrum irradiation.

Appl. Surf. Sci. 467–468, 320–327.

<https://doi.org/10.1016/j.apsusc.2018.10.165>

Wang, R., Lu, K., Tang, Z., Xu, Y., 2017. Recent progress in carbon quantum

dots: synthesis, properties and applications in photocatalysis. *J. Mater.*

Chem. A 5, 3717–3734. <https://doi.org/10.1039/C6TA08660H>

Wang, Y., Man, Y., Li, S., Wu, S., Zhao, X., Xie, F., Qu, Q., Zou, W.-S.,

2020. Pesticide-derived bright chlorine-doped carbon dots for selective determination and intracellular imaging of Fe(III). *Spectrochim. Acta*

Part A Mol. Biomol. Spectrosc. 226, 117594.

<https://doi.org/10.1016/j.saa.2019.117594>

Wang, Z., Liu, Q., Leng, J., Liu, H., Zhang, Y., Wang, C., An, W., Bao, C.,

Lei, H., 2021a. The green synthesis of carbon quantum dots and

- applications for sulcotrione detection and anti-pathogen activities. *J. Saudi Chem. Soc.* 25, 101373. <https://doi.org/10.1016/j.jscs.2021.101373>
- Wang, Z., Liu, Q., Leng, J., Liu, H., Zhang, Y., Wang, C., An, W., Bao, C., Lei, H., 2021b. The green synthesis of carbon quantum dots and applications for sulcotrione detection and anti-pathogen activities. *J. Saudi Chem. Soc.* 25, 101373. <https://doi.org/10.1016/j.jscs.2021.101373>
- Wang, Z., Zhao, X., Guo, Z., Miao, P., Gong, X., 2018. Carbon dots based nanocomposite thin film for highly efficient luminescent solar concentrators. *Org. Electron.* 62, 284–289. <https://doi.org/10.1016/j.orgel.2018.08.020>
- Wicht, M.M., Nassimbeni, L.R., Báthori, N.B., 2019. Werner clathrates with enhanced hydrogen bonding functionality. *Polyhedron* 163, 7–19. <https://doi.org/10.1016/j.poly.2019.01.069>
- Widiyandari, H., Prilita, O., Al Ja'farawy, M.S., Nurosyid, F., Arutanti, O., Astuti, Y., Mufti, N., 2023. Nitrogen-doped carbon quantum dots supported zinc oxide (ZnO/N-CQD) nanoflower photocatalyst for methylene blue photodegradation. *Results Eng.* 17, 100814. <https://doi.org/10.1016/j.rineng.2022.100814>
- Wong, K.T., Wong, V.L., Lim, S.S., 2020. Bio-sorptive Removal of Methyl Orange by Micro-Grooved Chitosan (GCS) Beads: Optimization of Process Variables Using Taguchi L9 Orthogonal Array. *J. Polym. Environ.* <https://doi.org/10.1007/s10924-020-01878-6>
- Wu, J., Zheng, W., Chen, Y., 2022. Definition of photocatalysis: Current

- understanding and perspectives. *Curr. Opin. Green Sustain. Chem.* 33, 100580. <https://doi.org/10.1016/j.cogsc.2021.100580>
- Wu, Y., Wei, H., Mei, H.C. Van Der, Vries, J. De, Busscher, H.J., Ren, Y., 2021. Materials Today Bio Inheritance of physico-chemical properties and ROS generation by carbon quantum dots derived from pyrolytically carbonized bacterial sources 12. <https://doi.org/10.1016/j.mtbio.2021.100151>
- Xie, X., Yang, Y., Xiao, Y.-H., Huang, X., Shi, Q., Zhang, W.-D., 2018. Enhancement of photoelectrochemical activity of Fe₂O₃ nanowires decorated with carbon quantum dots. *Int. J. Hydrogen Energy* 43, 6954–6962. <https://doi.org/10.1016/j.ijhydene.2018.02.099>
- Xu, J., Cui, K., Gong, T., Zhang, J., Zhai, Z., Hou, L., Zaman, F.U., Yuan, C., 2022. Ultrasonic-Assisted Synthesis of N-Doped, Multicolor Carbon Dots toward Fluorescent Inks, Fluorescence Sensors, and Logic Gate Operations. *Nanomaterials* 12. <https://doi.org/10.3390/nano12030312>
- Xu, J., Lv, H., Yang, S.-T., Luo, J., 2013. Preparation of graphene adsorbents and their applications in water purification. *Rev. Inorg. Chem.* 33, 139–160. <https://doi.org/10.1515/revic-2013-0007>
- Xu, L., Chen, Y., Shen, Z., Wang, Y., Li, M., 2018. I₂/Fe(NO₃)₃·9H₂O-catalyzed oxidative synthesis of aryl carboxylic acids from aryl alkyl ketones and secondary benzylic alcohols. *Tetrahedron Lett.* 59, 4349–4354. <https://doi.org/10.1016/j.tetlet.2018.10.060>
- Xue, B., Yang, Y., Sun, Y., Fan, J., Li, X., Zhang, Z., 2019. Photoluminescent

lignin hybridized carbon quantum dots composites for bioimaging applications. *Int. J. Biol. Macromol.* 122, 954–961.

<https://doi.org/10.1016/j.ijbiomac.2018.11.018>

Yadegari, A., Khezri, J., Esfandiari, S., Mahdavi, H., Karkhane, A.A., Rahighi, R., Heidarimoghadam, R., Tayebi, L., Hashemi, E., Farmany, A., 2019. Bottom-up synthesis of nitrogen and oxygen co-decorated carbon quantum dots with enhanced DNA plasmid expression. *Colloids Surfaces B Biointerfaces* 184, 110543.

<https://doi.org/10.1016/j.colsurfb.2019.110543>

Yang, P., Zhu, Z., Chen, M., Chen, W., Zhou, X., 2018. Microwave-assisted synthesis of xylan-derived carbon quantum dots for tetracycline sensing. *Opt. Mater. (Amst.)* 85, 329–336.

<https://doi.org/10.1016/j.optmat.2018.06.034>

Yang, W., Yang, H., Ding, W., Zhang, B., Zhang, L., Wang, L., 2016. High quantum yield ZnO quantum dots synthesizing via an ultrasonication microreactor method. *Ultrason. Sonochem.* 33, 106–117.

<https://doi.org/http://dx.doi.org/10.1016/j.ultsonch.2016.04.020>

Yang, X., Hou, S., Chu, T., Han, J., Li, R., Guo, Y., Gong, Y., Li, H., Wan, Z., 2021. Preparation of magnesium, nitrogen-codoped carbon quantum dots from lignin with bright green fluorescence and sensitive pH response.

Ind. Crops Prod. 167, 113507.

<https://doi.org/10.1016/j.indcrop.2021.113507>

Yang, Y., Peng, K., Deng, Y., Zhao, Y., Ai, J., Min, X., Hu, M., Huang, S.,

- Yu, L., 2022. Full-color-emission carbon quantum dots by controlling surface states in a system of solvent. *J. Lumin.* 243, 118614.
<https://doi.org/10.1016/j.jlumin.2021.118614>
- Yaqoob, A.A., Sekeri, S.H., Othman, M.B.H., Ibrahim, M.N.M., Feizi, Z.H., 2021. Thermal degradation and kinetics stability studies of oil palm (*Elaeis Guineensis*) biomass-derived lignin nanoparticle and its application as an emulsifying agent. *Arab. J. Chem.* 14, 103182.
<https://doi.org/10.1016/j.arabjc.2021.103182>
- You, Q., Zhang, Q., Gu, M., Du, R., Chen, P., Huang, J., Wang, Y., Deng, S., Yu, G., 2022. Self-assembled graphitic carbon nitride regulated by carbon quantum dots with optimized electronic band structure for enhanced photocatalytic degradation of diclofenac. *Chem. Eng. J.* 431, 133927. <https://doi.org/10.1016/j.cej.2021.133927>
- Youh, M., Chung, M., Tai, H., Chen, C., Li, Y., 2021. Fabrication of carbon quantum dots via ball milling and their application to bioimaging. *Mendeleev Commun.* 31, 647–650.
<https://doi.org/10.1016/j.mencom.2021.09.018>
- Yu, C., Qin, D., Jiang, X., Zheng, X., Deng, B., 2021. Facile synthesis of bright yellow fluorescent nitrogen-doped carbon quantum dots and their applications to an off–on probe for highly sensitive detection of methimazole. *Microchem. J.* 168, 106480.
<https://doi.org/10.1016/j.microc.2021.106480>
- Yu, J., Han, L., Liu, S.G., Ju, Y.J., Gao, X., Li, N.B., Luo, H.Q., 2019. Green

fluorescent carbon quantum dots as a label-free probe for rapid and sensitive detection of hematin. *Spectrochim. Acta Part A Mol. Biomol. Spectrosc.* 212, 167–172. <https://doi.org/10.1016/j.saa.2019.01.001>

Yu, Z., Zhang, L., Wang, X., He, D., Suo, H., Zhao, C., 2020. Fabrication of ZnO/Carbon Quantum Dots Composite Sensor for Detecting NO Gas. *Sensors* 20, 4961. <https://doi.org/10.3390/s20174961>

Zeng, L., Zhe, F., Wang, Y., Zhang, Q., Zhao, X., Hu, X., Wu, Y., He, Y., 2019. Preparation of interstitial carbon doped BiOI for enhanced performance in photocatalytic nitrogen fixation and methyl orange degradation. *J. Colloid Interface Sci.* 539, 563–574. <https://doi.org/10.1016/j.jcis.2018.12.101>

Zhang, J., Si, M., Jiang, L., Yuan, X., Yu, H., 2021. Core-shell Ag @ nitrogen-doped carbon quantum dots modified BiVO₄ nanosheets with enhanced photocatalytic performance under Vis-NIR light : Synergism of molecular oxygen activation and surface plasmon resonance. *Chem. Eng. J.* 410, 128336. <https://doi.org/10.1016/j.cej.2020.128336>

Zhang, J., Yan, M., Yuan, X., Si, M., Jiang, L., Wu, Z., Wang, H., Zeng, G., 2018. Nitrogen doped carbon quantum dots mediated silver phosphate/bismuth vanadate Z-scheme photocatalyst for enhanced antibiotic degradation. *J. Colloid Interface Sci.* 529, 11–22. <https://doi.org/10.1016/j.jcis.2018.05.109>

Zhang, L., Hou, S., Li, P., Zhou, S., Zhang, S., Li, H., 2021. *Colloids and Surfaces A : Physicochemical and Engineering Aspects* Decorating red-

light-emissive , N-doped carbon dots on bismuth sulfide to promote the photocatalytic activity. *Colloids Surfaces A Physicochem. Eng. Asp.* 618, 126397. <https://doi.org/10.1016/j.colsurfa.2021.126397>

Zhang, S., Sui, L., Dong, H., He, W., Dong, L., Yu, L., 2018. High-Performance Supercapacitor of Graphene Quantum Dots with Uniform Sizes. *ACS Appl. Mater. Interfaces* 10, 12983–12991. <https://doi.org/10.1021/acsami.8b00323>

Zhang, X., Guo, H., Chen, C., Quan, B., Zeng, Z., Xu, J., Chen, Z., Wang, L., 2023. Tunable photoacoustic and fluorescence imaging of nitrogen-doped carbon quantum dots. *Appl. Mater. Today* 30, 101706. <https://doi.org/10.1016/j.apmt.2022.101706>

Zhang, Z., Fan, Z., 2021. Application of cerium–nitrogen co-doped carbon quantum dots to the detection of tetracyclines residues and bioimaging. *Microchem. J.* 165, 106139. <https://doi.org/10.1016/j.microc.2021.106139>

Zhang, Z., Zheng, T., Li, X., Xu, J., Zeng, H., 2016. Progress of Carbon Quantum Dots in Photocatalysis Applications. *Part. Part. Syst. Charact.* <https://doi.org/10.1002/ppsc.201500243>

Zhao, C., Liao, Z., Liu, W., Liu, F., Ye, J., Liang, J., Li, Y., 2020. Carbon quantum dots modified tubular g-C₃N₄ with enhanced photocatalytic activity for carbamazepine elimination: Mechanisms, degradation pathway and DFT calculation. *J. Hazard. Mater.* 381, 120957. <https://doi.org/10.1016/j.jhazmat.2019.120957>

- Zhao, Wang, Zhao, Deng, Xia, 2019. Facile Synthesis of Nitrogen-Doped Carbon Quantum Dots with Chitosan for Fluorescent Detection of Fe³⁺. *Polymers (Basel)*. 11, 1731. <https://doi.org/10.3390/polym11111731>
- Zheng, S., Qin, F., Hu, C., Zhang, C., Ma, Y., Yang, R., Wei, L., Bao, L., 2021. Up-converted nitrogen-doped carbon quantum dots to accelerate charge transfer of dibismuth tetraoxide for enhanced full-spectrum photocatalytic activity. *Colloids Surfaces A Physicochem. Eng. Asp.* 615, 126217. <https://doi.org/10.1016/j.colsurfa.2021.126217>
- Zhou, Chengyun, Zeng, G., Huang, D., Luo, Y., Cheng, M., Liu, Y., Xiong, W., Yang, Y., Song, B., Wang, W., Shao, B., Li, Z., 2020. Distorted polymeric carbon nitride via carriers transfer bridges with superior photocatalytic activity for organic pollutants oxidation and hydrogen production under visible light. *J. Hazard. Mater.* 386, 121947. <https://doi.org/10.1016/j.jhazmat.2019.121947>
- Zhou, C., Zeng, Z., Zeng, G., Huang, D., Xiao, R., Cheng, M., Zhang, C., Xiong, W., Lai, C., Yang, Y., Wang, W., Yi, H., Li, B., 2019. Visible-light-driven photocatalytic degradation of sulfamethazine by surface engineering of carbon nitride : Properties, degradation pathway and mechanisms. *J. Hazard. Mater.* 380, 120815. <https://doi.org/10.1016/j.jhazmat.2019.120815>
- Zhou, Chengzhuang, Wang, Q., Zhou, Chengyun, 2020. Photocatalytic degradation of antibiotics by molecular assembly porous carbon nitride: Activity studies and artificial neural networks modeling. *Chem. Phys. Lett.* 750, 137479. <https://doi.org/10.1016/j.cplett.2020.137479>

- Zhou, L., Qiao, M., Zhang, L., Sun, L., Zhang, Y., Liu, W., 2019. Green and efficient synthesis of carbon quantum dots and their luminescent properties. *J. Lumin.* 206, 158–163.
<https://doi.org/10.1016/j.jlumin.2018.10.057>
- Zhou, Q., Yuan, G., Lin, M., Wang, P., Li, S., Tang, J., Lin, J., Huang, Y., Zhang, Y., 2021. Large-scale electrochemical fabrication of nitrogen-doped carbon quantum dots and their application as corrosion inhibitor for copper. *J. Mater. Sci.* 56, 12909–12919.
<https://doi.org/10.1007/s10853-021-06102-x>
- Zhou, Y., Zahran, E.M., Quiroga, B.A., Perez, J., Mintz, K.J., Peng, Z., Liyanage, P.Y., Pandey, R.R., Chusuei, C.C., Leblanc, R.M., 2019. Size-dependent photocatalytic activity of carbon dots with surface-state determined photoluminescence. *Appl. Catal. B Environ.* 248, 157–166.
<https://doi.org/10.1016/j.apcatb.2019.02.019>
- Zhu, J., Chu, H., Wang, T., Wang, C., Wei, Y., 2020. Fluorescent probe based nitrogen doped carbon quantum dots with solid-state fluorescence for the detection of Hg²⁺ and Fe³⁺ in aqueous solution. *Microchem. J.* 158, 105142. <https://doi.org/10.1016/j.microc.2020.105142>
- Zhu, L., Shen, D., Liu, Q., Wu, C., Gu, S., 2021. Sustainable synthesis of bright green fluorescent carbon quantum dots from lignin for highly sensitive detection of Fe³⁺ ions. *Appl. Surf. Sci.* 565, 150526.
<https://doi.org/10.1016/j.apsusc.2021.150526>
- Zou, C., Liu, Z., Wang, X., Liu, H., Yang, M., Huo, D., Hou, C., 2022. A

paper-based visualization chip based on nitrogen-doped carbon quantum dots nanoprobe for Hg(II) detection. *Spectrochim. Acta - Part A Mol. Biomol. Spectrosc.* 265, 120346.

<https://doi.org/10.1016/j.saa.2021.120346>

PUBLICATIONS

1. **Umairah Abd Rani**, Law Yong Ng, Ching Yin Ng, Ebrahim Mahmoudi. (2020). A review of carbon quantum dots and their applications in wastewater treatment, *Advances in Colloid and Interface Science*, Volume 278, 102124, ISSN 0001-8686, <https://doi.org/10.1016/j.cis.2020.102124>.
2. **Umairah Abd Rani**, Law Yong Ng, Ching Yin Ng, Ebrahim Mahmoudi, Yee-Sern Ng, Abdul Wahab Mohammad (2021). Sustainable production of nitrogen-doped carbon quantum dots for photocatalytic degradation of methylene blue and malachite green, *Journal of Water Process Engineering*, Volume 40, 101816, ISSN 2214-7144, <https://doi.org/10.1016/j.jwpe.2020.101816>.
3. **Rani, U.A.**, Ng, L.Y., Ng, C.Y., Wong, C.S., Mahmoudi, E. (2021). Preparation of Carbon-Based Photo-catalyst for Degradation of Phenols. In: Jawaid, M., Ahmad, A., Ismail, N., Rafatullah, M. (eds) *Environmental Remediation Through Carbon Based Nano Composites. Green Energy and Technology*. Springer, Singapore. https://doi.org/10.1007/978-981-15-6699-8_14.
4. **Umairah Abd Rani**, Law Yong Ng, Ching Yin Ng, Ebrahim Mahmoudi, Nur Hanis Hayati Hairom. (2021). Photocatalytic degradation of crystal violet dye using sulphur-doped carbon quantum dots, *Materials Today: Proceedings*, Volume 46, Part 5, Pages 1934-1939, ISSN 2214-7853, <https://doi.org/10.1016/j.matpr.2021.02.225>.
5. **Umairah Abd Rani**, Law Yong Ng, Yee Sern Ng, Ching Yin Ng, Ying Hui Ong, Ying Pei Lim. (2022). Photocatalytic degradation of methyl green dye by nitrogen-doped carbon quantum dots: Optimisation study by Taguchi approach, *Materials Science and Engineering: B*, Volume 283, 115820, ISSN 0921-5107, <https://doi.org/10.1016/j.mseb.2022.115820>.